UNIVERSITÉ DE SHERBROOKE
Faculté de génie
Département de génie mécanique

APPROCHE BASÉE SUR LA TEMPÉRATURE ÉQUIVALENTE POUR LA CONCEPTION THERMIQUE ET LA SÉLECTION DE FLUIDES DE TRAVAIL OPTIMAUX POUR LES CYCLES DE RANKINE ORGANIQUE ET DE RÉFRIGÉRATION

EQUIVALENT TEMPERATURE-BASED APPROACH FOR THERMAL DESIGN AND THE SELECTION OF OPTIMAL WORKING FLUIDS FOR REFRIGERATION AND ORGANIC RANKINE CYCLES

Thèse de doctorat
Spécialité : Génie Mécanique

HOSSEIN AKBARI

Sherbrooke (Québec) Canada

Avril 2020

Jury: Mikhail Sorin (directeur)

Sébastien Poncet (rapporteur)

Nicolas Galanis (examinateur)

Étienne Saloux (examinateur)

RÉSUMÉ

Les systèmes de réfrigération et de puissance représentent la plus grande part de la consommation d'énergie dans les secteurs résidentiel et commercial à travers le monde. Les projections de la demande mondiale d'énergie montrent même une tendance vers une hausse significative au cours des prochaines années. Par conséquent et en raison des sources d'énergie fossiles limitées et de l'impact environnemental, l'optimisation de ces cycles thermodynamiques a attiré beaucoup l'attention des chercheurs. Les performances économiques, environnementales et de fonctionnement des cycles dépendent fortement de la sélection du fluide de travail, ainsi que des caractéristiques de conception et de fonctionnement du cycle. Le choix du fluide de travail est un problème complexe car il implique la sélection du fluide de travail approprié parmi un grand nombre de candidats ainsi que l'ensemble des conditions de fonctionnement possibles pour chaque candidat. Pour résoudre ce problème, une approche systématique doit être définie pour filtrer les alternatives.

L'objectif principal de ce projet de recherche est d'introduire une approche systématique pour la conception thermique et la sélection des fluides de travail optimaux pour les cycles de Rankine organique et de réfrigération basés sur le concept de température équivalente. L'approche systématique introduite se compose de deux étapes, à savoir: l'optimisation des performances à l'échelle du système; et la conception à l'échelle des composants. Dans la première étape, l'efficacité maximale possible du système dans des circonstances idéales est déterminée, indépendamment du fluide de travail, basée sur les conditions existantes de la source externe. Étant donné que la température équivalente exprime implicitement la température de saturation, le sous-refroidissement et les degrés de surchauffe, l'utilisation d'une température équivalente au lieu de la température réelle nous fournit un nombre réduit de paramètres pour le problème d'optimisation. De plus, l'interprétation géométrique de la température équivalente sur le diagramme h-s ouvre la voie au calcul de la génération d'entropie à travers les composants du système qui reste un problème non résolu dans la littérature. Les résultats de l'optimisation des performances à l'échelle du système, ensuite, établissent des critères thermodynamiques pour présélectionner les fluides de travail potentiels. Dans la deuxième étape, une procédure de reconstruction est définie pour corréler les résultats d'optimisation, qui sont en termes de température équivalente, avec les paramètres de fonctionnement réels pour chaque fluide de travail présélectionné. Étant donné que les propriétés individuelles des fluides de travail présélectionnés sont disponibles, l'efficacité de la première loi et la conductance thermique totale sont considérées comme deux indicateurs économiques pour évaluer les performances de chaque fluide de travail. Par conséquent, le fluide de travail le plus approprié pourrait être sélectionné.

L'approche a d'abord été appliquée à la réfrigération par compression de vapeur et au cycle organique de Rankine. Les résultats ont démontré la supériorité de cette approche par rapport aux approches existantes dans la littérature. Il a été démontré que l'utilisation d'une température équivalente entraînait un problème d'optimisation précis et, à son tour, une meilleure conception des systèmes. Par la suite, l'approche a été étendue au système de réfrigération à éjection où la complexité du flux de fluide à l'intérieur de l'éjecteur crée un obstacle d'optimisation à l'échelle du système. De plus, certaines hypothèses préliminaires, concernant les différences de température dans les échangeurs de chaleur, empêchent les chercheurs d'atteindre une approche de conception systématique efficace. Pour simplifier la complexité des phénomènes à l'intérieur de l'éjecteur, il a été remplacé par un compresseur-expanseur hypothétique, puis le taux de génération d'entropie résultant a été caractérisé en utilisant l'efficacité de l'éjecteur. Nous avons ensuite déterminé les variables d'optimisation et jeté les bases d'une détermination systématique des états de fonctionnement des fluides de travail potentiels, sans aucune hypothèse préliminaire. Pour valider notre conception thermodynamique, une technique CFD a été utilisée pour déterminer les paramètres géométriques de l'éjecteur qui fournissent les conditions d’opération désirées.

Mots-clés: fluide de travail, conception thermique, cycles de Rankine organique et de réfrigération, température équivalente.

ABSTRACT

Refrigeration and power systems account for the largest portion of energy use by residential and commercial sectors around the world. Global energy demand projections show even a significant increasing trend by upcoming years. As a result and due to limited fossil fuel energy sources and the environmental impact of rising energy consumption, the optimization of such thermodynamic cycles has drawn much attention from researchers. The economic, environmental and operating performance of the cycles depends heavily on the selection of the working fluid, as well as the design and operating characteristics of the cycle. The choice of the working fluid is a complex problem because it implies the selection of the appropriate working fluid among a huge number of candidates as well as the sets of possible operating conditions for each candidate. To address this issue, a systematic approach needs to be defined to screen the alternatives.

The main objective of this research project is to introduce a systematic approach for the thermal design and selection of the optimal working fluids for organic Rankine and refrigeration cycles based on the equivalent temperature concept. The introduced systematic approach is composed of two steps, namely: system-scale performance optimization; and component-scale design. In the first step, the maximum possible efficiency of the system under ideal circumstances is determined, independently of the working fluid, based on the existing external source conditions. Since equivalent temperature implicitly expresses the saturation temperature, subcooling, and superheating degrees, using equivalent temperature instead of actual temperature provides us with a reduced number of parameters for the optimization problem. Furthermore, the geometrical interpretation of equivalent temperature on the h-s diagram paves the way for the calculation of entropy generation through the system components which remained an unsolved issue in the literature. The results of system-scale performance optimization, then, establish thermodynamic criteria to pre-select the potential working fluids. In the second step, a reconstruction procedure is defined to correlate the optimization results, which are in terms of equivalent temperature, with the actual operating parameters for each pre-selected working fluid. Since the individual properties of the pre-selected working fluids are available, first-law efficiency and total thermal conductance are considered as two economic indicators to evaluate the performance of each working fluid. As a result, the most appropriate working fluid could be selected.

The approach was, first, applied to the vapor-compression refrigeration and organic Rankine cycle (ORC). The results demonstrated the superiority of this approach compared to the existing approaches in the literature. It was shown that using equivalent temperature resulted in a precise optimization problem and, in turn, a better design of the systems. Afterward, the approach was extended to the ejector refrigeration system where the complexity of fluid flow inside the ejector creates an obstacle for system-scale optimization. Moreover, some preliminary assumptions, regarding temperature differences in heat exchangers, prevent researchers from reaching an efficient systematic design approach. To simplify the complexity of phenomena inside the ejector, it was replaced by a hypothetical expander-compressor, and then the resultant entropy generation rate was characterized by using the efficiency of the ejector. We subsequently determined the optimization variables and laid the foundation for a systematic determination of operating states for potential working fluids, without any preliminary assumptions. To

validate our thermodynamic design, a CFD technique was employed to determine the ejector geometry parameters that deliver the desired operating conditions.

Keywords: Working fluid, Thermal design, Organic Rankine cycle, Refrigeration, Equivalent temperature

ACKNOWLEDGMENTS

I would like to express my sincere gratitude to my advisor Prof. Mikhail Sorin for his continuous support and guidance through each step of this journey.

I would like to thank my committee members, Prof. Nicolas Galanis, Prof. Sébastien Poncet and Dr. Etienne Saloux for accepting their roles as examiners of this thesis.

I would also thank Prof. Bernard Marcos, who showed great interest in this work, especially in the optimization approaches.

I am grateful to all my friends and colleagues who provided me with a friendly environment at the Université de Sherbrooke. They have made truly memorable days for me during my Ph.D. study.

And also, special thanks go to my dear parents and my beloved wife for their continuous love and support.

TABLE OF CONTENTS

LIST OF FIGURES

LIST OF TABLES

Chapter 1

INTRODUCTION

1-1 Motivation

Nowadays, with a rapid pace of the development of technologies that rely on thermodynamic cycles, optimization of such cycles has drawn much attention from researchers. The economic, environmental and operating performance of a thermodynamic cycle depends heavily on its operating characteristics including the working fluid as well as operating states. The biggest barrier to find the optimal design conditions for thermodynamic cycles is the huge and increasing number of working fluids and their different optimal operating states for a fixed set of source conditions. To address this issue, systematic approaches have been introduced in the literature.

This study proposes a novel comprehensive approach for the design of thermodynamic cycles based on the equivalent temperature. The approach is composed of two steps: system-scale optimization and component-scale design. In the first step, a generalized optimization problem that is independent of working fluids is performed. The optimization problem comprises the method of thermodynamic optimization of finite-time systems based on chosen basic thermodynamic and heat transfer principles. The complexity of entropy generation associated with the system's component has caused a key issue in the optimization problems. The equivalent temperature concept was employed to address this issue by using some geometrical techniques. The optimization results provide us with some thermodynamic criteria that lead to the pre-selection of potential working fluids. Moreover, they laid the foundations for the reconstruction procedures to introduce a systematic selection of the working fluids and their corresponding optimal operating states. Based on the optimization results, a reconstruction approach is defined to determine the actual operating parameters such as operating pressures and temperatures, as well as the mass flow rate of each potential working fluids. Then,

economic indicators are employed to select the most appropriate working fluid and its operating states.

The approach is, first, applied to the vapor-compression refrigeration and organic Rankine cycles. The advantages of the approach are illustrated by comparing with other approaches existing in the literature. Afterward, the approach is developed to design the ejector refrigeration system. In this study, the economic performance of the system is evaluated in three different ways: the total thermal conductance of the systems where their operating performance of the system remains constant; an economic dimensionless factor; and exergoeconomic analysis.

1-2 Objectives

The main objective of the project is to introduce a systematic approach for the thermal design and selection of the most appropriate working fluid for refrigeration and organic Rankine cycles. This general objective includes the following specific points:

- Determination of entropy generation for each component of the systems, without recourse to the knowledge of working fluid properties.
- Establishment of links between entropy generation and the operating conditions of the system to constrain the optimization problems.
- Optimization problem statement and its solution for each cycle
- Introduction of thermodynamic criteria for pre-selection of potential working fluids based on the optimization problem
- Introduction of reconstruction procedure to correlate the optimization results with the actual operating states for each potential working fluids without any preliminary assumptions.
- Illustration of the advantages of the proposed approach for each cycle

1-3 Thesis outline

The present thesis contains seven chapters. In Chapter 2, an extensive literature review on the thermodynamic optimization of finite-time processes and systematic approach is provided.

Chapter 3 is devoted to the application of the proposed approach in the case of the vapor-compression refrigeration system. To compare the performances of potential working fluids, an economic dimensionless factor is used to facilitate the selection of optimal working fluid. Chapter 4 illustrates the application of the approach in the case of the organic Rankine cycle. Two case studies are used to show the advantages of the approach compared to the existing approaches in the literature. Since the operating performance of all potential working fluids is identical, the total thermal conductance of the system determines the most appropriate working fluid. Chapter 5 describes the application of the approach for the ejector refrigeration system. To simplify the complexity of flow inside the ejector, it is assumed as a hypothetical expander-compressor device and the optimization problem is carried out. The selection of the optimal working fluid is made by an exergoeconomic analysis. To validate our thermodynamic design, a CFD technique is employed to determine the ejector geometry parameters that deliver the desired operating conditions and the results are presented in Chapter 6. Finally, conclusions are presented in Chapter 7.

Chapter 2

STATE OF THE ART

The design of a thermodynamic system can be seen as a two-step approach. This chapter is devoted to an extensive review of studies conducted by previous researchers about both steps in detail.

2-1 System-scale performance optimization

The key attribute of system-scale optimization is that it is formulated generally and independently of working fluids. The upper bound of system efficiency was first introduced by Carnot. In 1824 Carnot introduced his well-known boundary of improvement for any ideal, reversible heat engine (Carnot cycle). This cycle is extremely idealized. In this cycle, the heat transfer from the reservoirs is assumed as a reversible process. To achieve a reversible heat transfer process, it is necessary to have infinitesimal temperature differences between the reservoirs and the engine, which makes the time of heat transfer infinite or the size of heat exchangers very large. Finite-time thermodynamics was introduced in the literature to address the issues related to the Carnot cycle. The reversible process does not occur in the real world and is merely an idealized version of the actual process. The factors that cause a process to be irreversible, such as friction and heat transfer across a finite temperature difference, are called irreversibilities. Irreversibility distributions have been determined to assess the effectiveness of each component separately. This minimization of excessive irreversibility and the trade-off between the contributions to the total irreversibility allow an optimum configuration to be achieved.

The optimization problem involves considerations of an objective function as well as a set of equalities and/or inequalities as optimization constraints.

2-1-1 Objective function

The optimization problem in thermodynamics is aimed to design the different components of a system with the sources/sinks, maximizing or minimizing a given criterion. This criterion can

be based on economic metrics. The capital and operating costs of the system are considered as two important economic metrics in the design of thermodynamic systems. Thermodynamic efficiencies represent the operating cost of the system (Khan and Zubair 1999, 2001) and (Ait-Ali 1996) while capital investments and maintenance costs are usually considered as the capital cost of a system (Bejan, Vargas and Sokolov 1995; Luo *et al.* 2002; Chen, Sun and Wu 2004). From an economic point of view, heat exchangers are important components since their areas affect the overall cost of the system. Moreover, the minimum total thermal conductance of the system and the optimal distribution of the total value between heat exchangers play key roles in the performance of the systems. Thus, the total heat conductance has attracted attention as another objective function (Nunes *et al.* 2015).

2-1-2 Constraints of the optimization problem

A process does not occur unless it obeys the first and second laws of thermodynamics. It means that the two laws are a fixed set of constraints in thermodynamic optimization problems. The second law, entropy generation, represents the efficiency of the system. The entropy generation is a measure of the magnitudes of irreversibilities present during a process. The calculation of entropy generation in a system is the most complex procedure in finite-time thermodynamics where working fluids and their properties are unknown. The procedure of entropy generation calculation in a system can be formulated as the following general schema:

The first step is to apply the energy, entropy and mass balances for the components. The entropy balance includes the entropy generation term which expresses the irreversibilities in the corresponding component. If the process is reversible then the entropy generation term equals zero; otherwise, its value must be positive. The second step is to derive the dependency of component efficiency on the rate of entropy generation. The efficiency of a component depends solely on the entropy generation rate. The third step is to find a link between the entropy generation rates of all components and the operating conditions of the system.

As to irreversibility analysis, Bejan (Bejan 1988) is the pathfinder who introduced the notion of irreversibility in the heat exchanger. Afterward, more attention was paid to the cycle irreversibilities and researchers have divided them into external and internal subsets. The

endoreversible concept (Ait-Ali 1995; Zhou *et al.* 2002) was introduced to investigate the impact of external irreversibility, i.e., heat transfer-type irreversibility associated with heat exchangers, on the proposed objective functions such as first- and second-law energy efficiencies of the systems. However, neglecting the internal irreversibility resulted in an appreciable deviation from the real system capacity. Numerous attempts have been made to distinguish between endoreversible and irreversible thermodynamic cycles and provide insight into real system behavior (Salah El-Din 2001a; Chen, Sun and Wu 2004; Sarkar and Bhattacharyya 2007; Qureshi 2015). Researchers (Ait-Ali 1996; Khan and Zubair 2001) considered the generic source of internal irreversibility by a dimensionless numerical coefficient using Clausius inequality and derived extensive mathematical expressions to measure the impact of internal entropy generation on performance parameters. It should be noted that although this generic coefficient paves the way for the development of the system design, its value has been selected arbitrarily and independently of the operating conditions, thus it can prevent precise us from a determination of the design variables. Hence, the entropy generation analysis or second-law analysis is an essential part of the optimization problem statement which constrains the problem and prevents obtaining infeasible design conditions.

2-1-3 Optimization problem modeling

The optimization problem modeling is the process of identifying the objective function, variables, and constraints for a given problem. All variables used in the optimization problem can be categorized into three groups. The first group belongs to input variables or known parameters needed to design the system. They include the variables that characterize the conditions of reservoirs such as their operating temperatures, mass flow rates, and heat capacities. It is worth noting that the complexity of an optimization problem increases exponentially with the number of input variables. The second group represents independent variables that are degrees of freedom in the optimization problem, which must be optimal to minimize or maximize the objective function. The last category belongs to the dependent variables and is composed of parameters obtained through the optimization problem for each selected independent variable. In a thermodynamic optimization of finite-time systems,

dependent variables are calculated based on chosen basic thermodynamic and heat transfer principles. Figure 2-1 depicts a schematic representation of a generic optimization problem.

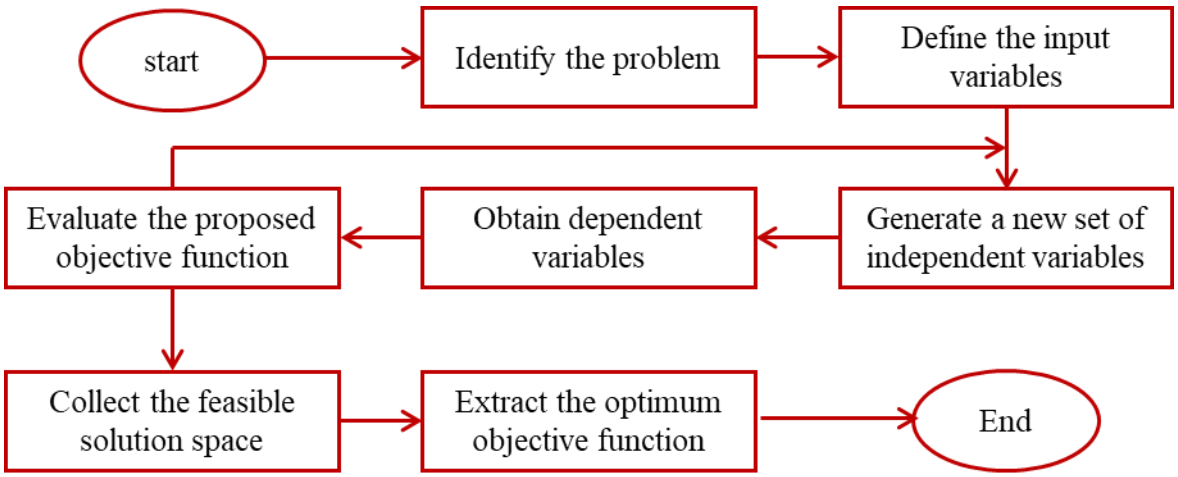

Figure 2-1: Optimization flowchart

The purpose of the system-scale optimization problem is to seek the independent variable values that lead to the optimal condition of the system according to the proposed objective function.

2-1-4 Optimization algorithm

Once the optimization problem has been modeled, an optimization algorithm is needed to find its solution. The optimization algorithms are based on an iterative procedure. The algorithms begin with an initial guess of independent variables and improve the initial guess sequentially in each iteration until they terminate at a solution. The approach employed to improve each iteration distinguishes one algorithm from another. A good optimization algorithm should satisfy the following criteria (Nocedal and Wright 2006):

- Robustness: it should execute well on a wide range of initial guesses.
- Efficiency: its computational cost should be reasonable.
- Accuracy: it should result in a precise solution.

Optimization algorithms can be categorized into two general groups: deterministic and stochastic. Deterministic optimization, also called mathematical programming, relies heavily on analytical properties of the problem to generate a sequence of iteration, to obtain an optimal solution. Stochastic optimization refers to algorithms that are performed based on some random selection in each iteration. It is proven that deterministic algorithms need a lower number of iterations to converge to a solution compared to stochastic algorithms. Moreover, since deterministic algorithms are based on a mathematical formulation, their results are replicable, unlike the stochastic algorithms, due to the presence of randomness in each iteration. The big disadvantage of deterministic algorithms is that they can get stuck in a locally optimal point which is not necessarily the global optimal point (Cavazzuti 2013). In this study, we used sequential quadratic programming (SQP), one of the deterministic algorithms that have recently drawn the attention because it satisfies all the criteria mentioned above. Moreover, it showed the capability to perform nonlinear and linear optimization problems (Adefarati and Bansal 2019). This iterative method is utilized on optimization problems for which the objective function and the constraints are twice continuously differentiable. It is one of the most effective methods for nonlinearly constrained optimization problems. This method generates steps by solving quadratic subproblems; it can be used both in line search and trust-region frameworks. SQP is suitable for small and large problems and it is well-suited to solving optimization problems with significant nonlinearities.

2-2 Component-scale design

The component-scale design includes the determination of the operating states of the system working fluid and the selection of the most appropriate working fluid among potential candidates.

2-2-1 Selection of working fluids and operating conditions

The selection of working fluid can play a significant role in the design of a thermodynamic system. The working fluid operating in the system should meet the following requirements from thermo-physical, environmental, safety and economic points of views:

1. Thermo-physical properties:

- To minimize the circulation rate per unit of cooling capacity in a refrigeration cycle, its latent heat of vaporization should be large enough.
- To avoid heavy construction of the pressure vessel and to minimize the input work, its pressure at the evaporator or condenser should be as low as possible.
- The working fluid should have desirable transport characteristics that influence heat transfer, e.g., viscosity and thermal conductivity.

2. Environmental impact: The refrigerant should be environmentally friendly, with zero ozone depletion potential (ODP) and global warming potential lower than 2500, according to the international agreements (Eldakamawy, Sorin and Brouillette 2017). It should be mentioned that according to the new regulations, working fluids with GWP of 150 or more will be phased out by 2022 (Dincer 2017).
3. Safety: The fluid should be non-toxic, non-corrosive, non-explosive, low inflammable and chemically stable.
4. Economics and availability: The fluid should be low cost and easily available.

The working fluids are traditionally categorized into three groups, based on the shape of the saturation vapor curve of the fluid in the temperature-entropy diagram: wet, dry and isentropic (Figure 2-2). Wet working fluids refer to those fluids that their slopes of the saturation vapor curve in the T-s diagram is negative. Dry or retrograde fluids have negative slopes of the saturation vapor curve in the T-s diagram (regardless of a short negative slope somewhat below the critical point). The third category, i.e. isentropic fluids, refers to those fluids that have a vertical saturation curve. The advantages and disadvantages of each category have been stated in the literature in detail (Eldakamawy, Sorin and Brouillette 2017). For instance, the retrograde fluids have smaller specific volumes that result in a lower work consumed in the compression process. Moreover, the retrograde fluids do not need to be superheated at the entrance of expander devices. For regular or wet fluids, we need some degrees of superheating to ensure a droplet-free expansion. On the other hand, due to the positive slope of the saturated vapor curve, a retrograde fluid has smaller latent heat and, in turn, leads to a smaller refrigeration effect at the same evaporation temperature, compared to a wet fluid.

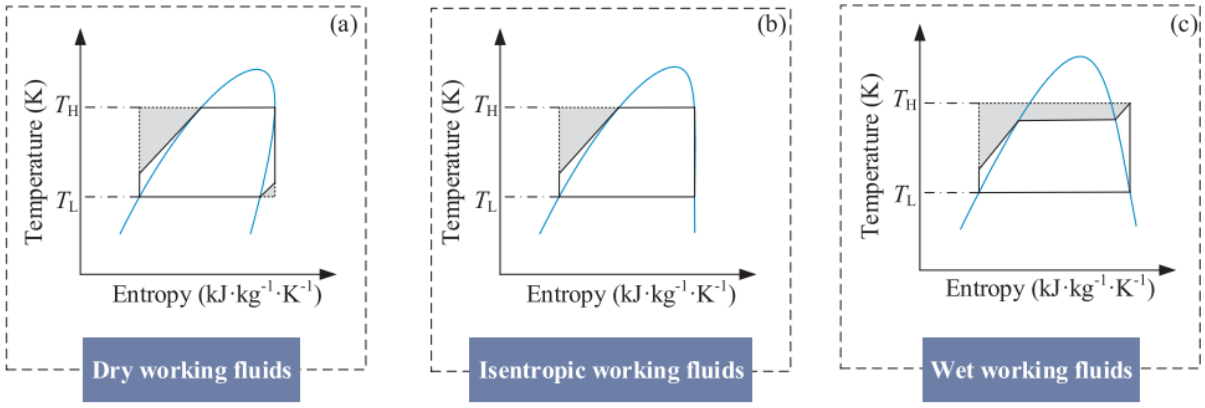

Figure 2-2: T-s diagram of ORC: (a) Dry working fluids; (b) Isentropic working fluids; (c) Wet working fluid (Xu *et al.* 2018)

Since there is a very large and increasing number of working fluids, a designer needs to screen all possible working fluids by using a systematic approach and selects the most appropriate one for the proposed application.

The component-scale design of a thermodynamic system includes the determination of operating states of potential working fluids as well as their mass flow rates. The determination of the operating conditions lay the foundations for the evaluation of the performance of the system for each working fluid. In the following chapters, systematic approaches for each thermodynamic cycle will be presented.

2-2-2 Economic performance of a system

To select the most appropriate working fluid and its corresponding operating condition, some indicators, especially economic ones, are needed to be evaluated. Capital and operating costs are two main indicators that have been used in the literature to economically evaluate the performance of a system. In the early stage of the economic evaluation of the system, total thermal conductance of the system, UA, has been used as an indicator of the capital cost of the system, due to the fact a large part of total capital cost belongs to the purchase of heat exchangers. For the operating cost, thermodynamic efficiencies such as the first- and second-law efficiencies have been usually used as two indicators. If the comparison of thermal conductance and thermodynamic efficiencies are not sufficient to select the best component-scale design, exergy-based methods such as exergoeconomic evaluation (Lazzaretto and

Tsatsaronis 2006), Advanced exergy-based method (Mehrpooya and Mousavi 2018) will be used. Exergy is the only rational basis for allocating monetary values to the process that an energy- conversion system undergoes with its surroundings and to the sources of thermodynamic imperfections within it.

In this study, Exergoeconomic evaluation will be used as it provides us with a clear understanding of the economic performance of the system, which relies on exergy analysis and economic principles. The main outcome of exergoeconomic analysis is the final cost of each product generated by the system. This analysis involves cost balances related to each component of the system. A cost balance simply expresses that the total cost of the exergy streams leaving the component equals the total cost of the entering streams plus the capital investment of the component and its operating and maintenance expenses (Bejan, Tsatsaronis and Moran 1996).

2-3 Comprehensive approaches for the design of thermodynamic cycles

A comprehensive approach is composed of two aforementioned steps, system scale optimization, and component-scale design. Neveu et al. (Neveu and Azoumah 2015) introduced a comprehensive approach for an organic Rankine cycle (ORC). They replaced the actual temperature by equivalent temperature to perform their theoretical optimization. The key attribute of equivalent temperature is to replace the varying-temperature processes with a constant-temperature one. It means that in condenser or evaporator, the value of equivalent temperature implicitly constitutes saturation temperature and the degrees of superheating (or desuperheating) and subcooling depending on the nature of working fluids. Their system-scale optimization was based on economic considerations and the limited information, i.e. temperature of the sources. They chose water as a candidate-working fluid and found all thermodynamic states of the cycle based on the optimization results, by using a simple reconstruction procedure. Due to some simplifications, they assumed that the equivalent temperature and saturation temperature of the condenser is equal which means that subcooling and superheating processes cannot take place in the condenser. This assumption will impose a

limit on the selection of optimal working fluid. For instance, dry fluids, which have saturation vapor lines with positive slopes on their *T-s* diagrams, cannot be investigated by this procedure. Afterward, Saloux et al. (Saloux *et al.* 2019) developed Neveu's approach optimization by using a genetic algorithm. They also overcome the aforementioned shortcoming of Neveu's reconstruction procedure by imposing technical constrains such as some degrees of subcooling at the inlet of the pump and then they determined the ORC thermodynamic states by using the *h-s* diagram. Saloux et al. (Saloux *et al.* 2018) introduced a procedure in which the mass flow rate was considered as the sole degree of freedom. First, they defined a range of the values of the mass flow rate for each potential fluid. Then they applied the reconstruction procedure for each selected mass flow rate by using *h-s* diagram attributes. Finally, they imposed some technical constraints such as the fluid superheating in the evaporator and the evaporator pressure as criteria, to select the most appropriate working fluid. The main drawback of this procedure is that the feasible distribution of temperature along the heat exchangers will not be guaranteed. A further disadvantage of this procedure is that the mass flow rate range related to each potential refrigerant must be defined beforehand.

The main objective of this study is to address the issues that have arisen in the previous equivalent temperature-based approaches. To formulate a precise optimization problem, a second-law analysis is introduced in which the entropy generation for each component of the systems, without recourse to the knowledge of working fluid properties, is determined. This analysis paves the way for an establishment of links between entropy generation and the operating conditions of the system to constrain the optimization problems. It should be mentioned that the optimization problem formulated by Saloux et al. (Saloux *et al.* 2018) is independent of the entropy generated in the mechanical components. This assumption causes plenty of room for error in an accurate optimization problem. Furthermore, the precise formulation of the optimization problem allows us to perform the problem by using a deterministic algorithm. Then, the definition of equivalent temperature is utilized to introduce the reconstruction procedure in which all the operating states and variables are automatically determined without any preliminary assumptions.

Chapter 3

An equivalent temperature based approach for selection of the most appropriate working fluids for refrigeration cycles

Avant-propos

Auteurs et affiliation:

Hossein Akbari: étudiant au doctorat, faculté de génie, département de génie mécanique, Université de Sherbrooke.

Mikhail Sorin: professeur, faculté de génie, département de génie mécanique, Université de Sherbrooke.

Bernard Marcos: professeur, faculté de génie, département de génie chimique et biotechnologique, Université de Sherbrooke.

Date d'acception: 7 août 2018

État de l'acceptation: version finale publiée

Revue: Energy Conversion and Management

Titre français: Une approche basée sur la température équivalente pour la sélection des fluides de travail les plus appropriés pour les cycles de réfrigération

Contribution au document:

Cet article contribue à la thèse par une application de l'approche proposée pour les cycles de réfrigération à compression de vapeur.

Résumé français:

Cet article présente une nouvelle approche compréhensive pour la sélection des fluides de travail les plus appropriés et la conception conceptuelle des cycles de réfrigération à compression de vapeur, soumis à une conductance globale minimale pour une capacité de réfrigération fixe avec un rendement isentropique connu du compresseur et des températures fixes des fluides externes entrant dans le condenseur et l'évaporateur. L'approche se compose de trois étapes séquentielles: la première étape est le calcul indépendant du fluide frigorigène de la conductance thermique minimale du système via une optimisation contrainte. L'analyse de la deuxième loi contraint le problème d'optimisation. Certaines considérations thermodynamiques du diagramme h-s et du concept de température équivalente permettent de calculer la génération d'entropie dans chaque composant du système. Les résultats d'optimisation établissent des critères thermodynamiques pour la présélection des réfrigérants potentiels. Étant donné que les conditions optimales obtenues sont exprimées en termes de températures équivalentes, dans la deuxième étape, une procédure de reconstruction est introduite pour corréler les températures équivalentes avec les caractéristiques thermodynamiques essentielles du système telles que les pressions de travail, les températures et le débit massique pour réfrigérant pré-sélectionné. La dernière étape de l'approche est la sélection finale du réfrigérant optimal parmi les candidats en utilisant un critère de performance des coûts d'exploitation. Une étude de cas a été présentée pour illustrer l'application de la nouvelle approche de sélection.

3-1 Abstract

This article presents a novel comprehensive approach for the selection of the most appropriate working fluids and the conceptual design of vapor-compression refrigeration cycles, subject to minimal overall conductance for fixed cooling capacity with known compressor isentropic efficiency, and fixed temperatures of the external fluids entering the condenser and the evaporator. The approach consists of three sequential steps: the first step is the refrigerant independent calculation of the minimum thermal conductance of the system via constrained optimization. The second law analysis constrains the optimization problem where some

thermodynamic considerations of *h-s* diagram and equivalent temperature concept provide the ability to calculate the entropy generation in each component of the system. The optimization results establish thermodynamic criteria for the pre-selection of potential refrigerants. Since the optimum conditions obtained are expressed in terms of equivalent temperatures, in the second step, a reconstruction procedure is introduced to correlate the equivalent temperatures with the essential thermodynamic characteristics of the system such as working pressures, temperatures, and mass flow rate for each pre-selected refrigerant. The last step of the approach is the final selection of the optimal refrigerant among the candidates using a capital-operating cost performance criterion. A case study was presented to illustrate the application of the novel selection approach.

Keywords: Vapor-compression refrigeration, Working fluid, Second-law analysis, Equivalent temperature

3-2 Introduction

The vapor-compression refrigeration cycle is the most widely used technology for the production of cold in residential, commercial and industrial applications (Energy Information Administration (EIA) 2017). Nowadays, in the context of the rapid growth of energy demand and cost, the optimization of such cycles has drawn much attention from researchers. The economic, environmental and operating performance of a refrigeration cycle depends heavily on the selection of the working fluid (Dalkilic and Wongwises 2010; Salhi, Korichi and Ramadan 2018), as well as the design (Molés *et al.* 2014; Farsi, Mohammadi and Ameri 2017) and operating characteristics of the cycle (Zhao *et al.* 2013; Bellos, Tzivanidis and Tsifis 2017).

Thermodynamic optimization models for the vapor-compression cycles can be categorized into empirical and theoretical groups. The former may contain several empirical coefficients, which typically are refrigerant-based (Khan and Zubair 1999; Belman *et al.* 2010). Due to the very large and increasing number of working fluids, the most appropriate working fluid corresponding to given conditions of external reservoirs needs to be selected based on systematic approach. Thus, the application of the empirical model in a systematic selection of the optimal working fluid, which necessitates having a huge volume of data, will be

unattainable. In this case, the alternative group, based on theoretical models (Ma *et al.* 2017), which are independent of the working fluid, will be very desirable. Theoretical model can provide preliminary design of the system based on the availability of the heat reservoirs, without the detailed characteristics of the system components. The main objective of a theoretical model is to calculate the optimal operating conditions of the system such as condensation and evaporation temperatures without recourse to the knowledge of working fluids and their thermo-physical properties. Several attempts have been made to develop the theoretical model by various endoreversible Carnot refrigerators using finite-time thermodynamics, which comprises external irreversibility associated with finite temperature-difference heat transfer (Ait-Ali 1995; Zhou *et al.* 2002). The endoreversible model does not account for internal irreversible processes. In order to deal with the internal losses, researchers considered the generic source of internal irreversibility by a dimensionless numerical coefficient using Clausius inequality and minimized the thermal conductance of the system for a fixed cooling capacity or maximized the cooling capacity for a constant overall thermal conductance (Ait-Ali 1996; Khan and Zubair 2001; Ahmadi *et al.* 2014). It should be noted that although this generic coefficient paves the way for the development of the system design, its value has been selected arbitrarily and independently of the operating conditions, thus it can prevent precise determination of the design variables.

Having obtained the optimal evaporation and condenser temperatures by using the theoretical model, a legitimate question is how to select the most appropriate working fluid, while respecting the optimization results. The selection of the working fluid, due to the very large number of choices, is always considered as a design challenge and requires the ability to systematically screen the alternatives (Linke, Papadopoulos and Seferlis 2015; Mavrou *et al.* 2015; Hærvig, Sørensen and Condra 2016).

Recently, Neveu et al. (Neveu and Azoumah 2015) introduced a comprehensive approach to minimizing the investment cost in the Rankine cycle for a given output power, based on limited information, i.e. temperatures of the sources. They replaced the actual temperature by the equivalent temperature to reduce the parameters of their theoretical optimization and, thus, obtained their results in terms of equivalent temperatures, which implicitly constitute the

saturation temperature, subcooling and superheating degrees. To find all thermodynamic states of the cycle as well as the mass flow rate of working fluid, they chose water as a candidate working fluid and performed their reconstruction procedure. Due to some simplifications, they assumed that the equivalent temperature and saturation temperature of the condenser are equal, which means that desuperheating and subcooling processes cannot take place in the condenser. This assumption will impose a limit for selection of the optimal working fluid. For instance, dry fluids, which have saturation vapor lines with positive slopes on their *T-s* diagrams, cannot be investigated by this procedure. In turn, Saloux et al. (Saloux *et al.* 2018) overcame the aforementioned shortcoming by imposing technical constraints such as some degrees of subcooling at the inlet of the pump and then they determined the ORC thermodynamic states by using *h-s* diagram.

The purpose of our research is to present a novel comprehensive approach to the design of a vapor-compression refrigeration cycle that leads to the selection of the optimal working fluid based on known compressor isentropic efficiency, and fixed inlet conditions for the external heat reservoirs. The method is composed of three steps. The first step, independent of the working fluid and its thermodynamic properties, is to define the optimal equivalent temperatures of the cycle corresponding to the minimum value of the overall system conductance. To constrain the optimization problem, the second-law analysis of the cycle is developed where some thermodynamic considerations of *h-s* diagram integrated with equivalent temperature properties are employed to calculate the entropy generation in each device based on the operating conditions, instead of applying arbitrary dimensionless coefficients used in the literature. Moreover, the optimization problem establishes thermodynamic criteria for the pre-selection of potential refrigerants. The second step is a reconstruction procedure that systematically correlates the optimal equivalent temperatures with operating conditions, such as working pressures, temperatures, mass flow rate, subcooling and desuperheating processes, for each pre-selected refrigerant. The third step is the final selection of the most appropriate working fluid based on a capital-operating cost performance criterion. To illustrate the application of the approach presented herein, a case study is presented.

3-3 System description

The vapor-compression refrigeration cycle is used to move heat from a cold reservoir to a hot reservoir. As shown schematically in Figure 3-1, it is essentially composed of two heat exchangers (a condenser and an evaporator) operating at high and low pressures, a non-isentropic compressor and an expansion valve. Heat is transferred by the working fluid from a low-temperature heat reservoir to a high-temperature heat reservoir due to the work consumed by the compressor.

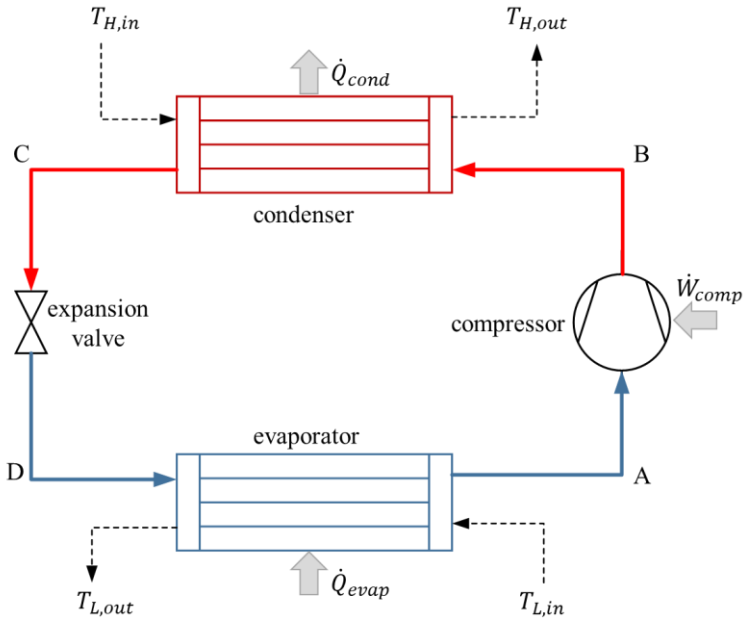

Figure 3-1 Vapor-compression refrigeration cycle

The use of the first and second laws of thermodynamics between two states yields the following property relation:

$$Tds = dh - vdp \tag{3-1}$$

The ratio of enthalpy to entropy variations between two states in constant-pressure process represents the equivalent temperature, also known as the exergy equivalent temperature (Saloux, Teyssedou and Sorin 2015).

$$\tilde{T} = \frac{\Delta h}{\Delta s} \tag{3-2}$$

A valuable diagram in the analysis of a thermodynamic cycle and its components is the enthalpy-entropy, Mollier, diagram (Figure 3-2a). The *h*-*s* diagram can provide intuitive insight into steady-state flow devices, as enthalpy h is a principal property of the first law of thermodynamics and entropy s is the characteristic that accounts for the second law. Equivalent temperature has an instructive geometric interpretation on the *h*-*s* diagram. The equivalent temperature $\tilde{T}$, which is defined in the constant-pressure process, corresponds to the slope of straight line in the Mollier diagram that can reasonably be fitted to the actual isobaric transformation (Neveu and Azoumah 2015). This key attribute of equivalent temperature concept will be used in the following section to determine entropy generation rates in thermodynamic processes.

3-4 Entropy generation

A detailed study of the component entropy generation is necessary to recognize the losses within the cycle. The model proposed herein is centred around the entropy generation of the system components based on the equivalent temperature, which is investigated in sections 3-4-1 to 3-4-5.

3-4-1 Condenser

Applying the first and second laws of thermodynamics to the condenser exchanging heat with variable-temperature heat reservoir yields:

$$\dot{Q}_{cond} = \dot{m}_{ref}(h_B - h_C) \tag{3-3}$$

$$\dot{m}_{ref}(s_C - s_B) = \dot{S}_{gen,cond} - \frac{\dot{Q}_{cond}}{\tilde{T}_H} \tag{3-4}$$

$\tilde{T}_H$ corresponds to the equivalent temperature of the high-temperature heat reservoir and it is determined by the following relation (Lee 2010):

$$\tilde{T}_H = \frac{T_{H,out} - T_{H,in}}{\ln \frac{T_{H,out}}{T_{H,in}}} \tag{3-5}$$

Combining Eqs. *(3-2)*, *(3-3)* and *(3-4)* yields the entropy production rate in condenser:

$$\dot{S}_{gen,cond} = \dot{Q}_{cond}\left(\frac{1}{\tilde{T}_H} - \frac{1}{\tilde{T}_{BC}}\right) \tag{3-6}$$

$\tilde{T}_{BC}$ denotes the equivalent temperature of the condenser. It should be noted that the entropy generation in a temperature-varying process, like the heat transfer process occurring in the condenser, where we normally have desuperheating and subcooling, can only be calculated due to the introduction of the equivalent temperature.

3-4-2 Evaporator

Like the condenser, applying the two laws of thermodynamics to the evaporator results in:

$$\dot{Q}_{evap} = \dot{m}_{ref}(h_A - h_D) \tag{3-7}$$

$$\dot{m}_{ref}(s_A - s_D) = \dot{S}_{gen,evap} + \frac{\dot{Q}_{evap}}{\tilde{T}_L} \tag{3-8}$$

$$\dot{S}_{gen,evap} = \dot{Q}_{evap}\left(\frac{1}{\tilde{T}_{AD}} - \frac{1}{\tilde{T}_L}\right) \tag{3-9}$$

$\tilde{T}_L$and $\tilde{T}_{AD}$ represent the equivalent temperatures of the cold heat reservoir and evaporator, respectively.

$$\tilde{T}_L = \frac{T_{L,out} - T_{L,in}}{\ln \frac{T_{L,out}}{T_{L,in}}} \tag{3-10}$$

3-4-3 Compressor

The isentropic efficiency of the compressor is defined as

$$\eta_{is,comp} = \frac{h_{B,is} - h_A}{h_B - h_A} \tag{3-11}$$

$h_{B,is}$ represents the outlet enthalpy of an ideal compressor. We can apply the first and second laws of thermodynamics to the compressor:

$$\dot{W}_{comp} = \dot{m}_{ref}(h_B - h_A) \tag{3-12}$$

$$\dot{S}_{gen,comp} = \dot{m}_{ref}(s_B - s_A) \tag{3-13}$$

Combining the Eqs. *(3-12)* and *(3-13)* yields

$$\dot{S}_{gen,comp} = \dot{W}_{comp} \cdot \frac{s_B - s_A}{h_B - h_A} \tag{3-14}$$

From simple geometric considerations in Figure 3-2(b) and Eq. *(3-11)*, it can be demonstrated that the entropy-enthalpy ratio in the compressor is equal to

$$\frac{s_B - s_A}{h_B - h_A} = \frac{1 - \eta_{is,comp}}{\tan\alpha} \tag{3-15}$$

$\tan\alpha$ corresponds to the slope of condenser line in the *h-s* diagram and is equal to the equivalent temperature of the condenser. Taken together Eqs. *(3-14)* and *(3-15)* yield:

$$\dot{S}_{gen,comp} = \dot{W}_{comp} \cdot \frac{1}{\tilde{T}_{BC}} \cdot \left(1 - \eta_{is,comp}\right) \tag{3-16}$$

According to Eq.*(3-16)*, the rate of entropy generation during the compression process is a function of the compressor isentropic efficiency and the equivalent temperature of the condenser (condenser pressure) as well as the work consumed by the compressor. It is worth noting that in a real case where the refrigerant is superheated at point B, $\tan\alpha$ is greater than $\tilde{T}_{cond}$ and this difference causes a slight deviation for the entropy generation calculation compared to the real case.

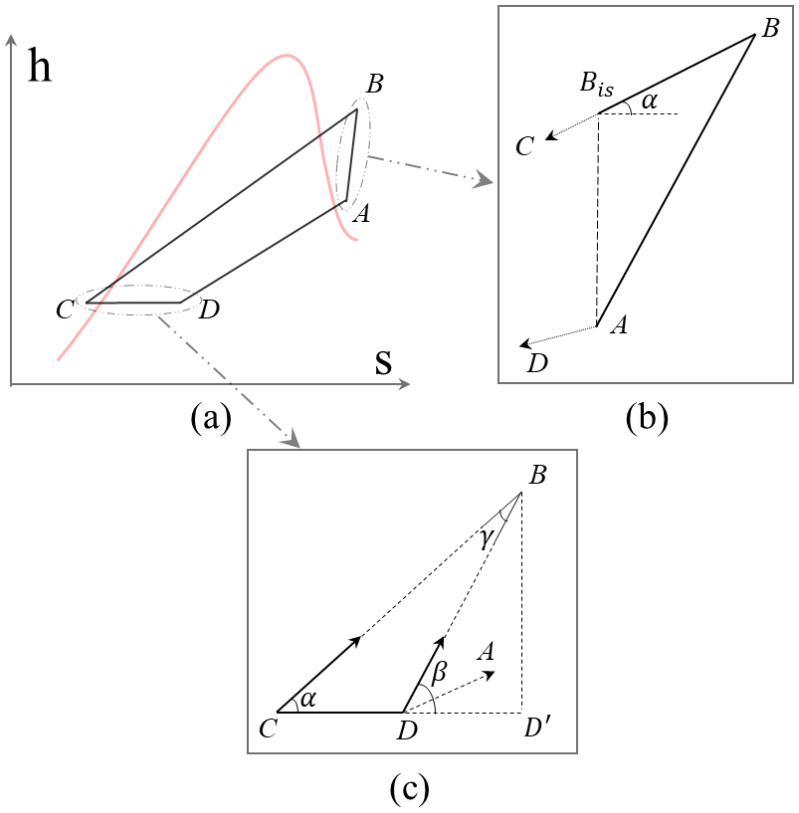

Figure 3-2: (a): Mollier diagram of a refrigeration cycle, (b): Compression process, and (c): Expansion process

3-4-4 Expansion valve

Unlike the processes in the condenser, evaporator and compressor, the ratio of enthalpy to entropy variations cannot be a useful parameter to calculate the entropy generation rate of the isenthalpic throttling process. Khennich et al. (Khennich, Sorin and Galanis 2014) replaced the isenthalpic process by a combination of isentropic and isobaric processes and made the application of equivalent temperature appropriate; nevertheless, their method highly depends on thermodynamic properties of refrigerant states at the inlet and the outlet of the expansion valve, such as enthalpies and mass flow rate. In this study, we propose to overcome this shortcoming by simple geometrical considerations in Figure 3-2(c). In the expansion process we have:

$$h_C = h_D \tag{3-17}$$

$$\dot{S}_{gen,exp} = \dot{m}_{ref}(s_D - s_C) \tag{3-18}$$

To calculate the entropy generation in the expansion valve, the straight line connecting the states B and D is used. In the triangle composed of states B, C and D (Figure 3-2(c)), the law of sine states

$$\frac{\overline{CD}}{\sin\gamma} = \frac{\overline{CB}}{\sin(\pi - \beta)} \tag{3-19}$$

$\overline{CD}$ corresponds to the value of entropy change in the throttling process and $\overline{CB}$ is the hypotenuse of triangle $BD'C$ (Figure 3-2(c)) and can be written as

$$\overline{CB} = \sqrt{{\Delta h_{BC}}^2 + {\Delta s_{BC}}^2} = \Delta h_{BC} * \sqrt{1 + \left(\frac{1}{\tilde{T}_{BC}}\right)^2} \tag{3-20}$$

Thus, Eq. *(3-19)* can be rewritten as

$$\frac{\dot{S}_{gen,exp}}{\sin\gamma} = \frac{\dot{Q}_{cond} * \sqrt{1 + \left(\frac{1}{\tilde{T}_{BC}}\right)^2}}{\sin(\pi - \beta)} \tag{3-21}$$

γ denotes the angle opposite $\overline{CD}$ and β is the angle formed by a horizontal line and the line $\overline{BD}$. In addition, using Eqs. *(3-7)* and *(3-16)*, and geometrical considerations, we have

$$\tan\beta = \frac{\Delta h_{BC}}{\Delta s_{DA} + \Delta s_{AB}} = \frac{\dot{Q}_{cond}}{\frac{\dot{Q}_{evap}}{\tilde{T}_{AD}} + \dot{W}_{comp} * \frac{1}{\tilde{T}_{BC}} * \left(1 - \eta_{is,comp}\right)} \tag{3-22}$$

$$\tan\gamma = \frac{\tan\beta - \tan\alpha}{1 + \tan\beta * \tan\alpha} \tag{3-23}$$

Finally, the combination of Eqs. *(3-21)* to *(3-23)* and trigonometric relationships yield

$$\dot{S}_{gen,exp} = \frac{\sqrt{1+\frac{1}{\tan^2\beta}}}{\sqrt{1+\frac{1}{\tan^2\gamma}}} * \dot{Q}_{cond} * \sqrt{1+\left(\frac{1}{\tilde{T}_{BC}}\right)^2} \quad (3\text{-}24)$$

Based on Eqs. *(3-22)* and *(3-24)*, we conclude that the individual contribution of entropy creation in each component is dependent on entropy generation in the other components (Alefeld 1987).

3-4-5 Refrigeration cycles

Enthalpy and entropy changes for closed systems such as refrigeration cycles are zero. Thus, the summations of enthalpy and entropy variations in foregoing components deduce:

$$\dot{Q}_{evap} + \dot{W}_{Comp} - \dot{Q}_{cond} = 0 \quad (3\text{-}25)$$

$$\dot{S}_{gen,tot} = \frac{\dot{Q}_{cond}}{\tilde{T}_H} - \frac{\dot{Q}_{evap}}{\tilde{T}_L} \quad (3\text{-}26)$$

$\dot{S}_{gen,tot}$ denotes the rate of total entropy generation of the refrigerant which comprises external entropy creation related to the heat transfer phenomena, i.e. in the condenser (Eq. *(3-6)*) and the evaporator (Eq. *(3-9)*); and internal entropy creation related to the compression (Eq. *(3-16)*) and the throttling (Eq. *(3-24)*) processes. The internal entropy production rate can be calculated by substituting Eqs. *(3-6)* and *(3-9)* into Eq.*(3-26)*:

$$\dot{S}_{gen,internal} = \dot{S}_{gen,exp} + \dot{S}_{gen,comp} = \frac{\dot{Q}_{cond}}{\tilde{T}_{BC}} - \frac{\dot{Q}_{evap}}{\tilde{T}_{AD}} \quad (3\text{-}27)$$

It is worth noting that the physical meaning of Eq. *(3-27)* is that the entropy variation of refrigerant in the condenser is equal to the summation of the refrigerant entropy variation in the three other components. Moreover, Eq.*(3-27)*, owing to the equivalent temperature, establishes a link between operating parameters of the cycle and entropy generation rates in the throttling valve and the compressor. The calculation of entropy generation in each component developed above lays the foundations for the optimization problem statement (following section).

Finally, it is worth noting that the coefficient of performance (COP) of the vapor-compression refrigeration system, the maximum COP of a refrigeration cycle operating between two reservoirs (Carnot efficiency), and the second-law efficiency (exergy efficiency) of the cycle can be calculated by

$$COP = \frac{\dot{Q}_{evap}}{\dot{W}_{comp}} \tag{3-28}$$

$$COP_{Carnot} = \frac{\tilde{T}_L}{\tilde{T}_H - \tilde{T}_L} \tag{3-29}$$

$$\eta_{\text{II}} = \frac{COP}{COP_{Carnot}} \tag{3-30}$$

3-5 Optimization Problem Statement and its Solution

In this section, the optimization of vapor-compression refrigeration cycle corresponds to the first step of the proposed comprehensive approach for the selection of the most appropriate working fluid is presented. The process of optimizing a thermodynamic cycle involves considerations of an objective function such as capital or operating performance criteria. From an economic point of view, heat exchangers are important components since their areas affect the overall system cost. Moreover, the minimum total thermal conductance and optimal distribution of the total value between the heat exchangers play key roles in the system performance (Bejan, Vargas and Sokolov 1995; Luo *et al.* 2002; Chen, Sun and Wu 2004). In this research, the optimization problem is defined to minimize the overall thermal conductance that satisfies a given cooling rate, independently of working fluids. The minimization is constrained by the entropy generation as presented by Eqs. (3-16), (3-24) and (3-27). It should also be mentioned that the proposed problem is equivalent to the maximization of a cooling generation that ensures a fixed total thermal conductance (Neveu and Azoumah 2015). The objective function can be expressed as

$$Minimize\ (UA)_{total} = (UA)_{cond} + (UA)_{evap} \tag{3-31}$$

$(UA)_{evap}$ and $(UA)_{cond}$ are the thermal conductances between cold- and hot-sides, respectively:

$$(UA)_{evap} = \frac{\dot{Q}_{evap}}{\Delta T_{LMTD_{evap}}} = \frac{\dot{m}_L c_{P,L}\left(T_{L,in} - T_{L,out}\right)}{\Delta T_{LMTD_{evap}}} \tag{3-32}$$

$$(UA)_{cond} = \frac{\dot{Q}_{cond}}{\Delta T_{LMTD_{cond}}} = \frac{\dot{m}_H c_{P,H}\left(T_{H,out} - T_{H,in}\right)}{\Delta T_{LMTD_{cond}}} \tag{3-33}$$

The logarithmic mean temperature differences (LMTDs) for evaporator and condenser are defined as:

$$\Delta T_{LMTD_{evap}} = \frac{\left(T_{L,in} - \tilde{T}_{AD}\right) - \left(T_{L,out} - \tilde{T}_{AD}\right)}{\ln \frac{\left(T_{L,in} - \tilde{T}_{AD}\right)}{\left(T_{L,out} - \tilde{T}_{AD}\right)}} \tag{3-34}$$

$$\Delta T_{LMTD_{cond}} = \frac{\left(T_{H,in} - \tilde{T}_{BC}\right) - \left(T_{H,out} - \tilde{T}_{BC}\right)}{\ln \frac{\left(T_{H,in} - \tilde{T}_{BC}\right)}{\left(T_{H,out} - \tilde{T}_{BC}\right)}} \tag{3-35}$$

It should be noted that the use of equivalent temperatures (constant temperature) in the condenser and evaporator, instead of actual temperatures where we have (de)superheating and subcooling, will produce a minimal estimation of the system thermal conductance. As will be illustrated in section 0, depending on the degrees of superheating and/or subcooling in the processes, the corresponding *UA* using real temperature will be up to 13% higher than when we use the equivalent temperature. In other words, the value of *UA* obtained by using equivalent temperature is the minimum value that a needed in the corresponding heat exchangers.

The optimization problem consists of solving Eqs. *(3-25)*, and *(3-31)* to *(3-35)*, while satisfying the following set of constraints.

$$\frac{\dot{Q}_{cond}}{\tilde{T}_{BC}} - \frac{\dot{Q}_{evap}}{\tilde{T}_{AD}} = \dot{S}_{gen,exp} + \dot{S}_{gen,comp} \tag{3-36}$$

$$T_{L,out} > \tilde{T}_{AD} \tag{3-37}$$

$$\tilde{T}_{BC} > T_{H,out} \tag{3-38}$$

The first constraint refers to the internal entropy generation caused by the expansion valve and non-isentropic compressor and their link to the entropy variations of working fluids in the condenser and evaporator. The last two constraints satisfy the driving forces for heat transfer in heat exchangers. All variables used in the optimization problem can be classified into three groups:

- Initial parameters for design, or known variables: Seven variables needed to design the system, including the high-temperature source information, i.e. the mass flow rate ($\dot{m}_H$), specific heat capacity ($c_{P,H}$) and inlet temperature of secondary fluid ($T_{H,in}$); low-temperature source information, i.e. specific heat capacity ($c_{P,L}$) and inlet temperature of secondary fluid ($T_{L,in}$); the isentropic efficiency of compressor ($\eta_{is,comp}$), and the desired cooling rate ($\dot{Q}_{evap}$).
- Independent variables: Variables including two equivalent temperatures, for the condenser and the evaporator, i.e. $\tilde{T}_{BC}$ and $\tilde{T}_{AD}$, respectively, and the final temperatures of hot- and cold-side secondary fluids, i.e. $T_{H,out}$ and $T_{L,out}$, respectively. Thus, there are four degrees of freedom in the optimization problem.
- Dependent variables: These parameters including $(UA)_{evap}$, $(UA)_{cond}$, $\dot{m}_L$, $\dot{Q}_{cond}$, $\dot{W}_{comp}$, $\tilde{T}_H$, $\tilde{T}_L$, $\dot{S}_{gen,exp}$, $\dot{S}_{gen,comp}$ can be obtained through the above equations and physical constraint equations (Eqs. *(3-36)* to *(3-38)*) for the selected independent variables.

In fact, the optimization problem in the first step of the comprehensive approach consists of searching for the values of the independent variables that minimize the overall thermal conductance, while providing a given cooling rate, independently of working fluids. The results obtained by the theoretical optimization problem establish thermodynamic criteria for the pre-selection of the potential refrigerants which can be used in the cycle. To establish the link between the equivalent temperatures and the real operating conditions of a vapor-compression refrigeration cycle for each pre-selected refrigerant candidates a special reconstruction procedure is required. This is the subject of the next section.

3-6 Reconstruction procedure

The objective of a reconstruction procedure, as the second step of the comprehensive approach, is to correlate the resultant equivalent temperatures with the operating parameters of the system such as operating pressures and temperatures and refrigerant mass flow rate. Since the optimization problem was formulated independently of the refrigerant, and each potential candidate pre-selected in the first step of the comprehensive approach has significantly different thermo-physical properties, the reconstruction procedure must be carried out to determine the corresponding operating conditions of each refrigerant candidates and, thus, to pave the way for the final selection of the optimal working fluid.

Saloux et al. (Saloux *et al.* 2018) introduced a procedure for ORC cycles in which the mass flow rate was considered as the sole degree of freedom. First, they defined a range mass flow rate values for each potential fluid. Then they applied their reconstruction procedure for each selected mass flow rate by using *h*-*s* diagram attributes. Finally, they imposed some technical constraints such as the fluid superheating in the evaporator and the evaporator pressure as criteria, to select the most appropriate working fluid. A different methodology is proposed in this paper. We consider the temperature differences at the outlets of evaporator and condenser as two degrees of freedom. The capital-operating cost for each working fluid will be assessed to select the optimal refrigerant. This method has some advantages. First, the feasible distribution of temperature along the heat exchangers will be guaranteed, which was not taken into consideration in Saloux's procedure. The second benefit is that the mass flow rate related to each potential refrigerant can be automatically calculated during the procedure and range of mass flow rate do not need to be defined beforehand.

A working fluid may experience three distinct states by exchanging heat while maintaining constant pressure: liquid phase (subcooled) in which the ratio of enthalpy to entropy variations (or equivalent temperature) between two points is less than saturation temperature related to the pressure; saturated liquid-vapor mixture phase, where the ratio remains constant and is equal to the saturation temperature; superheated region, where the equivalent temperature is higher than the saturation temperature. This concept is the foundation for the reconstruction procedure. It means that the deviation of equivalent temperature from saturation temperature determines the

degrees of superheating and sub-cooling in the condenser, and degree of superheating in the evaporator.

The procedure is started by assuming a value for the temperature difference at the evaporator outlet (ΔT_{evap}). Since the temperatures of the cold-side secondary fluid are known, the temperature at the outlet of the evaporator (point A in Figure 3-1) will be determined by the specified ΔT_{evap}. It should be noticed that ΔT_{evap} must be lower than the value of $T_{L,in} - \tilde{T}_{AD}$ to guarantee that the refrigerant will be superheated at the inlet of compressor. Meanwhile, the upper bound for evaporation temperature is given by the value of $\tilde{T}_{AD}$. Thus, the first approximation of the saturation temperature can be deduced by reducing the value of $\tilde{T}_{AD}$ by an amount of 0.01, which is equal to the accuracy of optimization results. Once the initial value of evaporator pressure is fixed, the thermo-physical properties of refrigerant at state A can be determined. The next step consists of setting the initial value of the evaporator inlet vapor quality. The minimum value that this parameter can take is one percent, which allows determining the refrigerant properties at state D. Next, condenser pressure is deduced. Since the inlet temperature of the secondary fluid is fixed, we need to assume a lower bound for temperature difference, ΔT_{cond}, at the condenser outlet to provide the driving force of heat transfer. On the other hand, due to superheated and subcooled states at the condenser, the relevant equivalent temperature, unlike the evaporator, cannot be the upper or lower value of saturation temperature. Assume that $T_{H,in} + \Delta T_{cond} + 0.01$ can be a first estimation of the condensation temperature. Once the condenser pressure is specified, the isentropic efficiency of compressor and isenthalpic process at the throttling valve are used to deduce states B and C. If the equivalent temperature between the two states, B and C, is different from $\tilde{T}_{BC}$ obtained by optimization method, the condensation temperature must be modified. Having obtained the proper condenser pressure, we now assess the temperature of refrigerant at the condenser outlet. A value lower than $T_{H,in} + \Delta T_{cond}$ makes the resolution of the procedure infeasible. In this case, we must modify the initial value of the quality of mixture at the evaporator inlet and iterate the aforementioned steps to find the satisfying value of vapor quality.

The next criterion which must be investigated is the equivalent temperature of the evaporator. If the value of enthalpy and entropy variations ratio between the resultant states D and A is lower than the optimal equivalent temperature, we must increase the last value of vapor quality at the state D. By contrast, if the value is higher than $\tilde{T}_{AD}$, a decrease in the evaporation temperature results in the modification of state D and A. The feasibility of temperature distribution along condenser constitutes the last step of the reconstruction procedure.

In the real application, compressor isentropic efficiency depends on pressure ratio (Yari and Mahmoudi 2011).

$$\eta_{is,comp} = 0.9343 - 0.04478 * (P_{cond}/P_{evap}) \tag{3-39}$$

Since the optimization procedure cannot provide any information about the pressure ratio of the compressor, we need to apply an iterative procedure to find the appropriate compressor isentropic efficiency. First, we assume that the compressor works isentropically, and perform the optimization and reconstruction procedures to obtain the pressure ratio. Then, using Eq. *(3-39)*, the compressor isentropic efficiency corresponding to the obtained pressure ratio will be calculated. The iterative procedure continues decreasing the assumed isentropic efficiency by the amount of 1% to the value which the assumed efficiency and the calculated one become the same. The algorithm proposed for determination of all thermodynamic states of the refrigerant in the cycle is illustrated in Appendix. Once all the thermodynamic states of the refrigerant are determined, the mass flow rate and the compressor work can be deduced by Eqs. *(3-7)* and *(3-12)*, respectively. The algorithm is repeated for each candidate refrigerant pre-selected in the first step of the comprehensive approach. In the final step of the approach, a comparison of the noteworthy design criteria permits the most appropriate refrigerant to be chosen.

It must be pointed out that the reconstruction procedure of our comprehensive approach not only allows the operating conditions such as condenser and evaporator pressures, and refrigerant mass flow rate to be determined, but also the degrees of superheating and sub-cooling in the condenser, as well as the degree of superheating in the evaporator, are automatically calculated.

The purpose of the theoretical optimization is to find the equivalent temperatures of the condenser and evaporator that minimize the overall thermal conductance. Therefore, the optimal equivalent temperatures obtained by the optimization problem will be the same for all candidates. However, individual thermo-physical properties of each candidate will result in different system characteristics, such as thermal conductance and compressor work. Thus, the comparison of these characteristics indicates the optimal working fluid, i.e. third step of the comprehensive approach.

3-7 Practical case study

The application of the optimization and reconstruction procedures described previously is illustrated in the following example presented by Xu and Chen (Xu and Chen 2013). The inlet hot- and cold-reservoir temperatures $\left(T_{H,in}\,, T_{L,in}\right)$ are fixed to 305 and 293 K, respectively, while the mass flow rate of the hot-side secondary fluid, $\dot{m}_H$, is set to 0.5 kg/s. The heat capacity of secondary fluids are considered to be the same and are equal to 1 kJ/(kg.K). The required cooling rate is 1000 W. The proposed comprehensive approach for the case study will be explained in the following subsections:

3-7-1 Theoretical optimization

The constrained nonlinear optimization problem, i.e. the first step of the comprehensive approach, was performed in MATLAB by using fmincon function to implement Sequential Quadratic Programming (SQP) (Luo *et al.* 2017). As it was mentioned above, in the context of theoretical optimization models, researchers defined the generic source of internal irreversibility by a dimensionless numerical coefficient called internal irreversibility parameter (Salah El-Din 2001a):

$$I = \frac{\left(\dot{Q}_{cond} \Big/ \tilde{T}_{BC}\right)}{\left(\dot{Q}_{evap} \Big/ \tilde{T}_{AD}\right)} \tag{3-40}$$

The main disadvantage of the existing theoretical optimization models is that the internal irreversibility parameter has been chosen arbitrarily and independent of operating conditions. Thus, it can prevent precise determination of the optimal design variables. The theoretical

optimization method presented herein overcomes the previous model's shortcoming by using Eq. *(3-36)*. For instance, the optimal results corresponding to the minimum overall thermal conductance of the system operated between the sources given above and for the isentropic efficiency of 1 and 0.8 are illustrated in Table 3-1.

Table 3-1: Results obtained from the optimization procedure

	$(\boldsymbol{UA})_{\boldsymbol{evap}}$(W/K)	$(\boldsymbol{UA})_{\boldsymbol{cond}}$(W/K)	$\widetilde{\boldsymbol{T}}_{\boldsymbol{BC}}$ (K)	$\widetilde{\boldsymbol{T}}_{\boldsymbol{AD}}$ (K)	$\dot{\boldsymbol{W}}_{\boldsymbol{comp}}$(W)	$\boldsymbol{I}$
$\eta_{is,comp} = 1$	83.5	87.8	319.20	280.00	143.6	1.003
$\eta_{is,comp} = 0.8$	83.5	93.2	318.83	280.00	175.8	1.03

Since the cooling rate is considered constant for all compressor isentropic efficiency, the parameters related to the evaporator in Table 3-1 remain fixed in the theoretical optimization, independent of compressor isentropic efficiency. It must be noted that the entropy generation in the throttling valve always causes the internal irreversibility parameter to be greater than unity, even if there is no entropy generation in the compressor ($\eta_{is,comp} = 1$), which means that the assumption of endoreversible cycle where the working fluid is expanded through the throttling valve is far from reality. The isentropic efficiency of 0.8 has been chosen arbitrarily to show the effect of compressor irreversibility on the optimum equivalent temperatures as well as internal irreversibility parameter (*I*). The performance parameters and the entropy generation rates for the refrigeration cycle operating between two reservoirs are given in Table 3-2.

Table 3-2: The performance parameters and entropy generation rates

	$\boldsymbol{COP}_{\boldsymbol{Carnot}}$	$\boldsymbol{COP}$	$\boldsymbol{\eta}_{\mathbf{II}}$ (%)	$\dot{\boldsymbol{S}}_{\boldsymbol{gen,comp}}$ (W/K)	$\dot{\boldsymbol{S}}_{\boldsymbol{gen,exp}}$ (W/K)	$\dot{\boldsymbol{S}}_{\boldsymbol{gen,tot}}$ (W/K)
$\eta_{is,comp} = 1$	20.6	6.9	33.6	0	0.01	0.31
$\eta_{is,comp} = 0.8$	20.6	5.7	27.6	0.13	0.01	0.42

A comparison between Table 3-1 and Table 3-2 reveals that, for the fixed cooling rate generation, the total entropy generation directly affects the performance and the thermal conductance of the system. An increase in entropy generation causes the compressor to consume more energy. Subsequently, the condenser needs higher thermal conductance to provide more energy (cooling rate and evaporator thermal conductance are fixed). Thus, the system with lower thermal conductance has better performance (Bejan, Vargas and Sokolov 1995; Luo *et al.* 2002; Chen, Sun and Wu 2004).

3-7-2 Reconstruction procedure

The theoretical optimization results were presented in terms of equivalent temperatures. To correlate the results with the essential thermodynamic characteristics of the system such as working pressures, temperatures, and mass flow rate for each refrigerant, reconstruction procedure must be performed. For the reconstruction procedure, the thermodynamic properties of refrigerant were taken from the CoolProp Library (Bell *et al.* 2014). Xu and Chen (Xu and Chen 2013) applied entransy theory to minimize the overall thermal conductance of the system for the isentropic compressor and R22 as the working fluid for the case study. To validate our proposed approach, the results obtained by the present approach are compared to those obtained by entransy theory in Table 3-3.

Table 3-3: The comparison between the optimal results of the present approach and Entransy theory presented in (Xu and Chen 2013).

	$(\boldsymbol{UA})_{evap}$(W/K)	$(\boldsymbol{UA})_{cond}$(W/K)	$(\boldsymbol{UA})_{tot}$(W/K)	$\boldsymbol{T}_{cond}$ (K)	$\boldsymbol{T}_{evap}$ (K)
Present approach	83.1	92.0	175.1	318.3	279.9
Entransy theory	86.8	91.7	178.5	321.4	280.1

T_{cond} and T_{evap} denote condensing and evaporating temperatures, respectively. Table 3-3 indicates that for the same fixed temperatures of the external fluids entering the condenser and the evaporator, the present approach results in 4.2% and 1.9% reduction in the evaporator and total thermal conductance, respectively, compared to entransy theory. However, the new approach causes the condenser thermal conductance increases 0.3%.

3-7-3 Working fluid selection

R 22 has ozone depletion potential (ODP) higher than zero, thus regarding the environmental regulation, it has to be replaced by an environmentally-friendly refrigerant. The aim of this step is to select the most appropriate working fluid for the presented case study. It should be mentioned that in order to show the application of the proposed comprehensive approach, a real vapor-compression refrigeration system with non-isentropic compression process will be investigated in which the compressor isentropic efficiency varies with pressure ratio Eq. *(3-39)*.

Table 3-1 shows that the equivalent temperature of the evaporator for different compressor isentropic efficiencies is fixed. Thus, we can now establish criteria for the pre-selection of potential refrigerants. The candidates must have atmospheric pressure boiling point temperatures lower than the evaporator equivalent temperature in order to avoid a vacuum pressure in the evaporator. Environmental, as well as thermodynamic criteria (Table 3-4), are considered as decisive factors to choose the candidate refrigerants. Six potential candidates have been pre-selected in this study for given source conditions: R152a, R134a, R290, Propylene (R1270), R600a and R1234ze (E). According to the international agreements, all candidates must have ozone depletion potential (ODP) of zero and global warming potential (GWP) lower than 2500 (Eldakamawy, Sorin and Brouillette 2017). Although all candidates are considered as non-toxic refrigerants, R134a has the safest operation conditions (toxicity and flammability). On the other hand, it presents relatively high GWPs, posing a potential limitation with respect to F-gas regulations. R290, Propylene, and R600a present the low ODP and GWP, however, they are relatively flammable fluids.

Table 3-4: Critical temperature and Environmental parameters of pre-selected refrigerants (*ASHRAE Handbook-Fundamentals* 2017)

Refrigerant	$T_{critical}$ (K)	$T_{boil}@1^{atm}$ (K)	ODP	GWP_{100}	Safety[1]	t_{lif} $(year)$
R22	369.3	232.3	0.034	1760	A1	11.9
R152a	386.4	249.1	0	138	A2	1.5
R134a	374.2	247.0	0	1300	A1	13.4
R290	369.9	231	0	5	A3	0.034
Propylene	364.2	225.3	0	1.8	A3	0.001
R600a	407.8	261.5	0	20	A3	0.016
R1234ze(E)	382.5	253.9	0	<1	A2L	0.045

The proposed optimization and reconstruction procedures, i.e. the first and second steps of the comprehensive approach, are performed to determine the operating conditions of each pre-selected refrigerants based on the optimal equivalent temperatures of the condenser and evaporator. As was described in the previous section, the arbitrary values for performing the reconstruction procedure are the values of temperature differences at the outlet of the evaporator and condenser. In this case study, they are assumed to be 8°C and 2°C, at the evaporator and condenser, respectively. The reconstruction procedure introduced herein is an iterative approach without any empirical coefficient. Thus, the small iteration step in reconstruction procedure (0.01) guarantees that the procedure can be applied to all refrigerants. In addition to safety and environmental constraints, the operational variable also plays a significant role in the selection of the refrigerant. Table 3-5and Table 3-6 show the optimization results for two isentropic efficiencies and essential operating conditions obtained by the reconstruction procedures for each pre-selected refrigerant, respectively. In Table 3-6, x_D indicates the vapor

[1] A: no toxicity, 1: no flame propagation, 2-2L: low flammability, 3: high flammability

quality at the inlet of the evaporator, Δh_{evap}, $\Delta T_{sh,cond}$ and $\Delta T_{sc,cond}$ represent latent heat at evaporation temperature, the degrees of superheating and subcooling along condenser, respectively. $\Delta T_{sh,evap}$ is the degree of superheating prior to the compressor entrance. Table 3-6 shows the compressor isentropic efficiency corresponding to the pressure ratio of each candidate refrigerant. The refrigerants experience evaporation and superheating processes along the evaporator. Thus, the superheating degree determines the difference between evaporation saturation and equivalent temperatures. On the other hand, the value of $T_A - \tilde{T}_{AD}$ is fixed and is not large enough (= 5°C) to cause superheating degree presenting a significant difference between saturation and equivalent temperatures. Hence, the saturation temperature and equivalent temperature at the evaporator will be roughly equal for all cases. Moreover, since the refrigerant must provide a certain amount of cooling rate at the evaporator, the mass flow rate of refrigerant depends mainly upon its latent heat at evaporation temperature and decreases with increasing Δh_{evap}.

Table 3-5: optimization results for compressor isentropic efficiencies of 79% and 81%

	$(\boldsymbol{UA})_{\boldsymbol{tot}}$(W/K)	$\widetilde{\boldsymbol{T}}_{\boldsymbol{BC}}$ (K)	$\widetilde{\boldsymbol{T}}_{\boldsymbol{AD}}$ (K)	$\dot{\boldsymbol{W}}_{\boldsymbol{comp}}$(W)	$\dot{\boldsymbol{S}}_{\boldsymbol{gen,comp}}$ (W/K)	$\dot{\boldsymbol{S}}_{\boldsymbol{gen,exp}}$ (W/K)
$\eta_{is,comp} = 0.79$	177.5	319.80	280.00	182.6	0.13	0.016
$\eta_{is,comp} = 0.81$	175.5	319.00	280.00	175	0.11	0.011

Table 3-6: Operating conditions for different refrigerants

Refrigerant	R22	R152a	R134a	R290	Propylene	R600a	R1234ze (E)
$\dot{m}_{ref}$ (g/s)	5.9	3.9	6.3	3.3	3.3	3.5	6.8
P_{cond} (kPa)	1708.9	1032.6	1179.9	1536.4	185.6	622.6	902.1
P_{evap} (kPa)	617.7	334.8	371.9	580.5	711.6	198.3	276.0
$\eta_{is,comp}$ (%)	81	79	79	81	82	79	78
Δh_{evap}(kJ/kg)	199.4	300.0	193.3	365.1	366.9	347.8	179.8
$\Delta T_{sh,cond}$(℃)	28.0	23.6	14.6	13.6	18.2	6.2	6.7
$\Delta T_{sc,cond}$(℃)	10.3	9.6	11.5	11.8	10.5	11.9	11.8
$\Delta T_{sh,evap}$(℃)	5.0	5.0	5.0	5.0	5.0	5.0	5.0
x_D (−)	0.17	0.17	0.20	0.20	0.20	0.19	0.21
$\dot{W}_{comp}$(Watt)	189.0	191.3	199.8	194.5	195.8	194.0	199.5
COP (−)	5.29	5.23	5.00	5.14	5.11	5.15	5.01

Although the equivalent temperatures in the evaporator and the condenser are identical for all refrigerants, the individual thermophysical properties of different working fluids lead to having completely different system performance and thermodynamic states for each refrigerant. The comparison between capital and operational costs for potential working fluids indicates the most appropriate refrigerant.

The compressor work (or COP) varies according to the rate of internal entropy creations by the refrigerant. The rate of entropy generation in compression and expansion processes calculated by the reconstruction procedure are shown in Table 3-7. The summation of entropy generation values at the compressor and the expansion valve determines the deviation of consumed work from the optimal value for each refrigerant. For instance, the summation of entropy generation

rates in compression and expansion processes is the lowest value for R152a among the alternatives to R22, thus the system operated by R152a needs the lowest compression work (the highest COP), followed by R600a. It is worth noting that as was mentioned in section 3-4-3, the superheating process causes the optimization method, where the equivalent temperature is used instead of actual temperature, to overestimate the entropy creation rate in the compression process calculated by Eq.*(3-16)*. In this regard, when the degree of superheating increases (Table 3-6), the difference between optimization result (Table 3-5) and reconstruction result (Table 3-7) increases.

Table 3-7: Entropy generation during compression and expansion processes obtained by reconstruction procedure

Refrigerant	R22	R152a	R134a	R290	Propylene	R600a	R1234ze (E)
$\left(\dot{S}_{gen,comp}\right)_{recons}$ (W/K)	0.10	0.11	0.13	0.11	0.11	0.13	0.13
$\left(\dot{S}_{gen,exp}\right)_{recons}$ (W/K)	0.05	0.05	0.06	0.06	0.07	0.05	0.06
$\left(\dot{S}_{gen,internal}\right)_{recons}$(W/K)	0.15	0.16	0.18	0.17	0.18	0.18	0.18

A parameter that affects the capital costs is the heat exchanger size, which is normally evaluated by the total thermal conductance of heat exchangers. The thermal conductance analysis proceeds by separating the condenser into three distinct sections, i.e. liquid section (f), two-phase (fg), and superheated (g). The heat transfer rate and thermal conductance for each section of the condenser for the seven refrigerants are given in Table 3-8. Two factors play a considerable role in the calculation of the condenser thermal conductance shown in Table 3-8. The heat transfer rate in the two-phase region, which can be directly affected by the mass flow rate and the latent heat at condensation, which has the major effect on the value of the thermal conductance. Another important factor is the superheating and subcooling degrees in the condenser, which exert a significant influence on the differences of ΔT_{LMTD} for each case study. Table 3-8 indicates that a cycle with R600a needs the smallest heat exchanger conductance for the condenser and its quantity is around 4 % lower than R22.

Table 3-8: Heat interaction and thermal conductance distribution of condenser

Refrigerant		R22	R152a	R134a	R290	Propylene	R600a	R1234ze (E)
$\dot{Q}_f$	(W)	81.2	70.9	108.4	109.4	95.9	102.8	115.5
$\dot{Q}_{fg}$	(W)	951.6	992.8	983.5	980.2	952.7	1036.3	1019.3
$\dot{Q}_g$	(W)	156.3	127.6	104.0	104.6	146.1	55.6	64.6
UA_f	(W/K)	13.4	9.8	16.8	17.4	14.3	15.8	17.6
UA_{fg}	(W/K)	82.7	83.2	78.2	77.4	78.3	80.4	78.6
UA_g	(W/K)	7.2	6.3	5.8	6.0	7.2	2.9	4.0
$\sum UA$	(W/K)	103.3	99.3	100.8	100.8	99.8	99.1	100.2

It is important to mention that due to the identical degree of superheating and saturation temperature at the evaporator for all candidates, the related thermal conductance variations are insignificant, and their average value is about 83.8 (W/K) which is 0.3% higher than the optimization result, i.e. Table 3-1. It must be noted that the overall UA obtained by optimization procedure (Table 3-5) is the minimum value that a system needs to provide the required heat transfer for the system due to the assumption of equivalent temperature (constant value) instead of temperature-varying processes occurring in the condenser and evaporator.

According to Table 3-6, R152a results in lower operational cost, while Table 3-8 illustrates that R600a needs the smallest overall heat exchanger conductance and, therefore, lower capital cost (thermal conductance of evaporator is constant for the refrigerants under consideration). Based on these observations, it is impossible to select the optimal refrigerants among the candidates. Dahmani et al. (Dahmani, Aidoun and Galanis 2011) introduced an economic indicator of the ejector refrigeration system in which both capital and operational costs have been taken into account and it can facilitate the comparison between refrigerants.

$$F = (UA)_{tot}\left(T_{H,in} - T_{L,in}\right)/\left(\dot{Q}_{cond}/COP\right) \tag{3-41}$$

$T_{H,in}$, $T_{L,in}$and $\dot{Q}_{cond}$ are fixed and F is a dimensionless factor and proportional to the overall thermal conductance and $\dot{W}_{comp}$. In the following, this economic indicator will be employed for different degrees of freedom of the reconstruction procedure to ascertain the optimal refrigerant and design. It should be noted that since the small value of UA for low capital cost and a high value of COP for low energy consumption (in the case of fixed cooling load) are desirable, the optimal system design has the smallest value of F.

As it was stated in section 3-6, the proposed reconstruction procedure has two degrees of freedom, i.e. temperature differences at the condenser and evaporator outlets. The effects of temperature difference at the condenser outlet on the thermal conductance of the condenser and the compressor work have been studied and the results are presented in Figure 3-3 and Figure 3-4, respectively. Figure 3-3 shows that, for all refrigerants, 8°C is the optimal temperature difference at the condenser outlet in the case of thermal conductance. Moreover, the system operating with R600a needs the smallest heat exchanger conductance for conductance and, therefore, the overall system. In Figure 3-4, regarding the reconstruction procedure, an increase of temperature difference causes a slight increase in the quality of vapor at the evaporator inlet and mass flow rate for the constant cooling rate; subsequently, the compressor work increases. Furthermore, Figure 3-4 shows that R152a among alternatives to R22 needs the lowest value of work to provide the desired cooling rate (the highest COP), however, it consumes 1.2 % more energy compared to R22.

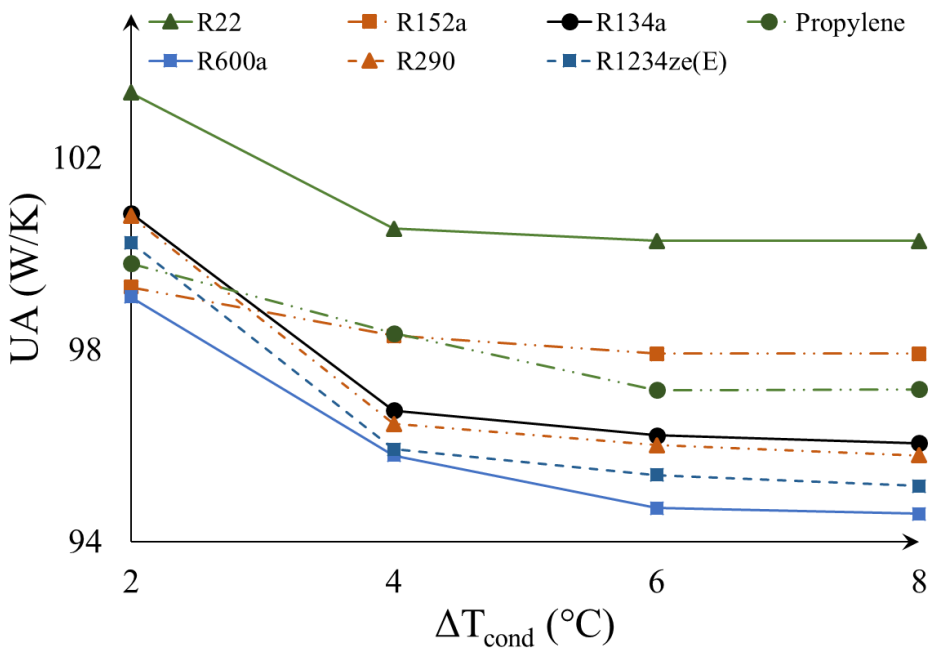

Figure 3-3: Effect of temperature difference at the condenser outlet on the thermal conductance of condenser (for $\Delta T_{evap} = 8°C$)

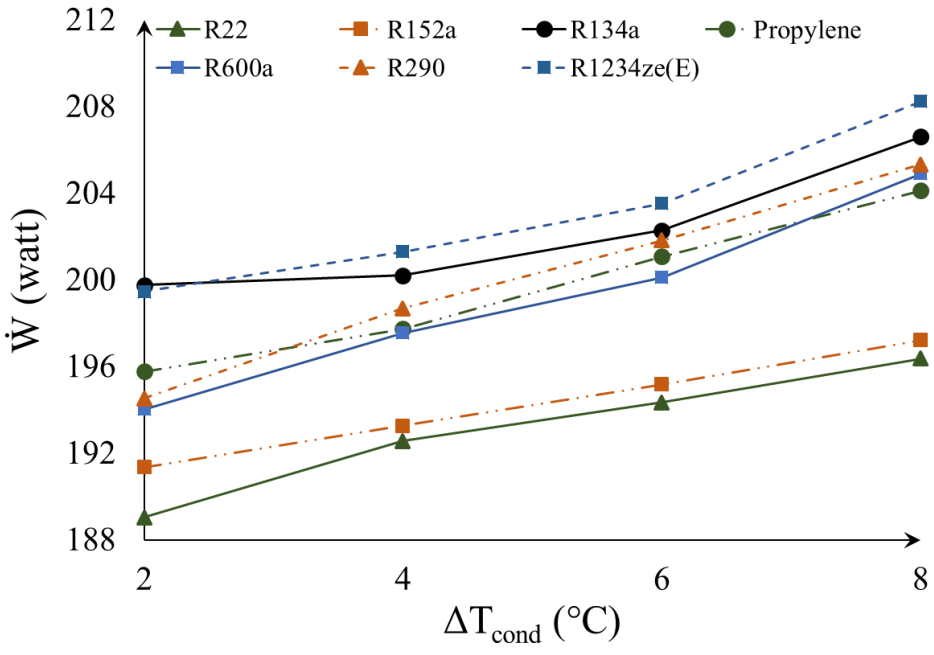

Figure 3-4: Effect of temperature difference at the condenser outlet on the work consumed by the compressor (for $\Delta T_{evap} = 8°C$)

The different optimal working fluids and temperature differences from the capital and operational costs of views necessitate employing the economic indicator to determine the

optimal ones. Figure 3-5 illustrates that $\Delta T_{cond} = 4℃$ is the optimal temperature difference at the outlet of the condenser for R600a, R1234ze (E), R134a and R290, while $\Delta T_{cond} = 2℃$ is the optimal temperature difference at the outlet of the condenser for R152a and propylene. Moreover, R152a has the smallest economic indicator.

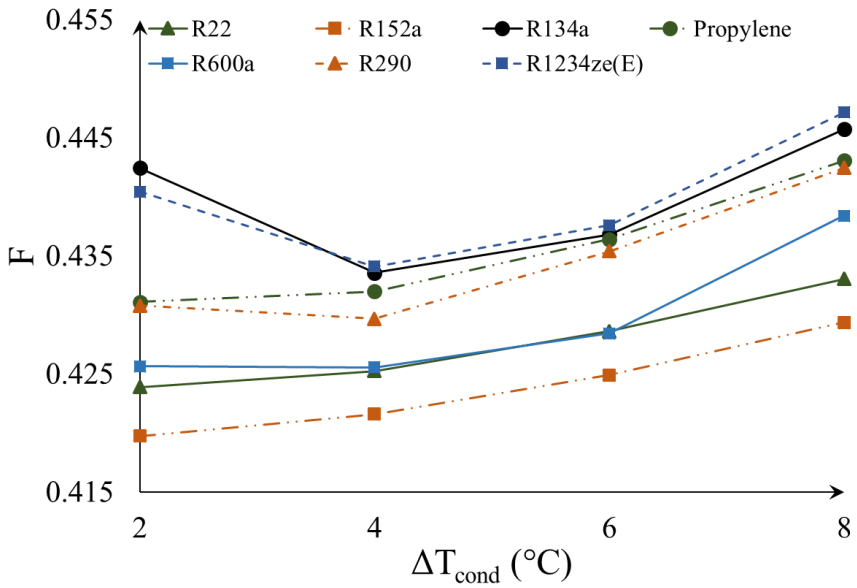

Figure 3-5: Economic indicator for different temperature differences at the condenser outlet (for $\Delta T_{evap} = 8℃$)

The other degree of freedom in the reconstruction procedure is the temperature difference at the evaporator outlet. Since this value affects all the operating parameters of the system obtained by the reconstruction procedure, the thermal conductance of the condenser and the amount of work needed by the compressor as two decisive factors in the selection of the optimal working fluid are investigated for different temperature differences at the evaporator outlet and optimal temperature difference at the condenser in Figure 3-6 and Figure 3-7.

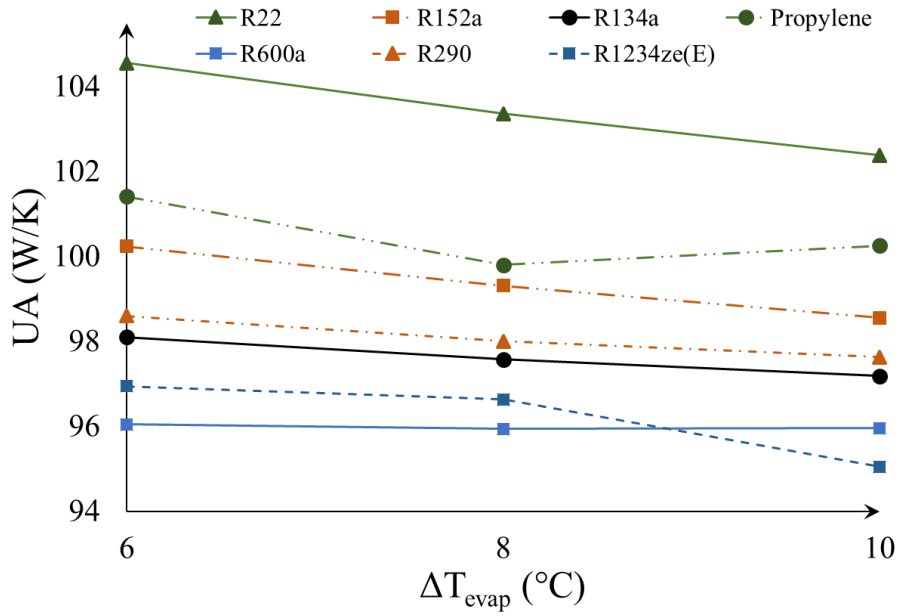

Figure 3-6: Effect of temperature difference at the evaporator outlet on the thermal conductance of condenser for the optimal ΔT_{cond}

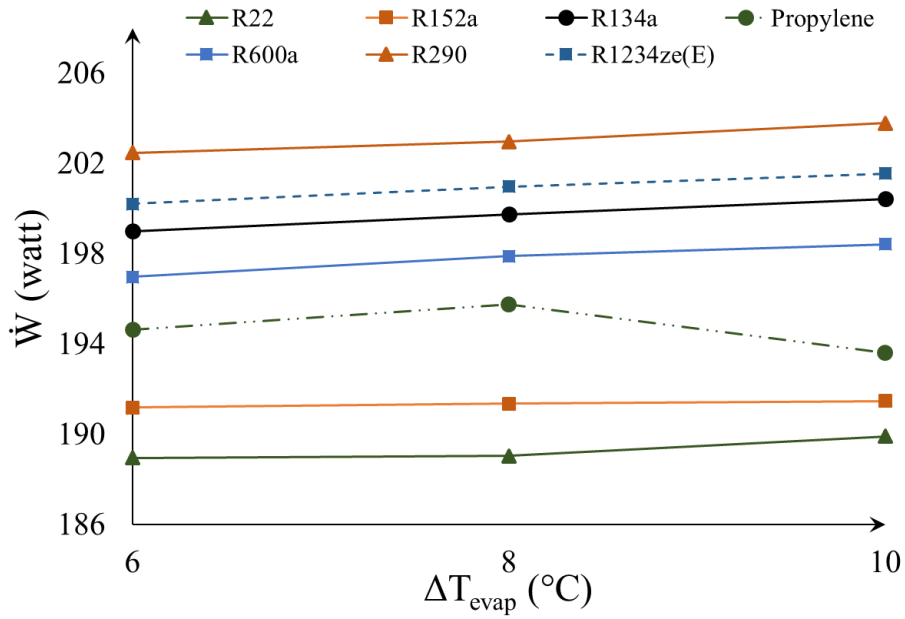

Figure 3-7: Effect of temperature difference at the evaporator outlet on the work consumed by the compressor for the optimal ΔT_{cond}

Figure 3-6 illustrates that the thermal conductance of the condenser slightly decreases with increasing the temperature difference at the evaporator, except for propylene where $\Delta T_{evap} =$ 8℃ is the optimal temperature difference. R1234ze (E) needs the lowest value of the thermal

conductance of the condenser at $\Delta T_{evap} = 10℃$ and, thus, the overall system. It should be noted that for the evaporation temperature (280K) and constant external fluid temperature (293K), $\Delta T = 10℃$ results in 3 degrees of superheating at the compressor inlet. According to Figure 3-7, from the operational cost point of view, R152a shows the best COP (lowest $\dot{W}_{comp}$) among pre-selected refrigerants.

Thus, the systems operating with R1234ze (E) and R152a have the lowest capital and operating costs, respectively. Owing to this conflict of interest and to facilitate the optimum selection, the economic indicator has been taken into account in Figure 3-8.

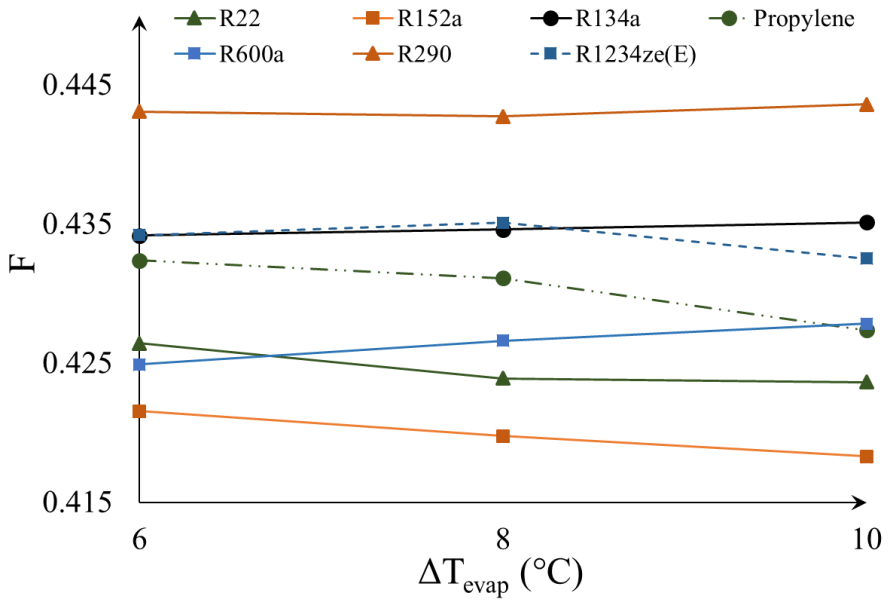

Figure 3-8: Economic indicator for different temperature differences at the evaporator outlet for the optimal ΔT_{cond}

Figure 3-8 reveals that R152a has the smallest economic indicator (even smaller than R22) and, thus, is the most appropriate refrigerant as an alternative to R22 for the case study presented herein.

3-8 Conclusions

In this paper, a novel systematic approach for the selection of the optimal working fluid for the vapor-compression refrigeration cycle according to the conditions of external reservoirs is presented. First, we define the minimal overall thermal conductance via the theoretical

optimization, independently of working fluids. Applying the concept of equivalent temperature and accounting for its graphical interpretation on the traditional h-s diagram lead to the derivation of new thermodynamic relations for the calculations of entropy generation in the cycle components, without recourse to the knowledge of working fluids. These relations establish a link between the operating parameters of the system and entropy generation in compressor and throttling valve, allow constraining the optimization problem (Eq. *(3-36)*). The optimization step overcame the previous methods' shortcoming to estimate the internal irreversibility parameter by using the second law-based analysis. Furthermore, the optimal evaporator equivalent temperature plays a key role in the pre-selection of the potential refrigerants and provides thermodynamic criteria to pre-select the candidate refrigerants among the very large number of working fluids.

The second step in the proposed approach is the reconstruction procedure to determine the essential operating states of each pre-selected refrigerants. The case study presented effectively demonstrated the proposed approach. Compared to entransy theory, the presented approach results in a 1.9% reduction in the overall thermal conductance of the system.

Finally, the approach was applied to find an environmental-friendly refrigerant as the best alternative to R22 in the presented case study. The approach indicated that the system operating with R600a needs the smallest thermal conductance while the system operating with R152a consumes the lowest amount of compressor work. Thus, a dimensionless economic indicator in which both capital and operating cost have been taken into account was employed to indicate the most appropriate refrigerant among pre-selected working fluids. The results showed that R152a compared to R22 not only has better environmental characteristics but also leads to having a system with a better economic indicator.

3-9 Acknowledgments

This project is a part of the Collaborative Research and Development (CRD) Grants Program at "Université de Sherbrooke". The authors acknowledge the support of the Natural Sciences and Engineering Research Council of Canada, Hydro-Québec, Rio Tinto, Alcan and Canmet ENERGY Research Center of Natural Resources Canada (RDCPJ451917-13).

3-10 Appendix

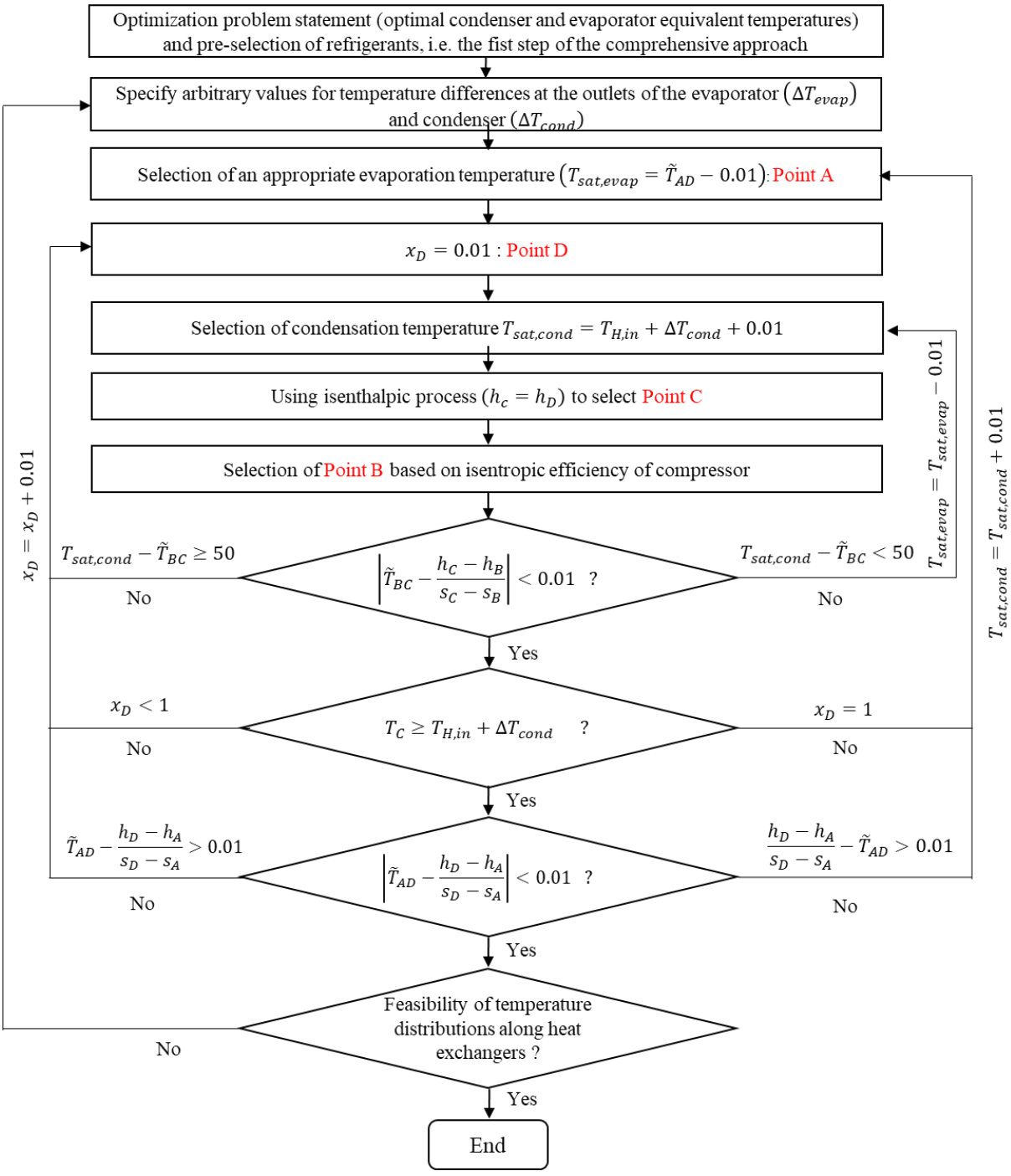

Figure 3-9: Proposed algorithm for reconstruction procedure

3-11 Nomenclature

COP	coefficient of performance
ds	entropy difference (kJ/kg.K)
dh	enthalpy difference (kJ/kg)
dp	pressure difference(kPa)
F	economic indicator (-)
P	pressure (kPa)
$\dot{Q}$	thermal power (W)
$\dot{S}_{gen}$	entropy generation rate (W/K)
T	temperature (°C or K)
$\tilde{T}$	equivalent temperature (K)
UA	product of the overall heat transfer coefficient and heat transfer surface area (W/K)
$\dot{W}$	power (Watts)
c_p	heat capacity at constant pressure (kJ/kg-K)
h	enthalpy (kJ/kg)
$\dot{m}$	mass flow rate (kg/s)
s	entropy (kJ/kg.K)
x	quality (-)

Subscripts

AD	refrigerant side in the evaporator
BC	refrigerant side in the condenser
H	high temperature
L	low temperature
LMTD	logarithmic mean temperature difference
c	critical
comp	compressor
cond	condenser
evap	evaporator
exp	expansion
f	saturated liquid
g	saturated vapor
is	isentropic
in	inlet
out	outlet

recons	reconstruction
ref	refrigerant
sat	saturation
sc	subcooling
sh	superheating
tot	total

Greek letters

Δ	difference
v	specific volume (m^3/kg)
η	efficiency

Chapter 4

Thermal design and selection of the optimal working fluid for organic Rankine cycles based on the equivalent temperature concept

Avant-propos

Auteurs et affiliation :

Hossein Akbari: étudiant au doctorat, faculté de génie, département de génie mécanique, Université de Sherbrooke.

Mikhail Sorin: professeur, faculté de génie, département de génie mécanique, Université de Sherbrooke.

Date d'acceptation: 28 décembre 2019

État de l'acceptation: version finale publiée

Revue: Applied Thermal Engineering

Titre français: Conception thermique et sélection du fluide de travail optimal pour les cycles organiques de Rankine sur la base du concept de température équivalente

Contribution au document: Cet article contribue à la thèse par une application de l'approche proposée pour les cycles organiques de Rankine.

Résumé français:

Une nouvelle approche, basée uniquement sur les conditions d'entrée des sources d'énergie externes, est proposée pour sélectionner l'ensemble des fluides de travail optimaux ainsi que les

paramètres de fonctionnement des Cycles de Rankine Organiques (ORC). L'approche se compose de deux étapes séquentielles. La première étape, formulée comme un problème d'optimisation, minimise la conductance thermique totale du système sans recourir aux propriétés du fluide de travail. Ici, une analyse de la seconde loi basée sur le concept de température équivalente contraint le problème d'optimisation non linéaire, où une caractéristique géométrique spécifique de température équivalente sur le diagramme h-s établit un lien entre les conditions de fonctionnement et la génération d'entropie dans chaque composant du système. La deuxième étape de l'approche, c'est-à-dire la procédure de reconstruction, met en corrélation les résultats d'optimisation, qui sont en termes de températures équivalentes, avec les caractéristiques thermodynamiques essentielles du cycle. La procédure de reconstruction ouvre également la voie à la sélection du fluide de travail le plus approprié parmi les candidats sur la base d'un critère de coût en capital. Pour illustrer l'application et les avantages de notre approche, deux études de cas sont présentées.

4-1 Abstract

A new approach, based solely on the inlet conditions of external energy sources, is proposed for selecting the set of optimal working fluids as well as operating parameters of Organic Rankine Cycles (ORC). The approach is composed of two sequential steps. The first step, formulated as an optimization problem, minimizes the total thermal conductance of the system without recourse to the working fluid properties. Here, a second-law analysis based on the equivalent temperature concept constrains the nonlinear optimization problem, where a specific geometrical feature of equivalent temperature on the *h-s* diagram establishes a link between operating conditions and entropy generation in each component of the system. The second step of the approach, i.e. reconstruction procedure, correlates the optimization results, which are in terms of equivalent temperatures, with the essential thermodynamic characteristics of the cycle. The reconstruction procedure also paves the way for the selection of the most appropriate working fluid among the candidates based on a capital cost criterion. To illustrate the application and the advantages of our approach, two case studies are presented.

Keywords: Organic Rankine Cycle, Working fluid, Second-law analysis, Equivalent temperature

4-2 Introduction

Nowadays, due to limited fossil fuel energy sources and environmental impact of rising energy consumption, the Organic Rankine Cycle (ORC) is considered as one of the most promising technologies for the recovery of low-grade waste heat (Badescu *et al.* 2019; Bianchi *et al.* 2019). The efficiency of the cycle depends heavily on the selection of the working fluid and operating conditions, which must be considered together to design an efficient system. The choice of the working fluid is a complex problem, because it implies the selection of the appropriate working fluid among a large number of candidates as well as the sets of possible operating conditions for each candidate. To address this issue, two different design approaches have been investigated in the literature: synergy or one-step active design methods and two-step classical design methods. In the synergy methods, both operating conditions and working fluid properties are considered at the same time, and the optimal design parameters and the fluid are determined. Thermodynamic cycle separating method (Wang *et al.* 2018), optimal heat source temperature method (Liu *et al.* 2015), and group contribution model (Su, Zhao and Deng 2017; White *et al.* 2018) are examples of the one-step active design model. In the two-step classical design methods, it was proposed (Bejan 1988; Qureshi 2015; Akbari, Sorin and Marcos 2018) to separate the design problem into two sequential steps: first, the definition of optimum operating conditions, based on the external source and sink conditions, and independent of the nature of the working fluids; second, the selection of the most appropriate working fluid, while respecting the optimal operating conditions. This paper addresses issues associated with the two-step classical design method.

The first step of the comprehensive approaches, i.e. the theoretical model (Akbari, Sorin and Marcos 2018), is always independent of the working fluid and its main objective is to define the optimal conceptual design of the system via constrained optimization methods, subject to the source and sink conditions. The most challenging issue in these optimization problems is to identify the sources of irreversibility. Irreversibility in a power cycle consists of external irreversibility associated with heat transfer across a finite temperature difference and internal

irreversibility related to the thermodynamic dissipation of the working fluid in pumping and expansion processes (Horlock 2003; Sarkar and Bhattacharyya 2007). Bejan (Bejan 1988) and Salah El-Din (Salah El-Din 2001b) took heat transfer irreversibility into account and employed finite-time and finite-size constraints to optimize the thermodynamic design of the power cycles. Qureshi (Qureshi 2015) and Ahmadi et al. (Ahmadi *et al.* 2014) characterized the generic source of internal irreversibility by a dimensionless numerical coefficient, the irreversibility parameter, using the Clausius inequality. The irreversibility parameter is generally a function of operating conditions. However, in many papers, the irreversibility parameter has been assumed to have an arbitrary constant value, in order to mathematically simplify the equations. Despite providing an average effect, assuming an arbitrary constant value for the irreversibility parameter can prevent precise determination of the design variables; there is no guarantee that the assumed value is compatible with the proposed operating conditions, and this simplification can lead to erroneous results (Akbari, Sorin and Marcos 2018).

Having obtained the optimal temperatures by using the theoretical model, a logical question is how to select the proper working fluid among a huge number of potential candidates, while respecting the optimization results. In the last decade, much more attention has been drawn to the selection of working fluids, and several papers have been published to evaluate thermal and economic advantages (Braimakis and Karellas 2018; White *et al.* 2018) as well as their environmental impacts (Yi *et al.* 2018; Zhang *et al.* 2018). The thermo-physical properties of working fluids have been studied to pinpoint the proper criteria for selecting the one that is the most appropriate. Some researchers investigated and compared a considerable number of working fluids, concluding that certain indicators could be used to evaluate the influence of the working fluid on system thermal efficiency. These indicators include operating conditions, such as critical temperature (Xu and Yu 2014) or boiling temperature (Aghahosseini and Dincer 2013), and sometimes they defined dimensionless parameters (Li *et al.* 2016; Yang *et al.* 2016; Ma *et al.* 2017), which are combinations of thermo-physical properties. The literature review reveals that there is no unique variable that can be defined as a decisive criterion for the selection of the optimal working fluid. Further, the enumeration of all possible refrigerants is a

cumbersome and time-consuming step. For this reason, recently Neveu et al. (Neveu and Azoumah 2015) and then Saloux et al. (Saloux *et al.* 2018, 2019) introduced an approach based on the concept of equivalent temperature to facilitate the selection of efficient working fluids by systematically screening the alternatives (Neveu and Azoumah 2015; Saloux *et al.* 2018, 2019).

The first step of Neveu's approach (Neveu and Azoumah 2015) is to minimize the total thermal conductance of the system, where only limited information about the external sources is available, such as the inlet conditions. They stated the optimization problem in terms of equivalent temperatures of the processes and obtained the optimal equivalent temperatures, independent of working fluids. Afterwards, Saloux et al. (Saloux *et al.* 2019) simplified the governing equations by eliminating the equivalent temperatures related to the expansion and pumping processes. However, their approach has shortcoming because their obtained optimal equivalent temperatures are independent of isentropic efficiencies of the expander and pump. In other words, the entropy generation rates through the mechanical processes were neglected. Moreover, the application of Genetic algorithms does not guarantee the global optimum solution. The second step of their approach is the reconstruction procedure, in order to correlate the optimal equivalent temperatures with the essential thermodynamic characteristics of the cycle, such as working pressures and temperatures. Neveu's reconstruction procedure was applicable only to wet fluids (Akbari, Sorin and Marcos 2018). This shortcoming was addressed by Saloux's procedure (Saloux *et al.* 2018), where they imposed some technical constraints and used the *h-s* diagram to determine the cycle operating conditions. However, the feasibility of temperature distributions along the heat exchangers in their procedure was not taken into account. Further, Saloux's reconstruction procedure provided them with a systematic approach for the selection of the most appropriate working fluid among candidates.

The purpose of this paper is to present a novel approach, which addresses the shortcomings of Saloux's approach (Saloux *et al.* 2018, 2019) for both stages, i.e. optimization and reconstruction procedure. The equivalent temperature concept and some thermodynamic considerations of *h-s* diagram are used to establish links between entropy generation rates through the mechanical processes and the operating conditions, in order to formulate a precise

optimization problem (the entropy generation rates will be considered as the optimization constraints). Then, the difference between the saturation temperature and corresponding optimal equivalent temperature lays the foundation for a new reconstruction procedure. This comprehensive approach consists of two sequential steps: the first step, formulated as an optimization problem, minimizes the total thermal conductance of the system without recourse to the working fluid properties. Since the optimum conditions obtained in the first step are expressed in terms of equivalent temperatures, in the second step, a reconstruction procedure is introduced to correlate the equivalent temperatures with the essential thermodynamic characteristics of the system such as working pressures, temperatures, and mass flow rate for each of the pre-selected working fluids. Then the reconstruction procedure is used to select the most appropriate working fluid based on a capital cost performance criterion. To illustrate the application and the advantages of our approach, two case studies are presented.

4-3 ORC and its thermodynamic model based on the equivalent temperature

Figure 4-1 illustrates the layout of a basic power (Rankine) cycle, which exchanges heat by two variable-temperature reservoirs, and its *T-s* diagram. The cycle is composed of two heat exchangers (i.e. evaporator and condenser), a pump, and an expander.

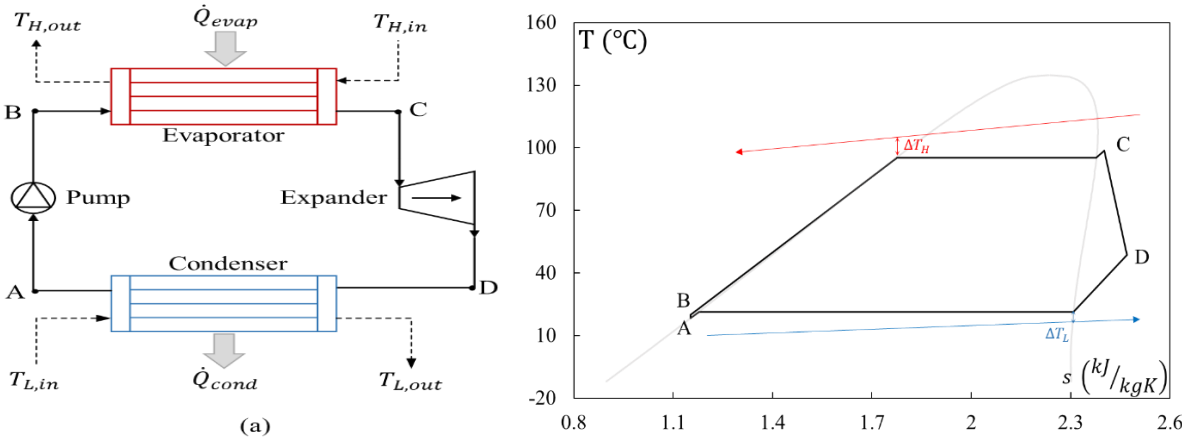

Figure 4-1: (a) Schematic of a typical basic power cycle, (b) T-s diagram of a simple ORC

According to the Gibbs relations (Çengel and Boles 2014) for a simple compressible substance between the initial and final states, we have:

$$Tds = dh - vdp \tag{4-1}$$

For the elementary components in which a heat transfer process occurs ideally, at constant pressure, the ratio of enthalpy to entropy variations between two states in Eq. (4-1) can be represented as the equivalent temperature or the exergy equivalent temperature (Saloux, Teyssedou and Sorin 2015).

$$\tilde{T} = \frac{\Delta h}{\Delta s} \tag{4-2}$$

The equivalent temperature corresponding to a constant-pressure processes can be defined as a ratio of enthalpy to entropy changes between the initial and final states of the working fluid. The actual temperatures of the fluid in a process can be replaced by a constant-value equivalent temperature. Thus, the equivalent temperature implicitly expresses the saturation temperature, subcooling and superheating degrees. This replacement helped some researchers (Neveu and Azoumah 2015; Saloux *et al.* 2018, 2019) reduce the number of parameters of their respective optimization problems. Moreover, another advantage of equivalent temperature is its interpretation on the *h-s* diagram. Since enthalpy and entropy, the principle properties of the first and second laws of thermodynamics, are the coordinates of the enthalpy-entropy diagram, this diagram is commonly used in the analysis of steady-state devices. The definition of equivalent temperature, Eq. (4-2), can be geometrically interpreted as the slope of the straight line that connects the initial and final states of the working fluid in an isobaric process in the *h-s* (Mollier) diagram (Akbari, Sorin and Marcos 2018). In the following section, this feature of the equivalent temperature definition and its interpretation on the *h-s* diagram will lay the foundation for the calculation of entropy generation rates in thermodynamic processes.

4-4 Entropy generation

The entropy generation calculation is necessary to recognize the individual component imperfections within the cycle. These calculations assist in a precise statement of the optimization problem to determine the design variables. Thus, our theoretical model preparation

begins with entropy generation calculations for the system components based on the concept of equivalent temperatures:

4-4-1 Evaporator

At the evaporator, a high-temperature reservoir heats the working fluid. Applying the first and second laws of thermodynamics in Eqs 4-3) and (4-4), and eliminating mass flow rate, the entropy production in the evaporator is shown in Eq. (4-5) (Akbari, Sorin and Marcos 2018).

$$\dot{Q}_{eva} = \dot{m}_{wf}(h_C - h_B) \tag{4-3}$$

$$\dot{m}_{wf}(s_C - s_B) = \dot{S}_{gen,eva} + \frac{\dot{Q}_{eva}}{\tilde{T}_H} \tag{4-4}$$

$$\dot{S}_{gen,eva} = \dot{Q}_{eva}\left(\frac{1}{\tilde{T}_{BC}} - \frac{1}{\tilde{T}_H}\right) \tag{4-5}$$

$\tilde{T}_H$ denotes the equivalent temperature of the thermal source and it is calculated in Eq. (4-6) (Lee 2010).

$$\tilde{T}_H = \frac{T_{H,out} - T_{H,in}}{\ln\frac{T_{H,out}}{T_{H,in}}} \tag{4-6}$$

4-4-2 Condenser

The combination of the first two laws of thermodynamics at the condenser results in:

$$\dot{S}_{gen,con} = \dot{Q}_{con}\left(\frac{1}{\tilde{T}_L} - \frac{1}{\tilde{T}_{AD}}\right) \tag{4-7}$$

$\tilde{T}_L$and $\tilde{T}_{AD}$ express the equivalent temperatures of the cold sink and condenser, respectively.

$$\tilde{T}_L = \frac{T_{L,out} - T_{L,in}}{\ln\frac{T_{L,out}}{T_{L,in}}} \tag{4-8}$$

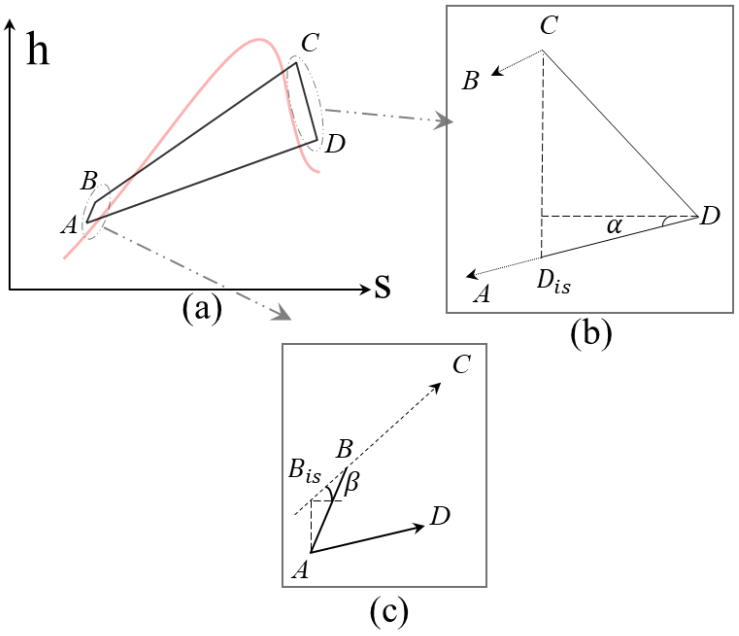

Figure 4-2: a) Mollier diagram of a basic power generation cycle, b) expansion process and c) compression process

4-4-3 Expander

The isentropic efficiency of an expander is defined as Eq. (4-9):

$$\eta_{is,exp} = \frac{h_D - h_C}{h_{D,is} - h_C} \tag{4-9}$$

$h_{D,is}$ represents the outlet enthalpy of an ideal expander. The combination of the thermodynamic laws yields:

$$\dot{S}_{gen,exp} = \dot{W}_{exp} \cdot \frac{s_D - s_C}{h_D - h_C} \tag{4-10}$$

The tangent law in Figure 4-2(b) and using Eq. (4-9) result in:

$$\frac{s_D - s_C}{h_D - h_C} = \frac{\left(\frac{1}{\eta_{is,exp}} - 1\right)}{\tan \alpha} \tag{4-11}$$

Since $\tan \alpha$ is equal to the equivalent temperature of the condenser, thus:

$$\dot{S}_{gen,exp} = \dot{W}_{exp} \cdot \frac{1}{\tilde{T}_{AD}} \cdot \left(\frac{1}{\eta_{is,exp}} - 1 \right) \quad (4\text{-}12)$$

4-4-4 Pump

The process in the pump is assumed to be a non-isentropic compression process with a constant isentropic efficiency defined as Eq. (4-13):

$$\eta_{is,pump} = \frac{h_{B,is} - h_A}{h_B - h_A} \quad (4\text{-}13)$$

$h_{B,is}$ represents the outlet enthalpy of an ideal pump. In the case of the pump, the combination of the first and the second laws of thermodynamics states:

$$\dot{S}_{gen,pump} = \dot{W}_{pump} \cdot \frac{s_B - s_A}{h_B - h_A} \quad (4\text{-}14)$$

From simple geometric considerations in Figure 4-2 (c) and Eq. (4-13), it can be demonstrated that the entropy-enthalpy ratio in the pump is equal to Eq. (4-15)

$$\frac{s_B - s_A}{h_B - h_A} = \frac{1 - \eta_{is,pump}}{\tan \beta} \quad (4\text{-}15)$$

$\tan \beta$ corresponds to the slope of the evaporator line in the *h-s* diagram and is equal to the evaporator equivalent temperature. Taken together, Eqs. (4-14) and (4-15) yield:

$$\dot{S}_{gen,pump} = \dot{W}_{pump} \cdot \frac{1}{\tilde{T}_{BC}} \cdot \left(1 - \eta_{is,pump}\right) \quad (4\text{-}16)$$

4-4-5 Closed cycle

In a closed cycle such as the ORC, the total enthalpy and entropy changes are zero. The summations of enthalpy and entropy variations in the four components are:

$$\dot{Q}_{eva} + \dot{W}_{pump} - \dot{Q}_{con} - \dot{W}_{exp} = 0 \quad (4\text{-}17)$$

$$\Delta S_{tot} = \dot{S}_{gen,exp} + \dot{S}_{gen,pump} + \dot{S}_{gen,con} + \dot{S}_{gen,eva} - \frac{\dot{Q}_{con}}{\tilde{T}_L} + \frac{\dot{Q}_{eva}}{\tilde{T}_H} = 0 \quad (4\text{-}18)$$

ΔS_{tot} expresses the total entropy variations of the working fluid. The total entropy generation includes external entropy generation associated with the heat exchanging processes in the evaporator (Eq. (4-5)) and the condenser (Eq. (4-7)); and internal entropy production related to the expansion (Eq. (4-12)) and the pumping (Eq. (4-14)) processes. Substituting Eqs. (4-5) and (4-7) into Eq. (4-18) yields the internal entropy generation rate:

$$\dot{S}_{gen,int} = \dot{S}_{gen,exp} + \dot{S}_{gen,pump} = \frac{\dot{Q}_{con}}{\tilde{T}_{AD}} - \frac{\dot{Q}_{eva}}{\tilde{T}_{BC}} \tag{4-19}$$

As mentioned above, the previous theoretical models introduced in the literature did not consider the internal entropy generation based on the operating conditions. In this work, the equivalent temperature concept and the resultant equations ((4-12), (4-16) and (4-19)) establish a link between general operating parameters of the cycle and the internal entropy production. This attribute paves the way for the optimization problem statement in the following section.

Finally, the performance of the system can be assessed by the first (thermal) and the second (exergetic) efficiencies.

$$\eta_{th} = \frac{\dot{W}_{net}}{\dot{Q}_{eva}} \tag{4-20}$$

$$\eta_{II} = \frac{\sum \dot{E}_{W_{net}}}{\sum \dot{E}_{Q_{eva}}} = \frac{\dot{W}_{net}}{Q_{eva} \cdot \left(1 - {T_r}/{\tilde{T}_H}\right)} \tag{4-21}$$

T_r denotes the reference temperature.

4-5 Optimization problem statement and its solution

This section presents the optimization of the organic Rankine cycle as the first step of our comprehensive approach for the selection of the optimal working fluid as well as operating parameters of ORC. In this study, the minimization of the total thermal conductance required for given power output is proposed as the objective function of the optimization problem. This optimization problem is equivalent to the maximization of a net power output produced when

the total thermal conductance is fixed (Neveu and Azoumah 2015). The objective function can be expressed as

$$Minimize\ (UA)_{total} = (UA)_{con} + (UA)_{eva} \quad (4\text{-}22)$$

$(UA)_{eva}$ and $(UA)_{con}$ are the thermal conductances of the evaporator and the condenser, respectively (Mills 1998; Dimian and Bildea 2008):

$$(UA)_{eva} = \frac{\dot{Q}_{eva}}{\Delta T_{LMTD_{eva}}} = \frac{\dot{m}_H c_{P,H}\left(T_{H,in} - T_{H,out}\right)}{\Delta T_{LMTD_{eva}}} \quad (4\text{-}23)$$

$$(UA)_{con} = \frac{\dot{Q}_{con}}{\Delta T_{LMTD_{con}}} = \frac{\dot{m}_L c_{P,L}\left(T_{L,out} - T_{L,in}\right)}{\Delta T_{LMTD_{con}}} \quad (4\text{-}24)$$

The logarithmic mean temperature differences (LMTDs) for evaporator and condenser are defined as (Mills 1998; Dimian and Bildea 2008):

$$\Delta T_{LMTD_{eva}} = \frac{\left(T_{H,in} - \tilde{T}_{BC}\right) - \left(T_{H,out} - \tilde{T}_{BC}\right)}{\ln \frac{\left(T_{H,in} - \tilde{T}_{BC}\right)}{\left(T_{H,out} - \tilde{T}_{BC}\right)}} \quad (4\text{-}25)$$

$$\Delta T_{LMTD_{con}} = \frac{\left(\tilde{T}_{AD} - T_{L,out}\right) - \left(\tilde{T}_{AD} - T_{L,in}\right)}{\ln \frac{\left(\tilde{T}_{AD} - T_{L,out}\right)}{\left(\tilde{T}_{AD} - T_{L,in}\right)}} \quad (4\text{-}26)$$

The optimization problem consists of solving Eqs. (4-17), and 4-22) to (4-26), while satisfying the following equality and inequality constraints.

$$\frac{\dot{Q}_{con}}{\tilde{T}_{AD}} - \frac{\dot{Q}_{eva}}{\tilde{T}_{BC}} = \dot{S}_{gen,exp} + \dot{S}_{gen,pump} \quad (4\text{-}27)$$

$$\tilde{T}_L < \tilde{T}_{AD} \quad (4\text{-}28)$$

$$\tilde{T}_{BC} < \tilde{T}_H \quad (4\text{-}29)$$

The equality constraint Eq. (4-27) refers to the entropy generated by the non-isentropic expander and pump and their link to the entropy variations of working fluid in the heat

exchanging processes. The two inequality constraints, Eqs. (4-28) and (4-29), guarantee the driving forces for heat transfer in the heat exchangers.

In fact, the first step of the approach, i.e. the optimization problem, aims to obtain the optimal equivalent temperatures and the amount of heat transferred in the heat exchangers that minimizes the total thermal conductance, while providing the desired power rate, independent of the working fluid. The initial parameters for design or known variables consist of six variables, including the inlet temperatures of external fluids ($T_{H,in}$ and $T_{L,in}$); the specific heat capacities of external fluids ($c_{P,H}$ and $c_{P,L}$); the mass flow rate of the high-temperature source ($\dot{m}_H$), and the desired output power. The optimal parameters obtained by the theoretical optimization problem establish decisive criteria for the pre-selection of the potential working fluids which can be used in the system. In section 4-6, a special reconstruction procedure is introduced to determine the real operating conditions such as pressures and temperatures of each pre-selected working fluid states by using the optimal equivalent temperatures. It should be mentioned that the optimization problem formulated by Saloux et al (Saloux *et al.* 2019) is independent of the entropy generated through the expansion and pumping processes. To apply the second law of thermodynamics as a constraint, they considered that the left hand side of Eq. (4-27) is greater than or equal to zero ($\frac{\dot{Q}_{cond}}{\tilde{T}_{AD}} - \frac{\dot{Q}_{evap}}{\tilde{T}_{BC}} \geq 0$). Since the lowest possible value of the left hand side of this inequality leads to the minimum total thermal conductance, i.e. objective function, and there is no additional relationship between the entropy generation rates through the mechanical processes and the operating parameters (the left side of Eq. (4-27)), the solver intended to consider the right hand side of this inequality equals zero. In other words, the solver obtained the optimal equivalent temperatures for a system without internal entropy generation. In this paper, the link established between entropy generation rates (Eqs. (4-12), (4-16)) and operating conditions (Eq. (4-27)) overcomes the Saloux procedure shortcomings. Thus, the adequate constraints introduced herein prepare the way for a more realistic formulation of the optimization statement.

4-6 Reconstruction procedure

The optimization problem described above was formulated independently of the working fluids. To select the most appropriate working fluid based on the optimization results (in terms of equivalent temperatures), a reconstruction procedure, as the second step of our comprehensive approach, must be performed to find out the corresponding operating conditions of each working fluid candidate.

A novel reconstruction procedure will be introduced to overcome the shortcomings of Saloux's approach (Saloux *et al.* 2018). Although they considered some environmental, safety and technical constraints through the working fluid selection, the feasibility of the temperature distribution along the heat exchangers was not guaranteed in their procedure. Moreover, the definition of an appropriate range of mass flow rate for each potential refrigerant can be complicated. In this paper, the feasibility of temperature distribution along the heat exchangers is considered as a criterion. Furthermore, the mass flow rate related to each working fluid under consideration will be automatically calculated in the new proposed reconstruction procedure.

The reconstruction procedure introduced herein is based on the differences between the saturation temperature and the value of equivalent temperature in the condenser and the evaporator (ideal constant-pressure processes). The saturation and equivalent temperatures are equal when there are no degrees of superheating and subcooling. When the working fluid experiences a superheated state, the ratio of enthalpy to entropy variations (equivalent temperature) increases. On the other hand, the subcooling state causes the equivalent temperature between two states to have a lower value than the saturation temperature related to that pressure. In other words, the deviation of equivalent temperature from saturation temperature determines the degrees of superheating (or desuperheating) and of sub-cooling in heat transfer processes.

The outline of methodology for the reconstruction procedure is presented as a flow chart in the Appendix. A complementary description of the procedure is given as follows:

1. The input data for the procedure are obtained by the first step of the comprehensive approach (optimization problem).

2. The temperature difference at the outlet of the condenser is the sole degree of freedom in the procedure.
3. To safely operate the pump in the system, some degrees of subcooling at the pump inlet is assumed.
4. To determine the pump outlet state, an iterative procedure is proposed. In the first estimation, the enthalpy of the condenser outlet is equal to the enthalpy of evaporator inlet. Using the values of equivalent temperature and heat transfer in the evaporator leads to the calculation of the enthalpy and entropy of the evaporator outlet and as a result, the evaporator pressure is determined. Then we introduce the isentropic efficiency of the pump and determine the pump outlet state. Thus, an iterative procedure calculates the working fluid states at the evaporator.
5. To ensure the feasibility of the solution, three constraints must be satisfied: first, the minimum temperature difference at the heat exchanger must be greater than 2.5 K; second, the enthalpies at the expander outlet and the condenser inlet must be identical (thermodynamic constraint of a closed cycle); finally the working fluid must be in the saturated vapor or superheated state in the expander. It should be mentioned that if these technical constraints are not satisfied by a refrigerant, it means that this refrigerant cannot be an acceptable candidate for the optimal conditions obtained in the preceding optimization step.
6. Finally, the increment of the temperature difference at the outlet of the condenser (sole degree of freedom) is chosen as 0.1 K for each iteration, owing to the accuracy of the equivalent temperatures.

It must be noted that the purpose of the theoretical optimization is to find the optimal equivalent temperatures and heat transfer values of the condenser and the evaporator that minimize the total thermal conductance. Therefore, the optimal equivalent temperatures, $\dot{Q}_{evap}$, and $\dot{Q}_{cond}$ obtained by solving the optimization problem will be the same for all working fluid candidates. However, the reconstruction procedure and individual thermo-physical properties of each candidate will determine the working fluid states. Thus, the comparison of the system characteristics for potential working fluids indicates the most appropriate working fluid.

In section 4-7 two case studies will be presented to illustrate the application of the novel approach.

4-7 Case studies

To illustrate the application and the advantages of the approach introduced herein, two case studies will be investigated. The first case study will compare our approach with the results of Saloux et al. (Saloux *et al.* 2018, 2019), based on their equivalent temperature model. The second case study will show the application of the approach in an organic Rankine cycle designed for low-grade waste heat recovery (Muhammad *et al.* 2015). The operating conditions of the case studies for desired powers are given in Table 4-1.

Table 4-1: Operating conditions used for the two case studies (case 1: Saloux et al., 2018, 2019) and (case 2: Muhammad et al., 2015)

Case studies	$T_{H,in}$ (°C)	$T_{L,in}$ (°C)	$c_{P,H}$ $(kJ/kg.K)$	$c_{P,L}$ $(kJ/kg.K)$	$\dot{m}_H$ (kg/s)	$\dot{W}_{net}$ (kW)	T_{SC} (°C)
1	120	10	1	1	0.30	1	3
2	135.4	4.9	2.38	4.02	0.063	0.812	3

4-7-1 Case study 1

As was described in section 4-5, the operating conditions of the external fluids presented in Table 4-1 are the initial design parameters of the comprehensive approach. For the first step of the approach, the fmincon function in MATLAB was used to perform the constrained nonlinear optimization problem to implement Sequential Quadratic Programming (SQP) (Luo *et al.* 2017). For the first case study, the optimization results for different isentropic efficiencies of the expander are shown in Table 4-2. It must be noted that since the power of the liquid pump is too low compared with the heat input in the evaporator, and owing to some simplification, the required power for liquid pumping process was not separately taken into account in the optimization step but we assumed that the power generated by the expander is the net power output. Note that Saloux et al. (Saloux *et al.* 2018) stated that the equivalent temperatures and

other system parameters presented in Table 4-2 are independent of the isentropic efficiency of the expander.

Table 4-2: Results obtained from the optimization procedure for case study 1.

$\eta_{is,exp}$ $(-)$	$\widetilde{\boldsymbol{T}}_{\boldsymbol{BC}}$ (K)	$\widetilde{\boldsymbol{T}}_{\boldsymbol{AD}}$ (K)	$T_{H,out}$ (K)	$\dot{Q}_{eva}$ (kW)	$(\boldsymbol{UA})_{\boldsymbol{eva}}$ (kW/K)	$(\boldsymbol{UA})_{\boldsymbol{cond}}$ (kW/K)
1	358.3	304.5	371.2	6.670	0.279	0.279
0.95	357.9	304.3	370.1	7.033	0.298	0.299
0.9	357.6	304.1	368.7	7.436	0.320	0.322
0.85	357.2	303.9	367.3	7.885	0.345	0.349
0.8	356.8	303.6	365.6	8.389	0.374	0.380
0.75	356.3	303.3	363.7	8.959	0.408	0.417
0.7	355.8	302.9	361.6	9.52	0.449	0.461
Ref. (Saloux *et al.* 2018)	353.9	296.1	361.4	9.52	0.496	0.612

The performance parameters and the external and internal entropy generation rates for different expander isentropic efficiencies obtained by the optimization problem are given in Table 4-3. The reference temperature for the calculation of the exergetic efficiency is equal to 298.15 (K). As it mentioned in the section4-2, in the case of theoretical optimization models, previous researchers used an arbitrary dimensionless coefficient called the internal irreversibility parameter (Eq. (4-30)) to characterize the generic source of internal irreversibility. The equivalent temperature concept paves the way to calculate the entropy generation rate of each component according to the operating condition (instead of using an arbitrary coefficient) in the theoretical model introduced herein and results in the precise determination of the optimal design variables. The internal irreversibility parameter for each expander isentropic efficiency is given in Table 4-3.

$$I = \frac{\dot{Q}_{con}/\tilde{T}_{AD}}{\dot{Q}_{eva}/\tilde{T}_{BC}} \qquad (4\text{-}30)$$

Table 4-3: Entropy generation and the performance of the system obtained by the optimization for case study 1.

$\eta_{is,exp}$ $(-)$	$\dot{S}_{gen,ext}$ (W/K)	$\dot{S}_{gen,int}$ (W/K)	I $(-)$	η_{th} $(-)$	η_{II} $(-)$
1	2.5	0	1	0.150	0.682
0.95	2.8	0.1	1.009	0.142	0.651
0.9	3.1	0.3	1.018	0.135	0.619
0.85	3.5	0.5	1.026	0.127	0.588
0.8	3.9	0.8	1.035	0.119	0.558
0.75	4.3	1.1	1.044	0.112	0.527
0.7	4.8	1.4	1.051	0.105	0.496

It is interesting to mention that the optimization problem tends to evenly distribute the total thermal conductance among the evaporator and the condenser (Table 4-2). For instance, in the case of isentropic expansion ($\eta_{is,exp} = 1$), the equipartition principle of the total thermal conductance, first referred by Bejan (Bejan 1989), is satisfied. Table 4-2 and Table 4-3 show that the internal irreversibility causes the deviation from the equipartition principle. This shows that the higher internal entropy generation results in a lower evaporator to condenser conductance ratio. Moreover, the thermal efficiency of the cycle, Eq. (4-20), in the case of isentropic expansion, is equal to the efficiency of a Carnot engine at maximum power output as reported by Curzon and Ahlborn (Curzon and Ahlborn 1975).

Prior to the reconstruction procedure, the optimal equivalent temperatures presented in Table 4-2 will be used to establish thermodynamic criteria for the pre-selection of potential working fluids. The condenser equivalent temperature must be higher than the boiling temperatures at

atmospheric pressure of candidates in order to avoid a vacuum pressure in the condenser. Furthermore, the critical temperature of the working fluid under investigation should be higher than the maximum operating temperature of the cycle (Papadopoulos, Stijepovic and Linke 2010). Environmental characteristics, as well as the thermodynamic criteria of working fluids shown in Table 4-4, are considered as decisive factors to choose the candidate working fluids. Isobutane (R600a), Isopentane (R601a), R245fa, c2butene and dimethyl ether (RE170) have been pre-selected in this paper. According to the international agreements, working fluids operating in the system must have zero ozone depletion potential (ODP) and global warming potential (GWP) lower than 2500 (Eldakamawy, Sorin and Brouillette 2017). Although R245fa has the safest operation condition form the flammability viewpoint, it is relatively toxic and has the highest GWP. The other fluids have GWP less than or equal to 20 whilst they are categorized as the fluids with high flammability potential.

Table 4-4: Critical temperature and Environmental parameters of pre-selected refrigerants (*ASHRAE Handbook-Fundamentals* 2017)

Working Fluids	$T_{critical}$ (K)	$T_{boil}@1^{atm}$ (K)	ODP	GWP	Safety[2]
R600a	407.9	261.4	0	20	A3
R601a	460.4	300.8	0	20	A3
R245fa	427.2	288.3	0	1030	B1
c2butene	435.8	276.9	0	20	A3
dimethyl ether	400.4	248.4	0	1	A3

Although the optimization results, i.e. the equivalent temperatures and heat transfer values in the condenser and the evaporator, are identical for all working fluids, the different individual thermo-physical properties of each candidate lead to completely different results in the

[2] A: no toxicity, B: toxicity, 1: no flame propagation, 3: high flammability

reconstruction procedure. Table 4-5 and show the essential operating conditions of the system operating with the working fluids under investigation for two different expander isentropic efficiencies. $\Delta T_{sh,cond}$ and $\Delta T_{sh,evap}$ represent the degrees of superheating at the evaporator outlet and the condenser inlet, respectively. The thermodynamic properties of working fluids were taken from the CoolProp Library (Bell *et al.* 2014). The working fluids under investigation are categorized as dry fluids, except dimethyl ether. Since dry fluids have positive slopes of the saturation vapor lines in their *T-s* diagrams, the superheating process in the evaporator outlet is not necessary. Dimethyl ether (dme), by contrast, needs some amount of superheating at the evaporator outlet, in order to avoid condensation through the expander.

Table 4-5: Operating conditions for different working fluids for case study 1 ($\eta_{is,exp} = 0.85$)

Working Fluids	R600a	R601a	R245fa	c2butene	Dimethyl ether
$\dot{m}_{wf}$ (kg/s)	0.019	0.0171	0.033	0.017	0.017
P_{cond} (kPa)	405.3	105.1	177.5	255.4	692.62
P_{evap} (kPa)	2148	717.45	1303	1350	3226.8
$\Delta T_{sh,cond}$ (°C)	16.9	29.8	19.6	8.6	3.0
$\Delta T_{sh,evap}$ (°C)	0	0	0	0	9
$\dot{W}_{exp}$ (kW)	1.059	1.016	1.025	1.028	1.063
$\dot{W}_{pump}$ (kW)	0.059	0.016	0.025	0.028	0.063

Table 4-6: Operating conditions for different working fluids for case study 1 ($\eta_{is,exp} = 0.7$)

Working Fluids	R600a	R601a	R245fa	c2butene	Dimethyl ether
$\dot{m}_{wf}$ (kg/s)	0.023	0.021	0.040	0.021	0.021
P_{cond} (kPa)	388.4	102	167.9	244.5	673.6
P_{evap} (kPa)	2078.6	697.1	1257.9	1306.9	3174.8
$\Delta T_{sh,cond}$ (°C)	22.9	34.6	25.8	16.2	3.4
$\Delta T_{sh,evap}$ (°C)	0	0	0	0	5.0
$\dot{W}_{exp}$ (kW)	1.071	1.020	1.030	1.035	1.080
$\dot{W}_{pump}$ (kW)	0.071	0.020	0.030	0.035	0.080

Though the operating states of the working fluids are completely different, the terms of Eq. (4-20) (thermal efficiency) and Eq. (4-21) (exergetic efficiency) are independent of working fluids and thus the performance parameters of all the working fluids are identical and equal to values presented in Table 4-3. The parameter that determines the optimal working fluid is the total thermal conductance of heat exchangers, known as an indicator of the size and cost of the system (Bejan, Vargas and Sokolov 1995; Dahmani, Aidoun and Galanis 2011). The thermal conductance calculation proceeds by separating each heat exchanger into liquid (f), two-phase (fg) and superheated (g) regions (Akbari, Sorin and Marcos 2018) by using Eqs. (4-23)-(4-26). For instance, the thermal conductance of the evaporator and the condenser for each working fluid for expander isentropic efficiency of 0.70 are given in Table 4-7. The last column to the right in the table shows the results obtained in Ref. (Saloux *et al.* 2018). The proposed comprehensive approach introduced herein resulted in 6% smaller heat exchanger compared to Saloux's procedure (Saloux *et al.* 2018). The discrepancy between two approaches is mainly due to the optimal equivalent temperatures (Table 4-2) obtained by the optimization procedures. In the present approach, the novel entropy generation calculations based on the equivalent

temperature concept, which constrain the optimization problem, led to a superior solution. Moreover, the optimal equivalent temperatures used by Saloux et al. (Saloux *et al.* 2018) resulted in unsatisfactory system characteristics operating with R245fa, owing to the presence of liquid droplets in the expander.

Table 4-7: Thermal conductance (kW/K) *of condenser and evaporator for* $\eta_{is,exp} = 0.7$

Refrigerant	R600a	R601a	R245fa	c2butene	Dimethyl ether	R600a (Saloux *et al.* 2018)
$(UA_f)_{con}$	0.0100	0.0092	0.0094	0.0079	0.0086	$(-)$
$(UA_{fg})_{con}$	0.4269	0.4412	0.4319	0.4371	0.4486	$(-)$
$(UA_g)_{con}$	0.0360	0.0446	0.0345	0.0209	0.0054	$(-)$
UA_{con}	0.4729	0.4950	0.4758	0.4659	0.4626	0.7729
$(UA_f)_{eva}$	0.2305	0.1679	0.1921	0.1434	0.1706	$(-)$
$(UA_{fg})_{eva}$	0.5028	0.5059	0.4881	0.4513	0.4104	$(-)$
$(UA_g)_{eva}$	0	0	0	0	0.0267	$(-)$
UA_{eva}	0.7333	0.6738	0.6802	0.5947	0.6077	0.5123
UA_{tot}	1.2062	1.1688	1.1560	1.0606	1.0703	1.2852

The total thermal conductance of the working fluids for different expander isentropic efficiencies are illustrated in Figure 4-3. The system operating with R600a needs the largest total thermal conductance compared to the other working fluids. It should be noted that the pre-selected working fluids requires higher total thermal conductances than the optimization results, because, in the optimization problem, the real temperatures of the working fluids in a process were replaced by a constant equivalent temperature. For instance c2butene needs 23% higher total thermal conductance than the optimization results, because, according to Table 4-6,

c2butene experiences a 16.2 K temperature difference (16.2 K de-superheating processes) along the condenser whilst the saturation, de-superheated and subcooled temperatures are implicitly considered in the equivalent temperature definition and presented as a constant value.

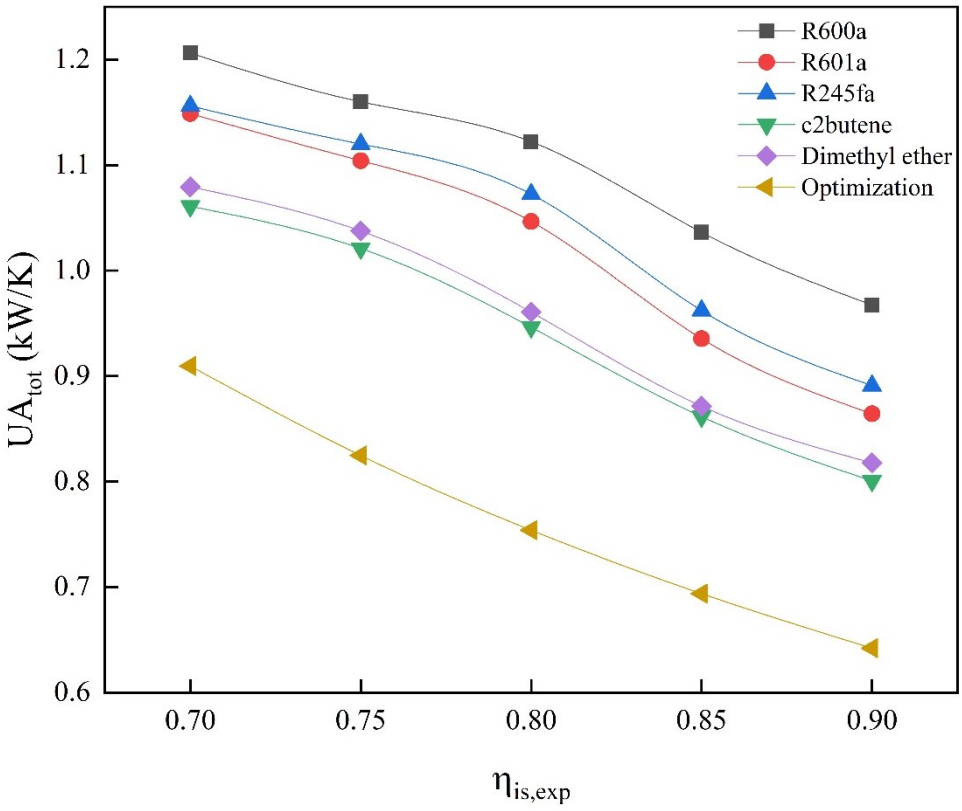

Figure 4-3: Total thermal conductance for different isentropic efficiencies (case study 1)

Since there are different desuperheating and subcooled degrees in the condenser and evaporator, respectively, for each working fluid and according to Table 4-8 each region has its own overall heat transfer coefficient, the calculation of heat transfer area for each region was conducted by using Eq. (4-31) and the results are shown in Table 4-9.

$$A = \frac{\dot{Q}}{U \times \Delta T_{LMTD}} \qquad (4\text{-}31)$$

Table 4-8: Approximate overall heat transfer coefficients (Mills 1998; Dimian and Bildea 2008)

Hot fluid	Cold fluid	U
$(-)$	$(-)$	(W/m^2K)
Evaporator		
Steam	Hydrocarbons (two-phase)	1250
Steam	Hydrocarbons (vapor)	20
Steam	Hydrocarbons (liquid)	600
Condenser		
Hydrocarbons (two-phase)	Water	850
Hydrocarbons (vapor)	Water	30
Hydrocarbons (liquid)	Water	600

Table 4-9: Heat exchanger area for different working fluids for case study1, (m^2)

Refrigerant	R600a	R601a	R245fa	c2butene	Dimethyl ether
$(A_f)_{con}$	0.017	0.015	0.016	0.013	0.014
$(A_{fg})_{con}$	0.502	0.519	0.508	0.514	0.528
$(A_g)_{con}$	1.199	1.487	1.150	0.696	0.180
A_{con}	1.718	2.021	1.674	1.223	0.722
$(A_f)_{eva}$	0.384	0.280	0.320	0.239	0.284
$(A_{fg})_{eva}$	0.402	0.405	0.390	0.361	0.328
$(A_g)_{eva}$	0	0	0	0	1.335
A_{eva}	0.786	0.685	0.710	0.600	1.967
A_{tot}	2.504	2.706	2.384	1.823	2.689

Table 4-9 reveals that c2butene needs the smallest heat exchanger surface area and is the optimal working fluid for case study 1.

4-7-2 Case study 2

The second case study was presented by Muhammad et al. (Muhammad *et al.* 2015), designed to experimentally investigate the overall performance of a small scale organic Rankine cycle using waste steam. The initial design parameters of the comprehensive approach were given in Table 4-1. The optimal equivalent temperatures, as well as other system characteristics that result in the minimum total thermal conductance of the system, are given in Table 4-10. It must be mentioned that the results are obtained for an expander isentropic efficiency of 0.60 and 0.70 (Muhammad *et al.* 2015).

Table 4-10: Optimization results for case study 2

$\eta_{is,exp}$ $(-)$	$\widetilde{\boldsymbol{T}}_{\boldsymbol{BC}}$ (K)	$\widetilde{\boldsymbol{T}}_{\boldsymbol{AD}}$ (K)	$T_{H,out}$ (K)	$\dot{Q}_{eva}$ (kW)	$(\boldsymbol{UA})_{\boldsymbol{eva}}$ (kW/K)	$(\boldsymbol{UA})_{\boldsymbol{cond}}$ (kW/K)
0.6	379.0	296.3	356.6	7.81	0.379	0.394
0.7	360.4	298.0	359.1	6.70	0.293	0.302

The reconstruction procedure results for the pre-selected refrigerants for two different expander isentropic efficiencies are given in Table 4-11 and Table 4-12. It should be mentioned that since R601a has a boiling temperature at atmospheric pressure, greater than the optimal condenser equivalent temperature, this refrigerant cannot meet the thermodynamic criterion for the pre-selection of potential working fluids.

Table 4-11 Reconstruction procedure results for the case study 2 ($\eta_{is,exp} = 0.6$)

Working Fluids	R600a	R245fa	c2butene	Dimethyl ether
$\dot{\boldsymbol{m}}_{\boldsymbol{wf}}$ (kg/s)	0.018	0.030	0.016	0.016
$\boldsymbol{P}_{\boldsymbol{cond}}$ (kPa)	312.6	125.5	193.9	555.7
$\boldsymbol{P}_{\boldsymbol{evap}}$ (kPa)	2641	1597	1549	3719
$\Delta \boldsymbol{T}_{\boldsymbol{sh,cond}}$ (℃)	29.8	35.5	24.5	14.8
$\Delta \boldsymbol{T}_{\boldsymbol{sh,evap}}$ (℃)	0	0	0	9.9
$\dot{W}_{exp}$ (kW)	0.885	0.843	0.846	0.886
$\dot{W}_{pump}$ (kW)	0.073	0.031	0.034	0.074

Table 4-12: Reconstruction procedure results for the case study 2 ($\eta_{is,exp}$ =0.70)

Working Fluids	R600a	R245fa	c2butene	Dimethyl ether
$\dot{m}_{wf}$ (kg/s)	0.015	0.026	0.014	0.014
P_{cond} (kPa)	332.9	137.0	207.5	585.6
P_{evap} (kPa)	2753	1670	1621	3940
$\Delta T_{sh,cond}$ (℃)	26.2	31.7	19.7	4.7
$\Delta T_{sh,evap}$ (℃)	0	0	0	8
$\dot{W}_{exp}$ (kW)	0.873	0.851	0.843	0.863
$\dot{W}_{pump}$ (kW)	0.061	0.039	0.031	0.051

Since the performance parameters such as net power and evaporator heat input are identical for all working fluids, the heat exchanger surface area corresponding to each refrigerant can determine the most appropriate working fluid. The heat exchanger surface area, as distributed between the evaporator and the condenser, as well as their sum for each refrigerant for the expander isentropic efficiency of 0.60 are given in Table 4-13.

Table 4-13: Heat exchanger area for different working fluids for case study 2 for $\eta_{is,exp}$ =0.6, (m^2)

Refrigerant	R600a	R245fa	c2butene	Dimethyl ether
$(A_f)_{con}$	0.015	0.014	0.011	0.012
$(A_{fg})_{con}$	0.439	0.451	0.442	0.441
$(A_g)_{con}$	1.148	1.147	0.764	0.534
A_{con}	1.602	1.612	1.217	0.987
$(A_f)_{eva}$	0.390	0.347	0.268	0.276
$(A_{fg})_{eva}$	0.253	0.307	0.288	0.215
$(A_g)_{eva}$	0	0	0	1.273
A_{eva}	0.643	0.654	0.556	1.764
A_{tot}	2.245	2.266	1.773	2.751

Table 4-13 reveals that for the identical performance, c2butene requires the lowest heat exchanger surface area, followed by R600a. It should be mentioned that the experimental investigation conducted by Muhammad et al. (Muhammad *et al.* 2015) was performed with R245fa as its working fluid. However, Table 4-13 shows that this refrigerant needs a higher heat exchanger surface area compared to c2butene and R600a.

4-8 Conclusions

In this article, a novel systematic approach is presented for the selection of the most appropriate working fluid for Organic Rankine Cycles (ORC) given fixed known external reservoir conditions. The novelty resides in the theoretical optimization statement, independent of the working fluid properties, that accounts for the entropy generation in each component. The equivalent temperature concept lays the foundation for establishing a link between the entropy generation and the operating conditions of each component, and it constrains the optimization problem. The optimization problem seeks the optimal equivalent temperatures and heat transfer values at the condenser and the evaporator, in order to minimize the total thermal conductance of the system. To correlate the optimization results with essential parameters of the system, such as the working fluid mass flow rate and operating pressures and temperatures, an original reconstruction procedure was introduced. The differences between saturation temperatures and the optimal equivalent temperatures in the condenser and evaporator were utilized to automatically obtain the superheating and subcooling as well as the mass flow rate. The reconstruction procedure systematically selects the most appropriate working fluid among potential candidates. The proposed approach was compared with the existing procedures in the literature and its application was shown in two case studies. The advantages of the new approach were illustrated: the precise optimization problem formulation, the capability of evaluating more working fluids, and the investigation of the temperature distribution feasibility within the heat exchangers.

4-9 Acknowledgments

This project is a part of the Collaborative Research and Development (CRD) Grants Program at “Université de Sherbrooke”. The authors acknowledge the support of the Natural Sciences

and Engineering Research Council of Canada, Hydro-Québec, Rio Tinto, Alcan and Canmet ENERGY Research Center of Natural Resources Canada (RDCPJ451917-13).

4-10 Appendix

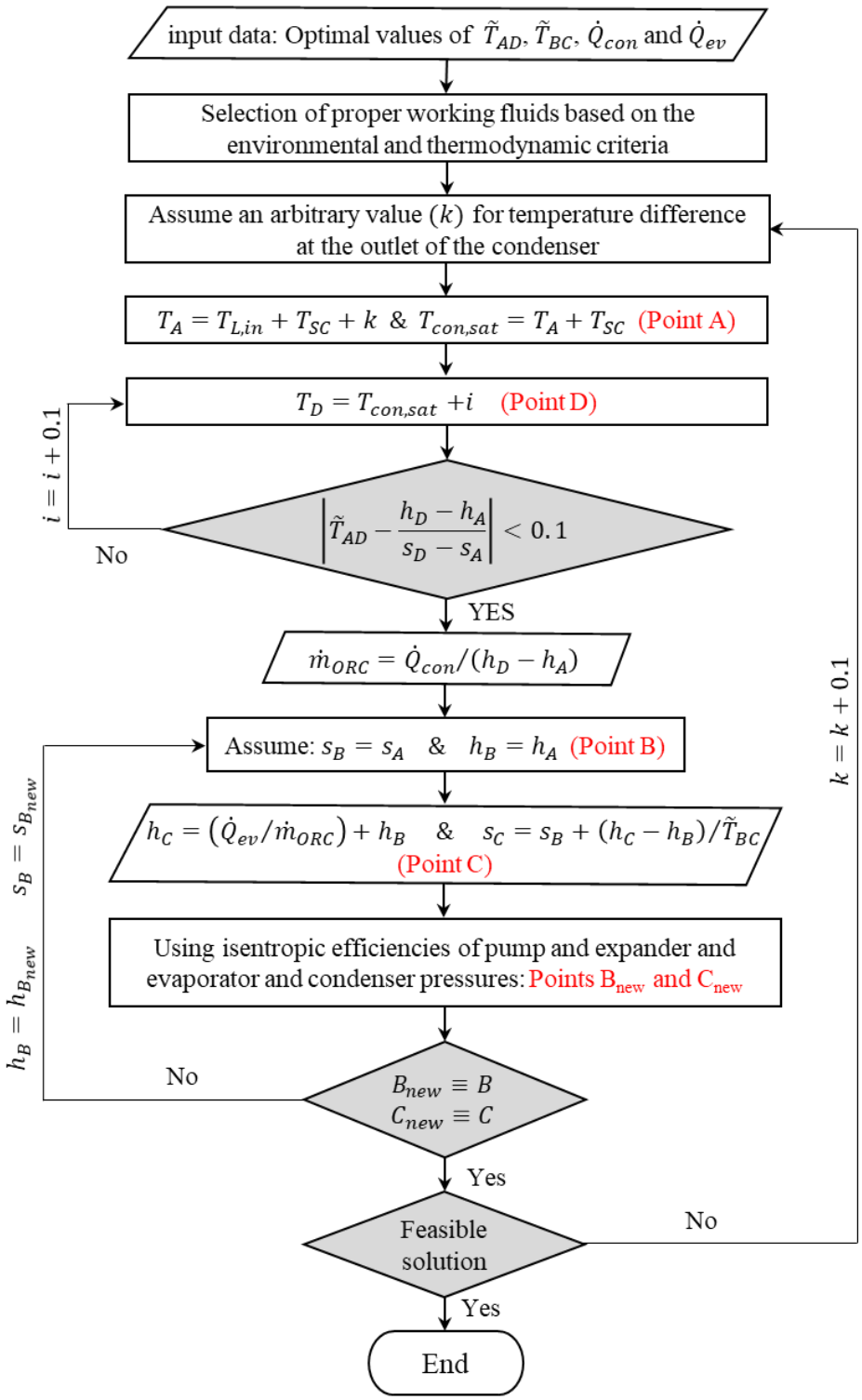

Figure 4-4: Proposed algorithm for reconstruction procedure

4-11 Nomenclature

ds	entropy difference (kJ/kg-K)
dh	enthalpy difference (kJ/kg)
dp	pressure difference(kPa)
P	pressure (kPa)
$\dot{Q}$	thermal power (kW)
$\dot{S}_{gen}$	entropy generation rate (kW/K)
T	temperature (K)
$\tilde{T}$	equivalent temperature (K)
UA	thermal conductance, i.e. product of the overall heat transfer coefficient and heat transfer surface area (kW/K)
$\dot{W}$	power (kW)
dme	Dimethyl ether
c_p	heat capacity at constant pressure (kJ/kg-K)
h	enthalpy (kJ/kg)
$\dot{m}$	mass flow rate (kg/s)
s	entropy (kJ/kg-K)

Subscripts

AD	refrigerant side in the condenser
BC	refrigerant side in the evaporator
H	high temperature
L	low temperature
LMTD	logarithmic mean temperature difference
con	condenser
eva	evaporator
exp	expander
ext	external
f	saturated liquid
g	saturated vapor
is	isentropic
in	inlet
int	internal
out	outlet
r	reference condition
Sc	Subcooling

sh	Superheating
tot	Total
wf	Working fluid

Greek letters

Δ	Difference
v	specific volume (m^3/kg)
η	Efficiency

Chapter 5

Optimal component-scale design of ejector refrigeration systems based on equivalent temperature

Avant-propos

Auteurs et affiliation :

Hossein Akbari: étudiant au doctorat, faculté de génie, département de génie mécanique, Université de Sherbrooke.

Mikhail Sorin: professeur, faculté de génie, département de génie mécanique, Université de Sherbrooke.

Date d'acception: 18 février 2020

État de l'acceptation: version finale publiée

Revue: Energy Conversion and Management

Titre français: Conception optimale à l'échelle des composants des systèmes de réfrigération à éjecteurs basés sur une température équivalente

Contribution au document: Cet article contribue à la thèse par une application de l'approche proposée pour le système de réfrigération à éjecteur.

Résumé français:

L'article propose une approche exhaustive pour la conception et l'optimisation d'un système de réfrigération à éjecteur, y compris la sélection du fluide de travail optimal. Le système de réfrigération à éjecteur est modélisé comme la combinaison d'un sous-cycle de puissance et d'un sous-cycle de compression de vapeur, et l'éjecteur est modélisé comme un dispositif d'expansio-compression. L'approche applique le concept de température équivalente en deux

étapes. La première étape est une optimisation à l'échelle du système de réfrigération à éjecteur qui est indépendante du fluide de travail. La minimisation de la conductance thermique totale du système a été choisie comme fonction objective où l'analyse de la seconde loi contraint le problème d'optimisation. La première étape comprend la présélection des réfrigérants candidats en fonction de certains critères thermodynamiques, environnementaux et sécuritaires. La deuxième étape est la conception à l'échelle des composants du système de réfrigération à éjecteur, comprenant le calcul de toutes les températures, pressions et débits massiques inconnus restants. La deuxième étape comprend la sélection du fluide de travail. Si le coefficient de performance et la conductance thermique totale, en tant qu'indicateurs économiques, ne sont pas suffisants pour choisir le fluide de travail optimal, une analyse exergoéconomique est utilisée pour effectuer la sélection finale. L'approche globale proposée a été appliquée sur une étude de cas et validée par rapport aux résultats publiés dans la littérature.

5-1 Abstract

The article proposes a comprehensive approach for the design and optimization of an ejector refrigeration system, including the selection of the optimal working fluid. The ejector refrigeration system is modeled as the combination of a power sub-cycle and a vapor compression sub-cycle, and the ejector is modeled as an expander-compressor device. The approach applies the equivalent temperature concept in two steps. The first step is a system-scale optimization of the ejector refrigeration system that is independent of the working fluid. Minimization of the total system thermal conductance was chosen as the objective function where a second-law analysis constrains the optimization problem. The first step includes the pre-selection of refrigerant candidates based on some thermodynamic, environmental and safety criteria. The second step is the component-scale design of the ejector refrigeration system, comprising the calculation of all remaining unknown temperatures, pressures, and mass flow rates. The second step includes the selection of the working fluid. If the coefficient of performance and total thermal conductance, as economic indicators, are not sufficient to choose the optimal working fluid, then an exergoeconomic analysis is used to make the final selection. The proposed comprehensive approach was demonstrated with a case study and validated against published results.

Keywords: Ejector refrigeration system, System-scale optimization, Component-scale design, Equivalent temperature

5-2 Introduction

Air conditioning and refrigeration account for the largest portion of electricity use by residential and commercial sectors around the world (*International Energy Outlook, Energy Information Administration (EIA)* 2018). Supplying such high-grade energy to the vapor-compression cycle, which is the most widely used technology for the production of cold, is accompanied by high cost and growing environmental concerns. These issues can be partially addressed by the utilization of alternative systems such as an ejector refrigeration system (ERS) which consumes very little electricity. In the ejector refrigeration cycle, a pump, a generator, and an ejector replace the mechanical compressor (the main consumer of electricity) in the conventional vapor-compression cycle. The ejector possesses the ability to compress the working fluid by utilizing low-grade energy sources, such as solar energy (Xu *et al.* 2019), geothermal energy (Rostamnejad Takleh and Zare 2019), or waste heat recovery (Reddick, Sorin and Rheault 2014), thus resulting in a reduction of operating costs, as well as curbing environmental degradation. Owing to these advantages, ERS design has attracted attention in both academic and industrial fields.

The design of a thermodynamic cycle can be seen as a three sequential-step process: system-scale performance optimization; component-scale design; and local-scale analysis (Besagni 2019). The system-scale performance optimization determines the maximum possible efficiency of the system under ideal circumstances based on the existing external thermal sources. In this step, each component of the system is considered as a black box that is responsible for the corresponding process while respecting the first two laws of thermodynamics. This step comprises the method of thermodynamic optimization of finite-time systems based on chosen basic thermodynamic and heat transfer principles. Entropy generation minimization (Bejan 1996), thermodynamic equipartition technique (Thiel *et al.* 2014) and equivalent temperature-based (Akbari, Sorin and Marcos 2018) methods are three available examples in the open literature. Since the results of system-scale performance optimization are

independent of working fluids, this step provides the basis for introducing a systematic approach for the second step of the cycle design. The second step, i.e. component-scale design, deals with the boundary conditions of the system components while taking into account the thermo-physical properties of potential working fluids. Since the individual properties of the selected working fluids are available, the actual performance of the system and its components can be evaluated by using exergy and entropy analyses (Sayed Ahmed *et al.* 2018). As a result, the most appropriate working fluid can be selected. In the third step, i.e. local-scale analysis, the complex flow phenomena within the components are taken into consideration to design the final geometries and other characteristics of the system components.

The complexity of fluid flow inside an ejector creates an obstacle for the system-scale optimization and to the best knowledge of the authors, no study deals with the system-scale performance analysis of ejector refrigeration system. However, the last two steps have been investigated by a vast number of researchers. In the component-scale analysis, the focus has been to evaluate the effects of different operating conditions on the ejector behavior by using different optimization techniques (Rashidi, Aghagoli and Raoofi 2017), numerical models (Taslimitaleghani, Sorin and Poncet 2018) and experimental investigations (Narimani *et al.* 2019). Since an ejector is characterized by complicated fluid dynamics, such as that of a shock wave, mixing process, under-expanded jets, etc., its local-scale analysis has attracted much more attention from researchers compared to the other system components. Researchers have shed light on the local phenomena such as choking conditions (Lamberts, Chatelain and Bartosiewicz 2018) and polytropic efficiencies of the ejector (Haghparast, Sorin and Nesreddine 2018a) by using computational fluid dynamics (CFD). Moreover, they have investigated the effects of ejector geometry parameters on system behavior and performance (Tashtoush, Al-Nimr and Khasawneh 2019).

The enumeration of all possible working fluids, as well as their individual optimal operating conditions, pose major difficulties with the design of thermodynamic cycles. To overcome this issue, some thermodynamic and environmental criteria must be considered to reduce the number of potential working fluids. Subsequently, a systematic approach can facilitate the determination of optimal operating conditions for each pre-selected working fluid. The

systematic approaches existing in the literature for the design of operating conditions (Dahmani, Aidoun and Galanis 2011) and the selection of working fluid (Eldakamawy, Sorin and Brouillette 2017) are based on a set of pre-defined minimum approach temperature at the heat exchangers. In order to retrieve the optimal component-scale design, the values of the minimum approach temperature must be manually tuned. Thus, the huge number of possible permutations for their values makes the design problem a cumbersome process.

The main purpose of this paper is to introduce a comprehensive approach for selecting the most appropriate working fluid as well as optimal operating conditions of the ERS, which can also deal with the issues relating to the first two steps of the aforementioned design steps of such cycle. In the first step, system-scale optimization will be performed according to the inlet conditions of external sources. To overcome the complexity of phenomena within the ejector, it will be considered as a hypothetical expander-compressor device and, in turn, the ERS as a combination of power and vapor-compression refrigeration systems. This assumption will pave the way for the system-scale optimization by using the equivalent temperature based model recently introduced by Akbari et al. (Akbari, Sorin and Marcos 2018). In that model, the system-scale optimization for the hypothetical power and compression cycle is formulated independently of working fluids where a second-law analysis, as a constraint, guarantees the feasibility of results. In order to correlate the irreversibilities of the hypothetical expander and compressor with that of ejector, the ejector efficiency definition will be utilized. The resultant optimal equivalent temperatures of the heat-exchange processes establish a thermodynamic criterion to pre-select the potential working fluids among a vast number of existing refrigerants. The optimal entrainment ratio of the ejector, as well as the equivalent temperatures, will provide the basis for a systematic approach, i.e. the second step of the comprehensive approach, for the determination of optimal operating conditions, which includes actual temperatures and pressures and the mass flow rates for each pre-selected working fluid. Individual properties of each potential working fluid result in different capital-operating cost performance. Hence, an economic analysis of the system determines the most appropriate working fluid. A case study is presented to illustrate the application and advantages of the approach compared to a systematic approach existing in the literature.

5-3 System description

As shown schematically in Figure 5-1, an ERS is similar to a conventional vapor-compression refrigeration cycle expect that the usual compressor is replaced by an ejector, a generator, and a pump. The ejector's motive gas (known as the power source of ejector) comes from the generator, where heat is absorbed from a high-temperature reservoir. The ejector utilizes the expansion of the primary high-pressure motive stream to entrain a low-pressure secondary vapor leaving the evaporator, and to increase the pressure of the entrained flow. Both streams are mixed inside the ejector and discharged at the condenser pressure. The mixture enters the condenser where it rejects heat to an external fluid. A fraction of the condensed refrigerant exiting the condenser returns to the generator by passing through the pump. The remaining condensed fluid expands through the expansion valve to the pressure of the evaporator, where the desired cooling load is produced.

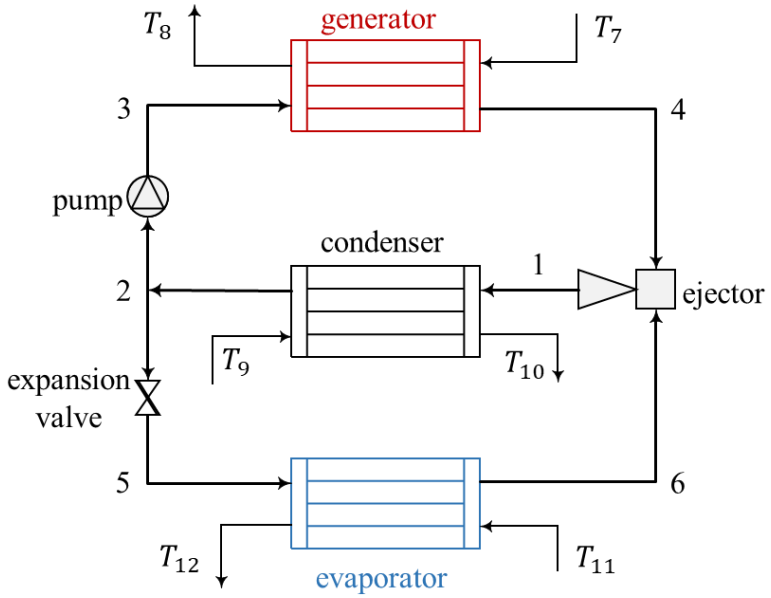

Figure 5-1: Ejector refrigeration system

5-4 System-scale performance optimization

The system-scale performance optimization introduced herein can be seen as the extension of the equivalent temperature based model introduced by Akbari et al. (Akbari, Sorin and Marcos 2018; Akbari and Sorin 2020) for the vapor-compression refrigeration and organic Rankine

cycles. Equivalent temperature replaces the actual temperatures of inlet and outlet states of an isobaric process according to the entropy and enthalpy changes through the process (Akbari, Sorin and Marcos 2018):

$$\tilde{T} = \frac{\Delta h}{\Delta s} \qquad (5\text{-}1)$$

Since the calculation of individual component entropy generation is an essential part of the system-scale performance optimization, in the following subsection we calculate the entropy generation of each component. It should be mentioned that the concept of equivalent temperature and its interpretation on the *h-s* (Akbari, Sorin and Marcos 2018) will be used to carry out this second-law based analysis.

5-4-1 Entropy generation

As a literature review reveals, the ejector is responsible for the most important irreversibility in the ERS (Chen *et al.* 2017; Eldakamawy, Sorin and Brouillette 2017; Taslimitaleghani, Sorin and Poncet 2018). From the local-scale point of view, the main sources of irreversibility inside the ejector are mixing, shock waves and parasitic friction (Eldakamawy, Sorin and Brouillette 2017). To identify these phenomena, we need to use some complex fluid dynamic equations, which are based on the thermo-physical properties of the working fluids. Since the system-scale performance optimization must be formulated independently of working fluid and, thus, thermo-physical properties of working fluid are unknown, the calculation of entropy generated through the ejector is the most complicated part of this optimization problem. To overcome this difficulty, we need to take a detailed look at the operating principle of the ejector. The main purpose of using an ejector is to provide the required compression of the entrained stream from the evaporator pressure to the condenser pressure. The ejector operating principle can be explained by analogy with a hypothetical expander-compressor (Köhler *et al.* 2007; Lucas and Koehler 2012). The main advantage of this hypothetical expander-compressor assumption is that we can determine the entropy generation through the ejector by two well-known isentropic efficiencies, i.e. compressor and expander isentropic efficiencies. An isentropic efficiency for the hypothetical compression process assists in the calculation of entropy generated by the entrained stream compressed from the evaporator pressure to the condenser pressure (Akbari,

Sorin and Marcos 2018). The other isentropic efficiency can be utilized to characterize the entropy generated by the motive stream expanded form the generator pressure to the condenser pressure (Akbari and Sorin 2020). Hence, we replace the ERS with two subcycles, i.e. power subcycle and refrigeration subcycle. T-s diagrams of the actual ERS and hypothetical expander-compressor systems are shown in Figure 5-2. It must be noted that the amount of power required to compress the entrained flow from the evaporator pressure to the condenser pressure is exactly the same amount of power extracted from the motive fluid expanding between the generator pressure and condenser pressure.

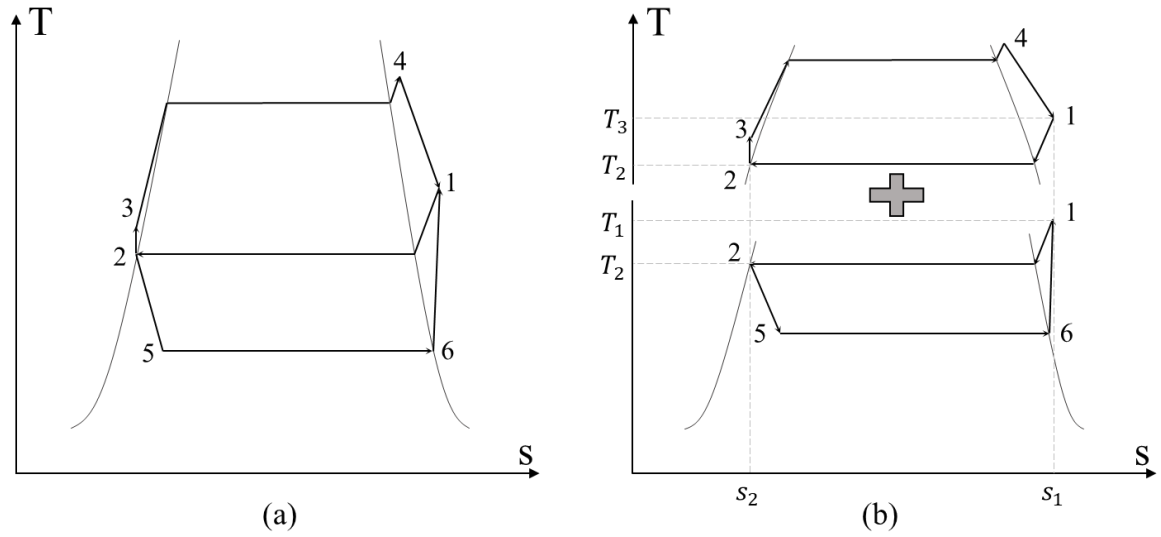

Figure 5-2: T-s diagrams of ERS. (a) actual system, (b) hypothetical expander-compressor system

The entropy generation calculation related to each component based on the concept of equivalent temperature is investigated in the following.

The rates of entropy generation in the generator, condenser, and evaporator can be determined with Eqs. (5-2)-(5-4) (Akbari, Sorin and Marcos 2018; Akbari and Sorin 2020):

$$\dot{S}_{gen} = \dot{Q}_{gen}\left(\frac{1}{\tilde{T}_{gen}} - \frac{1}{\tilde{T}_H}\right) \tag{5-2}$$

$$\dot{S}_{con} = \dot{Q}_{con}\left(\frac{1}{\tilde{T}_C} - \frac{1}{\tilde{T}_{con}}\right) \tag{5-3}$$

$$\dot{S}_{ev} = \dot{Q}_{ev}\left(\frac{1}{\tilde{T}_{ev}} - \frac{1}{\tilde{T}_L}\right) \quad (5\text{-}4)$$

$\tilde{T}_{gen}$, $\tilde{T}_{con}$ and $\tilde{T}_{ev}$ denote the equivalent temperatures of the generator, condenser, and evaporator respectively. The equivalent temperatures $\tilde{T}_H$, $\tilde{T}_C$ and $\tilde{T}_L$ correspond to those of the external fluids and they are calculated in Eqs. (5-5)-(5-7).

$$\tilde{T}_H = \frac{T_8 - T_7}{\ln\frac{T_8}{T_7}} \quad (5\text{-}5)$$

$$\tilde{T}_C = \frac{T_{10} - T_9}{\ln\frac{T_{10}}{T_9}} \quad (5\text{-}6)$$

$$\tilde{T}_L = \frac{T_{12} - T_{11}}{\ln\frac{T_{12}}{T_{11}}} \quad (5\text{-}7)$$

The processes in the pump and hypothetical compressor are assumed non-isentropic, with constant isentropic efficiencies. Based on some geometrical considerations of the *h-s* diagram and the concept of equivalent temperature (Akbari, Sorin and Marcos 2018; Akbari and Sorin 2020), the rates of entropy generation in the compression processes are equal to Eqs. (5-8) and (5-9):

$$\dot{S}_{pump} = \dot{W}_{pump} \cdot \frac{1}{\tilde{T}_{gen}} \cdot \left(1 - \eta_{is,pump}\right) \quad (5\text{-}8)$$

$$\dot{S}_{comp} = \dot{W}_{comp} \cdot \frac{1}{\tilde{T}_{con}} \cdot \left(1 - \eta_{is,comp}\right) \quad (5\text{-}9)$$

The rates of entropy generation in the hypothetical expander and expansion valve are defined as Eqs. (5-10) and (5-11) (Akbari, Sorin and Marcos 2018; Akbari and Sorin 2020):

$$\dot{S}_{exp} = \dot{W}_{exp} \cdot \frac{1}{\tilde{T}_{con}} \cdot \left(\frac{1}{\eta_{is,exp}} - 1\right) \quad (5\text{-}10)$$

$$\dot{S}_{txv} = \frac{\sqrt{1 + \frac{1}{\alpha^2}}}{\sqrt{1 + \frac{1}{\beta^2}}} * \dot{Q}_{con,R} * \sqrt{1 + \left(\frac{1}{\tilde{T}_{con}}\right)^2} \quad (5\text{-}11)$$

$$\alpha = \frac{\dot{Q}_{con,R}}{\frac{\dot{Q}_{ev}}{\tilde{T}_{ev}} + \dot{W}_{comp} \cdot \frac{1}{\tilde{T}_{con}} \cdot \left(1 - \eta_{is,comp}\right)} \quad (5\text{-}12)$$

$$\beta = \frac{\alpha - \tilde{T}_{con}}{1 + \alpha * \tilde{T}_{con}} \quad (5\text{-}13)$$

$\dot{Q}_{con,R}$ denotes the amount of heat transferred in the condenser associated with the mass flow rate of refrigeration subcycle, i.e. $\dot{m}_R$.

The total entropy changes in both hypothetical power and refrigeration subcycles are zero:

$$\dot{S}_{gen} + \dot{S}_{pump} + \dot{S}_{con,P} + \dot{S}_{exp} - \frac{\dot{Q}_{con,P}}{\tilde{T}_C} + \frac{\dot{Q}_{gen}}{\tilde{T}_H} = 0 \quad (5\text{-}14)$$

$$\dot{S}_{ev} + \dot{S}_{comp} + \dot{S}_{con,R} + \dot{S}_{txv} - \frac{\dot{Q}_{con,R}}{\tilde{T}_C} + \frac{\dot{Q}_{ev}}{\tilde{T}_L} = 0 \quad (5\text{-}15)$$

It is worth noting that Eqs. (5-14) and (5-15) and the corresponding entropy generation rates expressed in Eqs. (5-2)-(5-4) and Eqs. (5-7)-(5-10) establish the links between operating parameters of the cycles and the entropy generation rates in the components.

The summation of enthalpy variations in both subcycles result in:

$$\dot{Q}_{gen} + \dot{W}_{pump} - \dot{Q}_{con,P} - \dot{W}_{exp} = 0 \quad (5\text{-}16)$$

$$\dot{Q}_{ev} + \dot{W}_{comp} - \dot{Q}_{con,R} = 0 \quad (5\text{-}17)$$

The assumption of an ejector as a hypothetical expander-compressor system results in two following auxiliary equations:

$$\dot{W}_{exp} = \dot{W}_{comp} \quad (5\text{-}18)$$

$$\frac{\dot{Q}_{con,R}}{\dot{Q}_{con,P}} = \frac{\dot{m}_R}{\dot{m}_P} = ER \quad (5\text{-}19)$$

Eq. (5-18) states that the amount of power consumed by the compressor in the refrigeration subcycle is exactly the same amount of power produced by the expander in the power subcycle.

Furthermore, the amounts of heat transferred in the condenser, in the refrigeration and power subcycles, are related to each other by the ratio of corresponding mass flow rates (Eq. (5-19)), known as ejector entrainment ratio, *ER*.

Another auxiliary equation is needed to link the entropy generation of the hypothetical compressor and expansion processes to the entropy generation of the actual ejector, Eq. (5-20) (Lawrence and Elbel 2015; Haghparast, Sorin and Nesreddine 2018b). This equation states that the product of isentropic efficiencies of hypothetical compressor and expander equals to the ejector efficiency.

$$\eta_{ej} = \eta_{is,exp} \cdot \eta_{is,comp} \qquad (5\text{-}20)$$

It should be mentioned that this efficiency is equivalent to the ratio of the actual entrainment ratio to the isentropic or reversible entrainment ratio that would be achieved for the same inlet and exit states. However, the reversible process cannot be achievable in the case of the ejector, owing to the shock presence inside the ejector.

5-4-2 Problem statement of the system-scale optimization

The optimization problem involves considerations of an objective function as well as a set of equalities and/or inequalities as optimization constraints. The minimization of capital or the maximization of operating performance are criteria that are commonly chosen as an objective function of the optimization problem. Since the heat exchangers play a key role in the overall system cost and the optimal distribution of the total thermal conductance between heat exchangers affects the system performance (Chen, Sun and Wu 2004), the objective function of the optimization problem in this research minimizes the total thermal conductance, for a given cooling load. The proposed objective function can be expressed as:

$$Minimize\ (UA)_{tot} = (UA)_{gen} + (UA)_{con} + (UA)_{ev} \qquad (5\text{-}21)$$

$(UA)_{gen}$, $(UA)_{con}$ and $(UA)_{eva}$ correspond to the thermal conductances of the generator, condenser, and evaporator, respectively:

$$(UA)_{gen} = \frac{\dot{Q}_{gen}}{\Delta T_{LMTD_{gen}}} = \frac{\dot{m}_H c_{P,H}(T_7 - T_8)}{\Delta T_{LMTD_{gen}}} \quad (5\text{-}22)$$

$$(UA)_{con} = \frac{\dot{Q}_{con}}{\Delta T_{LMTD_{con}}} = \frac{\dot{m}_C c_{P,C}(T_{10} - T_9)}{\Delta T_{LMTD_{con}}} \quad (5\text{-}23)$$

$$(UA)_{ev} = \frac{\dot{Q}_{ev}}{\Delta T_{LMTD_{ev}}} = \frac{\dot{m}_l c_{P,L}(T_{11} - T_{12})}{\Delta T_{LMTD_{ev}}} \quad (5\text{-}24)$$

The logarithmic mean temperature differences (LMTDs) for generator, condenser, and evaporator are expressed as:

$$\Delta T_{LMTD_{gen}} = \frac{\left(T_7 - \tilde{T}_{gen}\right) - \left(T_8 - \tilde{T}_{gen}\right)}{\ln \frac{\left(T_7 - \tilde{T}_{gen}\right)}{\left(T_8 - \tilde{T}_{gen}\right)}} \quad (5\text{-}25)$$

$$\Delta T_{LMTD_{con}} = \frac{\left(\tilde{T}_{con} - T_{10}\right) - \left(\tilde{T}_{con} - T_9\right)}{\ln \frac{\left(\tilde{T}_{con} - T_{10}\right)}{\left(\tilde{T}_{con} - T_9\right)}} \quad (5\text{-}26)$$

$$\Delta T_{LMTD_{ev}} = \frac{\left(T_{11} - \tilde{T}_{ev}\right) - \left(T_{12} - \tilde{T}_{ev}\right)}{\ln \frac{\left(T_{11} - \tilde{T}_{ev}\right)}{\left(T_{12} - \tilde{T}_{ev}\right)}} \quad (5\text{-}27)$$

Eqs. (5-16) to (5-19) and (5-22) to (5-27) constitute the optimization problem while satisfying Eqs. (5-14) and (5-15) as well as the following set of inequalities as optimization constraints:

$$\tilde{T}_{gen} < \tilde{T}_H \quad (5\text{-}28)$$

$$\tilde{T}_C < \tilde{T}_{con} \quad (5\text{-}29)$$

$$\tilde{T}_{ev} < \tilde{T}_L \quad (5\text{-}30)$$

$$\Delta T_{min} \geq 2.5 \quad (5\text{-}31)$$

The equality constraints (Eqs. (5-14) and (5-15)) present the second law based analysis of the cycle. They refer to the entropy generation caused by a non-isentropic ejector (hypothetical expander-compressor system) and their links to the cycle variables established by the concept of equivalent temperature. The inequality equations impose some technical constraints on the

optimization problem to control the temperature distributions along the heat exchangers. It must be mentioned that Eq. (5-20) acts as an auxiliary equation that establishes a link between the isentropic efficiencies of hypothetical compressor and expander for each ejector efficiency value.

All variables used in the optimization problem can be categorized into three groups given in Table 5-1. Input variables or known parameters consist of seven variables needed to design the system. Each independent variable is a degree of freedom in the optimization problem, which must be optimal in order to minimize the objective function. The last category is composed of parameters obtained through the optimization problem for each selected independent variable.

Table 5-1: Three categories of optimization problem variables

Input variables	Independent variables	Dependent variables
T_7 , T_9 , T_{11}	$\tilde{T}_{gen}$, $\tilde{T}_{con}$, $\tilde{T}_{ev}$	$(UA)_{gen}$, $(UA)_{con}$, $(UA)_{ev}$
$\dot{m}_H$, $c_{P,H}$, η_{ej}	T_8 , T_{10} , T_{12}	$\dot{S}_{gen}$, $\dot{S}_{pump}$, $\dot{S}_{con}$, $\dot{S}_{exp}$
$\dot{Q}_{ev}$	ER	$\dot{S}_{ev}$, $\dot{S}_{comp}$, $\dot{S}_{exp.valve}$
		$\tilde{T}_H$, $\tilde{T}_C$, $\tilde{T}_L$, $\dot{Q}_{con}$, $\dot{Q}_{ev}$

The purpose of the first step of the approach, i.e., the system-scale optimization problem, is to seek the independent variable values that lead to the minimum total thermal conductance of the system and the optimal distribution of thermal conductance between the evaporator, condenser, and generator for different ejector's efficiencies. It is worth noting that the results of the system-scale optimization problem, as well as some environmental and safety criteria, will be considered for the pre-selection of working fluids among a huge number of potential working fluids. The details of working fluid pre-selection will be presented in section 5-6-1.

5-5 Component-scale design

The component-scale design step can be divided into two categories including the determination of operating conditions and the selection of most appropriate working fluid.

5-5-1 Operating conditions

The key attribute of the optimization problem described in section 5-4 is that it is formulated without recourse to the knowledge of working fluids and their thermo-physical properties. The optimal equivalent temperatures and the mass flow rates ratio (entrainment ratio) obtained through the optimization problem lay the foundation for a systematic approach to select the actual operating conditions of each pre-selected refrigerant including operating pressures, temperatures, and mass flow rates by introducing a reconstruction procedure. The reconstruction procedure proposed herein is based on the differences between the values of equivalent temperature and saturation temperature in the heat transfer processes (which are assumed as ideal constant-pressure processes). Equivalent temperature and saturation temperature are equal when the working fluid undergoes a constant-temperature process (no degrees of subcooling and/or superheating). A superheated state results in an increase in the ratio of enthalpy to entropy variations (equivalent temperature). On the other hand, a subcooled state decreases the equivalent temperature compared to the saturation temperature corresponding to that pressure. In other words, the difference between the saturation temperature and equivalent temperature can be utilized to determine the degrees of superheating (desuperheating) and of subcooling in heat transfer processes. The flow chart of the reconstruction procedure is illustrated in Appendix A complimentary description of the flow chart is given as follows:

- Appendix A shows the methodology for the determination of all thermodynamic states of the cycle, while Appendix B and Appendix C present the governing equations used for the calculation of the refrigerant properties inside the ejector and the 1D thermodynamic model. It must be mentioned that by Eldakamawy et al. (Eldakamawy, Sorin and Brouillette 2017) already validated this 1D model against experimental data, and found that the agreement was good. Moreover, some important constant values for the 1D model such as isentropic and mixing coefficients are listed in Table 5-2.
- The input data for the reconstruction procedure come from the optimization problem (first step of our comprehensive approach) for each ejector efficiency.

- The refrigerant states at the condenser and the evaporator are assumed to be saturated liquid and saturated vapor, respectively.
- Some technical constraints have been imposed throughout the reconstruction procedure to ensure the feasibility of the solution. The minimum approach temperature difference between the refrigerant and the external fluids at the heat exchangers must be greater than or at least 2.5 K. The length to diameter ratio of the ejector constant-area duct is the sole parameter of ejector geometry that has been proposed in Appendix B and Appendix C. Moreover, since refrigerant condensation inside the primary nozzle deteriorates the ejector performance (Eldakamawy, Sorin and Brouillette 2017), the droplet-free expansion is considered as a restriction.

Table 5-2: Constant values used for 1D model

Coefficient	Symbol	value
Primary nozzle isentropic efficiency	η_P	0.95
Secondary nozzle isentropic efficiency	η_S	0.95
Diffuser isentropic efficiency	η_d	0.85
Mixing coefficient	ϕ_m	0.98
Length to diameter ratio of constant-area duct	L/D	13.7
Pump isentropic efficiency	$\eta_{is,pump}$	1

5-5-2 Working fluid selection

Having performed the reconstruction procedure for all pre-selected candidates, individual thermo-physical properties of each candidate lead to different operating states and, in turn, different capital and operating costs. In the early stage of economic analysis, total thermal conductance and COPs of the pre-selected working fluids will be utilized as two economic

indicators to select the optimal working fluid. If two or more candidates are considered equally optimal, the final selection is based on exergoeconomic evaluation. Exergoeconomic evaluation provides us with a clear understanding of the economic performance of the system, which relies on exergy analysis and economic principles. The main outcome of exergoeconomic analysis is the final cost of each product generated by the system. This analysis involves cost balances related to each component of the system. A cost balance simply expresses that the total cost of the exergy streams leaving the component equals the total cost of the entering streams plus the capital investment of the component and its operating and maintenance expenses (Bejan, Tsatsaronis and Moran 1996):

$$\sum_{out}\left(c_{out}\dot{E}_{out}\right)_k + c_{w,k}\dot{W}_k = c_{q,k}\dot{E}_{q,k} + \sum_{in}\left(c_{in}\dot{E}_{in}\right)_k + \dot{Z}_k \quad (5\text{-}32)$$

$$C_j = c_j\dot{E}_j \quad (5\text{-}33)$$

Here C_j (\$/h) is the cost rate associated with each exergy stream, c_{out}, c_{in}, c_w and c_q represent the exergetic costs, i.e., cost per unit of exergy (\$/GJ), of the streams and $\dot{Z}_k$ (\$/h) denotes the sum of the capital investment and the operating and maintenance cost rates of the *k*th component and can be calculated as (Salimpour, Ahmadzadeh and Al-Sammarraie 2019):

$$\dot{Z}_k = \frac{(CRF \times \varphi)I_k}{N} \quad (5\text{-}34)$$

$$CRF = \frac{i(1+i)^n}{(1+i)^n - 1} \quad (5\text{-}35)$$

In Eqs. (5-34) and (5-35), CRF is the capital recovery factor, φ is the operating and maintenance factor, I_k represents the purchase cost of the *k*th component (Table 5-3), *N* is annual operating hours, i is the interest rate and *n* is the lifetime of the system (Salimpour, Ahmadzadeh and Al-Sammarraie 2019).

Table 5-3: Component cost functions

Component	Cost function (I_k)
Generator (Salimpour, Ahmadzadeh and Al-Sammarraie 2019)	$17500\left({A_{gen}}/{100}\right)^{0.6}$
Pump (Mehrpooya and Mousavi 2018)	$1120 \times \dot{W}_{pump}{}^{0.8}$
Condenser (Salimpour, Ahmadzadeh and Al-Sammarraie 2019)	$8000\left({A_{con}}/{100}\right)^{0.6}$
Evaporator (Salimpour, Ahmadzadeh and Al-Sammarraie 2019)	$16000\left({A_{ev}}/{100}\right)^{0.6}$
Ejector (Samaké, Galanis and Sorin 2018)	$15962.46(\dot{m}_P + \dot{m}_R)\left({T_{ev}}/{P_{ev}}\right)^{0.05} P_{con}{}^{-0.75}$
Expansion valve (Mohammadi and McGowan 2019)	$114 \times \dot{m}_R$

The exergy rates leaving or entering a component, as well as the exergy associated with the heat transfer, are calculated through Eqs. (5-36) and (5-37).

$$\dot{E}_{in} = \dot{m}(h_{in} - h_r) - T_0(s_{in} - s_r) \quad (5\text{-}36)$$

$$\dot{E}_q = \dot{Q}\left(1 - {T_r}/{\tilde{T}}\right) \quad (5\text{-}37)$$

In Eq. (5-32), the cost rates of all entering streams in a component, including material streams and energy streams, are known from the components they exit or from the energy costs. The cost rates of exiting streams in Eq. (5-32) are unknown variables that must be calculated for all system components. Since there are three components, which each have more than one exiting stream, i.e., generator, condenser and evaporator, the unknown variables cannot be obtained without using appropriate auxiliary equations. The cost balance and auxiliary equations for each component are indicated in Table 5-4.

Table 5-4: Cost balance and auxiliary equation of each component

Component	Cost balance	Auxiliary equation
Generator	$C_4 = C_3 + C_7 - C_8 + \dot{Z}_{gen}$	$c_7 = c_8$
Pump	$C_3 = C_2 + C_{W,pump} + \dot{Z}_{pump}$	$- - -$
Condenser	$C_2 = C_1 + C_9 - C_{10} + \dot{Z}_{con}$	$c_2 = c_1$
Evaporator	$C_6 = C_5 + C_{11} - C_{12} + \dot{Z}_{ev}$	$c_5 = c_6$
Ejector	$C_1 = C_4 + C_6 + \dot{Z}_{ej}$	$- - -$
Expansion valve	$C_5 = C_2 + \dot{Z}_{txv}$	$- - -$

Finally, the value of C_{12}, i.e., the cooling load cost rate, determines which pre-selected refrigerant is the most appropriate one for the proposed design conditions.

5-6 Practical case study

By using a solar ERS proposed by Salimpour et al. (Salimpour, Ahmadzadeh and Al-Sammarraie 2019) as a case study, for the given inlet conditions of external reservoirs in Table 5-5, the application of our comprehensive approach will be demonstrated and its advantages compared to the existing approach will be presented in section 5-7.

Table 5-5: External fluids operating conditions and desired cooling load

T_7 (K)	T_9 (K)	T_{11} (K)	$c_{P,H}$ $(kJ/kg.K)$	$c_{P,C}$ $(kJ/kg.K)$	$c_{P,L}$ $(kJ/kg.K)$	$\dot{m}_H$ (kg/s)	$\dot{Q}_{ev}$ (kW)
377	303	293	4.22	4.18	1.01	0.6	5

5-6-1 System-scale optimization

The Fmincon function in MATLAB was used to perform the system-scale optimization problem as the first step of the comprehensive approach. Lawrence and Elbel (Lawrence and Elbel 2015) stated that the maximum ejector efficiency reported in the open literature is about 0.3. However,

the optimization problem herein was performed for different ejector efficiencies up to 0.4. The optimal equivalent temperatures of the generator, condenser, and evaporator, as well as the entrainment ratio and the resultant performance of the system for each ejector efficiency, are shown in Table 5-6.

Table 5-6: System-scale performance optimization results for the case study, with ejector efficiency as a parameter

η_{ej} $(-)$	$\tilde{T}_{gen}$ (K)	$\tilde{T}_{con}$ (K)	$\tilde{T}_{ev}$ (K)	ER $(-)$	$\dot{Q}_{gen}$ (kW)	COP $(-)$	UA_{tot} (kW/K)
0.4	350.0	318.8	288.5	0.416	15.61	0.32	3.525
0.3	353.2	316.9	288.5	0.381	16.53	0.30	3.995
0.2	355.8	315.3	288.5	0.301	21.22	0.23	5.134
0.1	353.4	312.9	288.5	0.168	38.69	0.13	9.203

The optimal results and the inlet conditions of the external fluids will be used to specify the upper and lower bounds of the operating system temperatures and assist in establishing thermodynamic criteria for the pre-selection of potential working fluids. The critical temperature of the working fluid candidate must be hotter than the maximum possible temperature of the system, i.e. hotter than the temperature of the inlet temperature of the external fluid entering the generator. Furthermore, based on the assumption of no superheating degree at the evaporator outlet (see section 5-5), the evaporator equivalent temperature equals to the refrigerant evaporation temperature. In order to avoid sub-atmospheric pressure in the evaporator, the working fluid candidate must have an atmospheric pressure boiling temperature that is lower than the evaporator equivalent temperature. This candidate criterion is a consequence of the observation that the evaporator equivalent temperature is the lowest possible operating temperature of the system working fluid. Environmental characteristics of working fluid candidates are other criteria that must be considered during the working fluid pre-selection. Under international agreements, the following environmental criteria must be satisfied: working fluids must have negligible ozone depletion potential (ODP), and a global warming potential (GWP) lower than 2500 (Eldakamawy, Sorin and Brouillette 2017). The pre-

selected working fluids, as well as their associated thermodynamic, environmental and safety selection criteria parameters, are listed in Table 5-7. R245fa is the only refrigerant among the pre-selected candidates that has no flame propagation potential. It is, nevertheless, relatively toxic and has the highest GWP. From the flammability viewpoint, R1234ze is the second safest operation condition fluid, with a very low GWP and no toxicity. Although the other fluids have very low GWP values, they are highly flammable if any leakage were to occur.

Table 5-7: Comparison of pre-selected working fluids showing selection criteria parameters (*ASHRAE Handbook-Fundamentals* 2017)

Working Fluids	$T_{critical}$ (K)	$T_{boil}@1^{atm}$ (K)	ODP	GWP	Safety[3]
R600a	407.9	261.4	0	20	A3
R600	425.2	272.7	0	20	A3
1butene	419.3	266.8	0	20	A3
R245fa	427.2	288.3	0	1030	B1
R1234ze	382.6	254.2	0	6	A2L

5-6-2 Component-scale design

Having performed the optimization problem and pre-selected the potential working fluids, the actual operating temperatures and pressures of the system states can be determined using the reconstruction procedure. The reconstruction computational procedure started with the ejector efficiency of 0.4 in descending order by using the optimal equivalent temperatures of the evaporator, condenser, and generator, as well as optimal entrainment ratio corresponding to the ejector efficiency, until the constraints mentioned in section 5-4-2 and Appendix C were satisfied. Table 5-8 shows the results of the reconstruction procedure, i.e. component-scale design, for the working fluids under investigation where the thermodynamic properties of refrigerants were taken from the REFPROP libraries. $\Delta T_{sh,con}$ and $\Delta T_{sh,gen}$ represent the degree of desuperheating at the condenser and superheating degree at the generator outlets,

[3] A: no toxicity, B: toxicity, 1: no flame propagation, 2-2L: low flammability, 3: high flammability

respectively. Table 5-8 shows that none of the working fluids under investigation requires a superheating process at the generator outlet.

Table 5-8: Actual operating conditions for different working fluids obtained by the reconstruction procedure

Working Fluids		R600a	R600	1butene	R245fa	R1234ze
$\dot{m}_P$	(kg/s)	0.0466	0.0423	0.0415	0.0835	0.0939
$\dot{m}_s$	(kg/s)	0.018	0.016	0.016	0.0305	0.0357
P_{gen}	(kPa)	1741.4	1285.0	1585.3	1074.1	2502.1
P_{con}	(kPa)	533.7	377.2	460.9	244.8	756.2
P_{ev}	(kPa)	259.0	176.1	216.9	102.2	364.2
$\Delta T_{sh,gen}$	(°C)	0	0	0	0	0
$\Delta T_{sh,con}$	(°C)	18.6	21.2	19.1	22.4	22.6
η_{ej}	$(-)$	0.23	0.22	0.23	0.21	0.22
$\dot{Q}_{gen}$	(kW)	17.33	17.51	16.60	18.21	18.03
$\dot{W}_{Pump}$	(kW)	0.11	0.07	0.08	0.05	0.15

The reconstruction procedure results in different thermodynamic states for different working fluids even for that have the same ejector efficiency (See R600 and R1234ze or R600a and 1butene in Table 5-8). These discrepancies are mainly caused by their individual thermo-physical properties. Thus, the economic performance resulting from each refrigerant must be determined to select the most appropriate working fluid among the pre-selected candidates. The economic performance of the system includes the total capital investment, operating and maintenance expenses of the system's components and the operating cost. In the early stage of an economic analysis of the system, the comparison of the total thermal conductance as an indicator of the system capital cost and the coefficient of performance (COP) as an indicator of the system operating cost can give us a good picture of the economic performance of the system. These two economic parameters for each working fluid are shown in Figure 5-3. The figure reveals the superiority of 1butene and R600a over their rivals, where 1butene has the highest COP, while R600a needs the lowest total thermal conductance. This means that the optimal

refrigerant must be selected between 1butene and isobutane (R600a). It should be mentioned that the optimization curve, shown in Figure 5-3, indicates the minimum required total thermal conductance of the system that corresponds to each COP value. Replacing the optimal equivalent temperatures with the actual operating temperatures for each candidate by performing the reconstruction procedure, results in a higher value of total thermal conductance in the real systems. For instance, R600a requires at least 5.231 (kW/K) total thermal conductance to achieve a COP of 0.29. This amount of total thermal conductance is about 15% greater than that of thermal conductance for the same COP in the optimization curve.

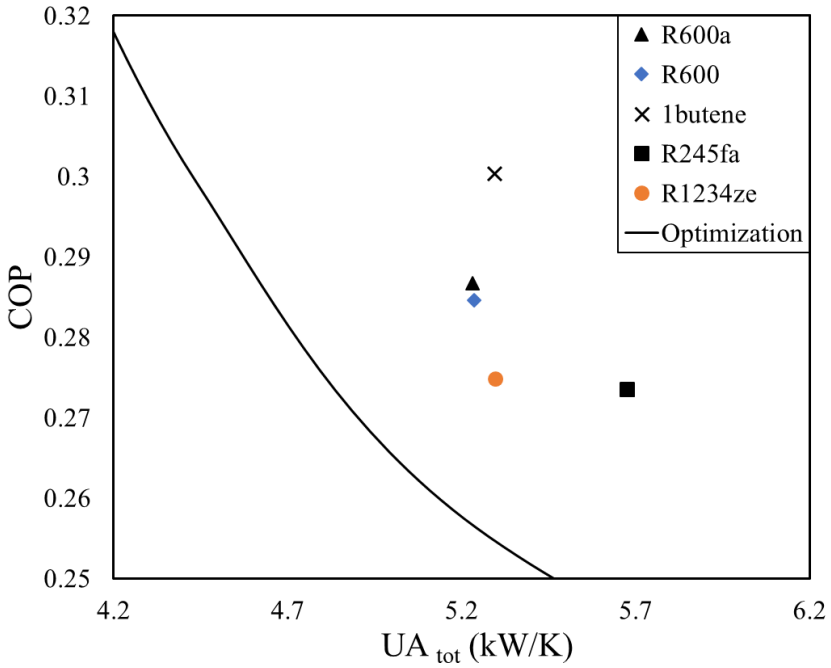

Figure 5-3: Economic performance indicators for pre-selected refrigerants

In order to facilitate the selection of the most appropriate working fluid between these two remaining candidates, exergoeconomic analysis was conducted to evaluate the final cost of cooling load resulted from 1butene and R600a. The exergoeconomic analysis was carried out based on some required input parameters given in Table 5-9. The set of simultaneous equations, including cost balance and auxiliary equations for each component, in Table 5-4, were solved

and the results are indicated in Table 5-10. Figure 5-1 shows the placement of the streams and W.F. refers to the working fluid.

Table 5-9: Input parameters for exergoeconomic analysis (Rostamnejad Takleh and Zare 2019)

Parameter	Unit	Value
Generator overall heat transfer coefficient, U_{gen}	$kW/(m^2.K)$	1.3
Condenser overall heat transfer coefficient, U_{con}	$kW/(m^2.K)$	0.5
Evaporator overall heat transfer coefficient, U_{ev}	$kW/(m^2.K)$	1.1
Operating and maintenance factor, φ	$---$	1.06
annually number of operating hours, N	$---$	7446
Lifetime of system, n	$year$	20
Interest rate, i	(%)	10
Cost of required electric power to run pump, $c_{w,pump}$	$\$/GJ$	10
Cost of solar source per 1 ℃	$\$/GJ$	2.086
Environment temperature, T_r	K	293
Environment pressure, P_r	kPa	101.3

Table 5-10: Exergoeconomic results of each stream

State (↓)	Temperature (K)		Mass flow rate (kg/s)		Exergy (kW)		Cost rate $(\$/h)$		Exergetic cost $(\$/GJ)$	
W.F. (→)	R600a	1butene	R600a	1butene	R600a	1butene	R600a	1butene	R600a	1butene
1	331.9	332.5	0.065	0.057	4.446	3.751	0.614	0.497	38.35	36.8
2	313.3	313.4	0.065	0.057	2.927	2.286	0.404	0.303	38.35	36.8
3	314	314	0.047	0.041	2.218	1.732	0.295	0.221	36.91	35.47
4	366.3	367.4	0.047	0.041	5.273	4.727	0.514	0.425	27.06	24.96
5	288.5	288.5	0.018	0.016	0.760	0.589	0.113	0.084	41.19	39.73
6	288.5	288.5	0.018	0.016	0.676	0.505	0.100	0.072	41.19	39.73
7	377	377	0.6	0.6	19.80	19.80	1.018	0.974	14.28	13.67
8	370.1	370.4	0.6	0.6	15.93	16.10	0.819	0.792	14.28	13.67
9	303	303	2.284	2.2	1.641	1.584	0	0	0	0
10	305.5	305.5	2.284	2.2	0.890	0.859	0.231	0.215	72.13	69.57
11	293	293	2.475	2.48	0	0	---	---	---	---
12	291	291	2.475	2.48	0.071	0.071	0.032	0.031	122.75	120.73

Table 5-10 reveals that the system operating with 1butene resulted in a 3% lower value of the final product cost, $C_{12} = 0.031(\$/h)$, i.e., cooling load cost, compared to the system operating with R600a, $C_{12} = 0.032(\$/h)$. Hence, 1butene is selected as the most appropriate working fluid for the proposed ERS.

5-7 Validation of results

In order to show the advantages of our comprehensive approach, a previous thermodynamic design approach presented in the literature (Dahmani, Aidoun and Galanis 2011; Grazzini, Milazzo and Paganini 2012; Eldakamawy, Sorin and Brouillette 2017) was applied to the case study given in Table 5-5. In their design approach, six temperature differences in the heat exchangers shown in Figure 5-4 were proposed as degrees of freedom. The main disadvantage of their approach is the huge number of possible permutations that must be investigated. For instance, if there are only five possibilities for each temperature difference value, we must investigate 5^6=15625 different system configurations. To facilitate the design problem, Dahmani et al. (Dahmani, Aidoun and Galanis 2011) and Eldakamawy et al. (Eldakamawy, Sorin and Brouillette 2017) made the following assumptions:

$$\Delta T_1 = \Delta T_3 = \Delta T_6 = \Delta T \tag{5-38}$$

$$\Delta T_2 = \Delta T_4 = \Delta T_5 = {}^{\Delta T}/_{2} \tag{5-39}$$

They reduced the degrees of freedom of their design problem from six to one by using Eqs. (5-38) and (5-39), then considered different values of ΔT to find the optimal one based on the economic performance criteria.

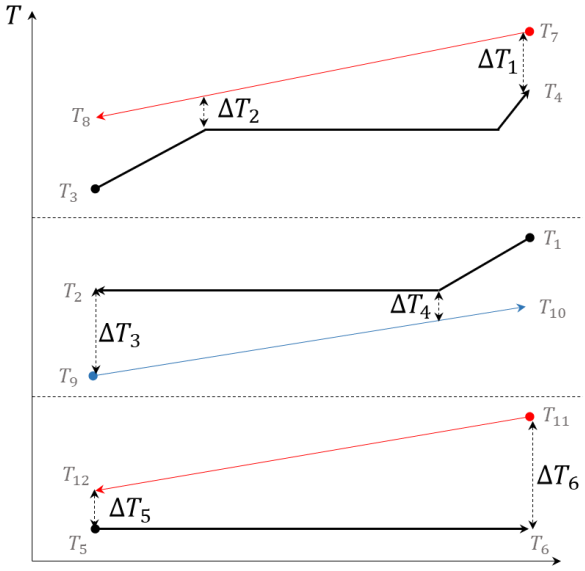

Figure 5-4: Temperature evolution in the heat exchangers

Dahmani's approach was applied to our case study and the resulting operating conditions, as well as the optimal temperature difference for the refrigerants under investigation, are given in Table 5-11.

Table 5-11: The operating conditions obtained by the design approach introduced by (Dahmani, Aidoun and Galanis 2011; Eldakamawy, Sorin and Brouillette 2017).

Working Fluids		R600a	R600	1butene	R245fa	R1234ze
$\dot{m}_P$	(kg/s)	0.0586	0.0412	0.0524	0.0961	0.1401
$\dot{m}_s$	(kg/s)	0.0182	0.0161	0.0161	0.0306	0.0362
P_{gen}	(kPa)	1780.1	1398.3	1588.7	1117.9	2728.0
P_{con}	(kPa)	517.4	357.8	445.1	234.4	746.0
P_{ev}	(kPa)	227.9	159.1	189.9	89.2	318.9
$\Delta T_{sh,gen}$	(°C)	0	0	1.1	1.4	0
$\Delta T_{sh,con}$	(°C)	22.1	23.7	22.2	25.3	11.5
$\dot{Q}_{gen}$	(kW)	22.13	17.45	21.20	21.37	24.29
$\dot{W}_{Pump}$	(kW)	0.14	0.07	0.10	0.07	0.25
ΔT_{opt}	(K)	9	8	9	8	9

The comparisons between the proposed two economic indicators (UA and COP) resulting from our comprehensive approach and the Dahmani's approach are illustrated in Figure 5-5 and Figure 5-6. Two remarks may be made from these figures. Firstly, the design approach introduced in this paper resulted in better performances from the capital and operating costs points of view for all working fluids under investigation. Secondly, the optimal working fluids selected by the two approaches are different. According to the resultant operating conditions obtained by our approach, 1butene showed the best economic performance, while according to Dahmani's approach R600 would be the optimal candidate.

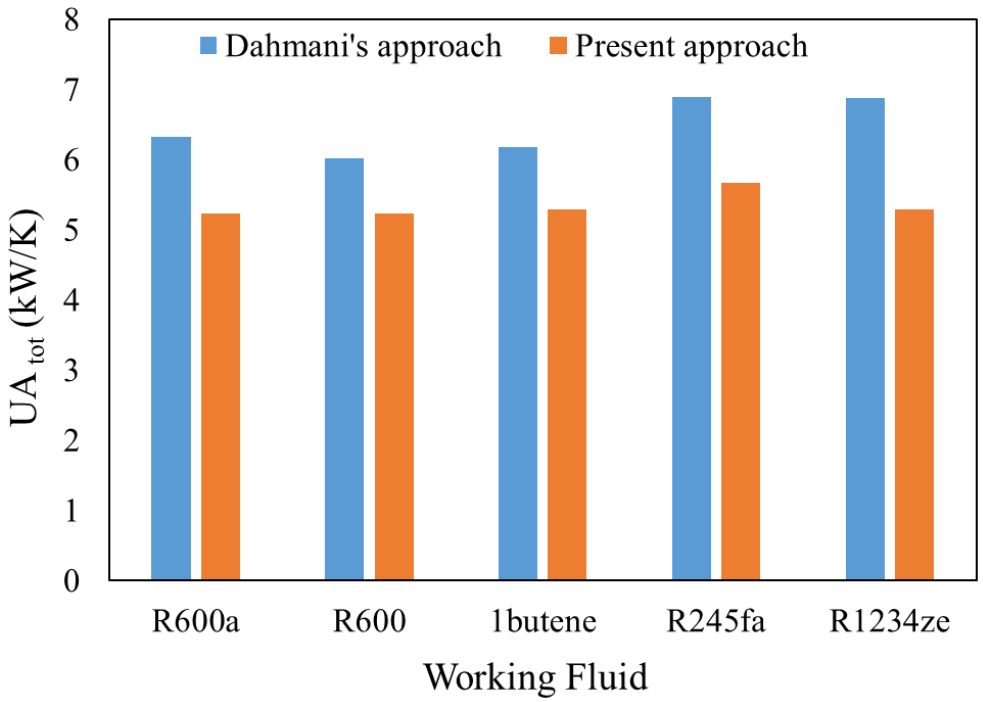

Figure 5-5: Total thermal conductance comparison resulting from Dahmani's approach and the present work

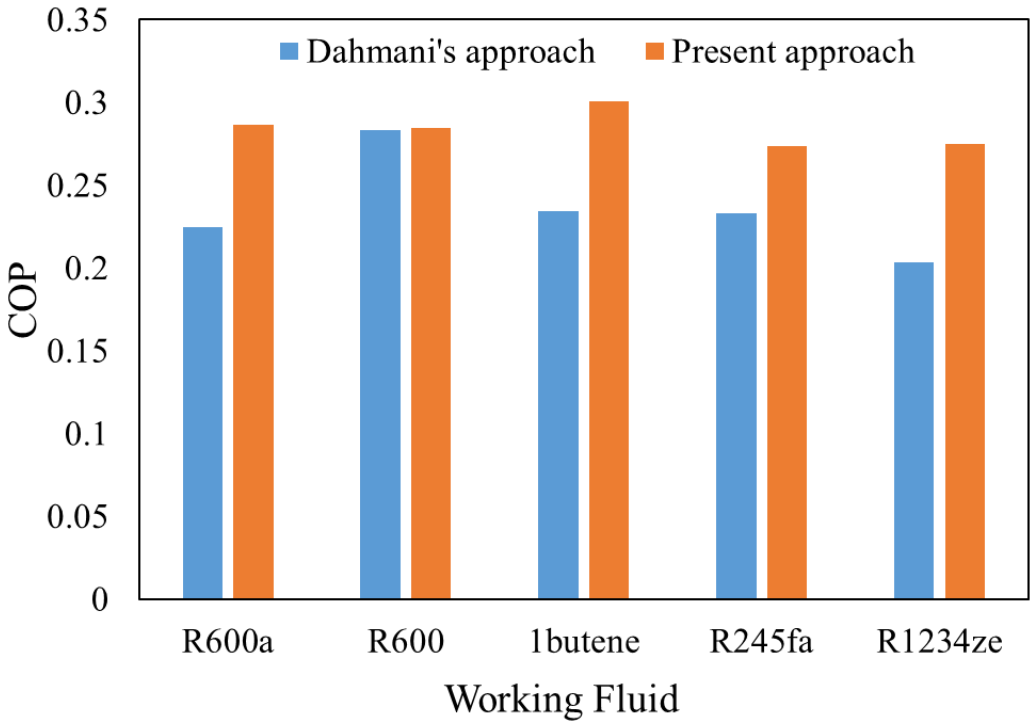

Figure 5-6: COP comparison resulting from Dahmani's approach and the present work

The comparison made above reveals that the assumptions of Eqs. (5-38) and (5-39) prevent us from finding the optimal operating conditions of the system. Moreover, the huge number of possible permutations for six temperature differences existed in Figure 5-6 makes the design problem a time-consuming and cumbersome process. One of the advantages of our approach is that these temperature differences are automatically calculated throughout the reconstruction procedure and only a minimum possible value is introduced (2.5 K, in Section 5-5) to ensure the feasibility of temperature distribution along the heat exchangers.

5-8 Conclusion

The comprehensive approach introduced in this paper presented a novel systematic approach for the selection of the most appropriate working fluid as well as its optimal operating conditions for ERS. First, the system-scale optimization was performed, independent of working fluids, based solely on the inlet conditions of external sources. Minimization of the total system thermal conductance was chosen as the objective function and the optimization problem was constrained by a second-law analysis of the system by using an equivalent

temperature based model. To simplify the complexity of phenomena inside the ejector, it was replaced by a hypothetical expander-compressor, and then the entropy generation rate inside the ejector was characterized by using the efficiency of the ejector. The optimal variables including the ejector's entrainment ratio and the equivalent temperatures of the isobaric processes were subsequently determined. The resultant equivalent temperature of the evaporator, then, was considered as a thermodynamic criterion for the pre-selection of working fluids among a huge number of potential working fluids. Moreover, the optimization results laid the foundations for a component-scale design model, i.e., reconstruction procedure, where the actual operating conditions including temperatures and pressures, as well as mass flow rates, corresponding to each potential working fluid, were systematically determined. Afterward, an early observation emerged from comparisons of total thermal conductance and coefficient of performance for each pre-selected working fluid, resulting in a reduction of optimal working fluid candidates. Finally, a detailed economic analysis determined the most appropriate working fluid and its corresponding operating conditions. The proposed approach was applied to a practical case study and was compared to the existing thermodynamic models in the literature. In this case study, the system-scale optimization established a thermodynamic criterion to pre-select five potential refrigerants, i.e., R600, R600a, 1butene, R245fa, and R1234ze, among a large number of candidates existing in the literature. Then, the reconstruction procedure results were used to compare COPs and total thermal conductance of each working fluid. The results revealed that the optimal refrigerant would be either R600a or 1butene, since R600a needed the lowest total thermal conductance, while 1butene showed the highest COP. In order to facilitate the final selection, an exergoeconomic analysis was conducted. It revealed that 1butene resulted in a 3% lower value of the final product cost, i.e., cooling load cost, compared to the system operating with R600a. Through a comparison of the present approach and another systematic approach existed in the literature, the present work has resulted in better performances from the capital and operating costs points of view for all working fluids under investigation. The new approach also automatically determined the optimal thermodynamic states of each potential working fluid without any preliminary assumption about temperature distributions. Furthermore, the present approach provided the minimum thermal conductance versus the corresponding COP curve, independent of working fluid.

5-9 Acknowledgments

This project is a part of the Collaborative Research and Development (CRD) Grants Program at “Université de Sherbrooke”. The authors acknowledge the support of the Natural Sciences and Engineering Research Council of Canada, Hydro-Québec, Rio Tinto, Alcan and Canmet ENERGY Research Center of Natural Resources Canada (RDCPJ451917-13).

5-10 Appendices

5-10-1 Appendix A

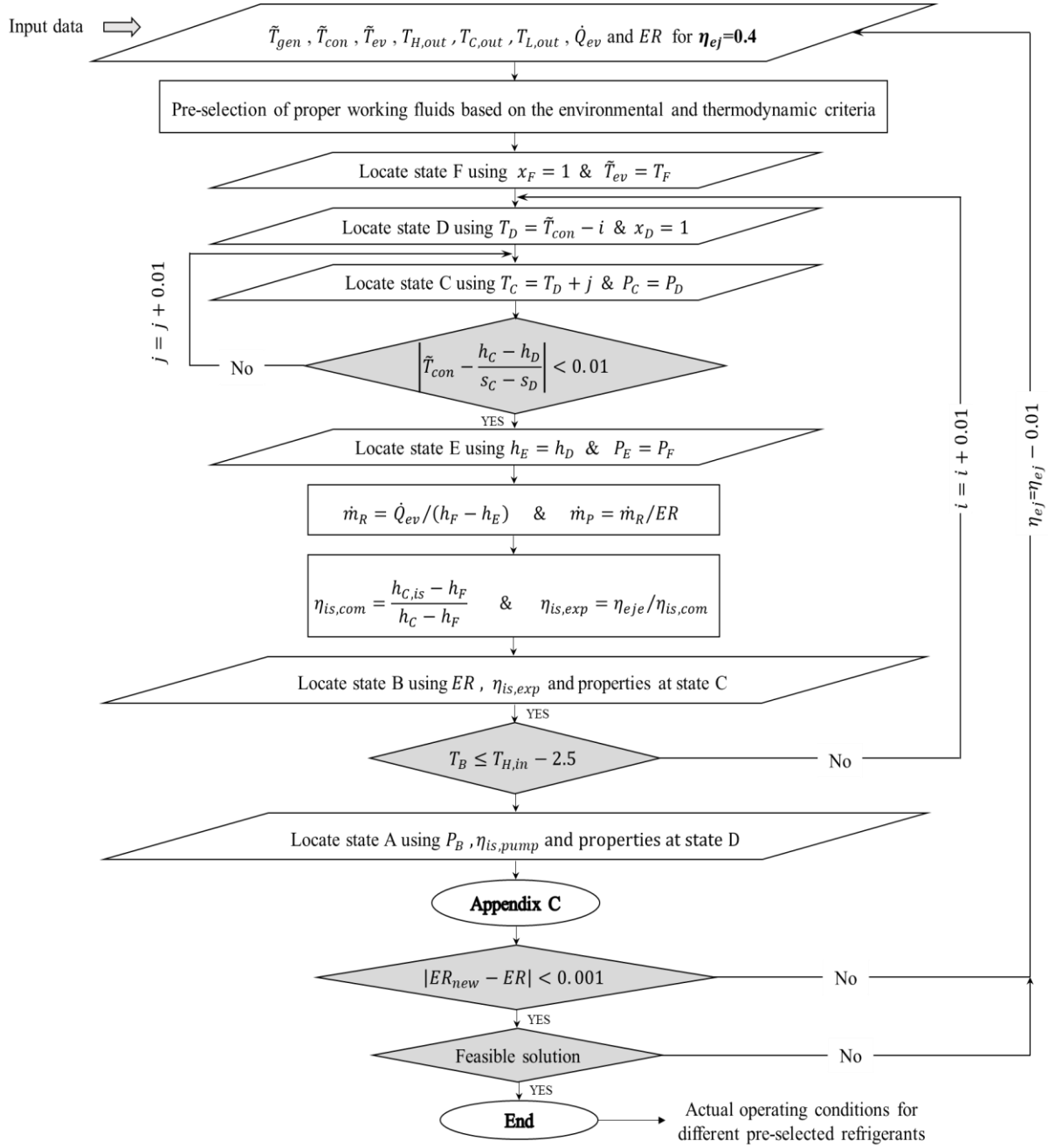

Figure 5-7: Reconstruction procedure algorithm

5-10-2 Appendix B

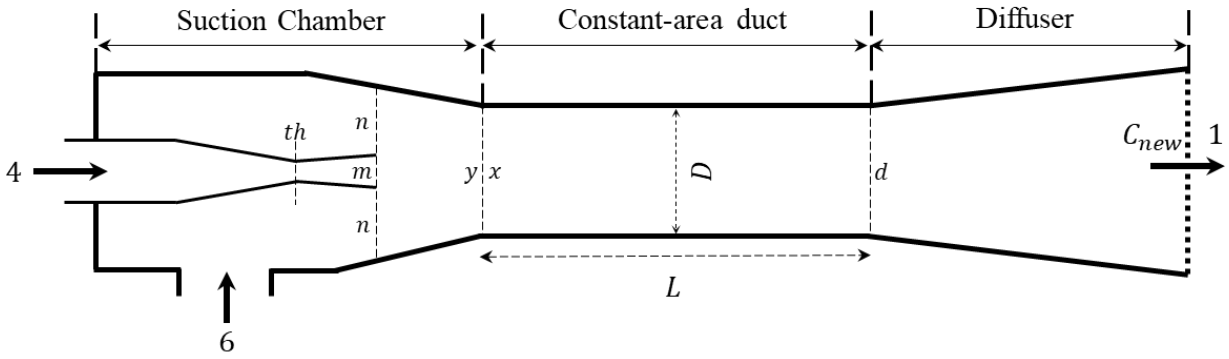

Figure 5-8: Ejector's layout

Table 5-12: Governing equations for different states inside the ejector

State	Equations
n	$s_{n_{is}} = s_6 \quad \& \quad P_{n_{is}} = P_n \quad \& \quad \eta_s = \frac{(h_6 - h_n)}{(h_6 - h_{n_{is}})} \quad \& \quad c_n = \sqrt{2(h_6 - h_n)} \quad \& \quad G_n = \frac{c_n}{\nu_n}$
m	$s_{m_{is}} = s_4 \quad \& \quad P_{m_{is}} = P_m = P_n = P_y \quad \& \quad \eta_p = \frac{(h_4 - h_m)}{(h_4 - h_{m_{is}})} \quad \& \quad c_m = \sqrt{2(h_4 - h_m)}$
y	$c_y = \varphi_m \frac{(c_m + w \cdot c_n)}{(1 + w)} \quad \& \quad h_y = \frac{(h_m + (c_m^2)/2 + w \cdot h_n + w\,(c_n^2)/2)}{(1 + w)} - \frac{(c_y^2)}{2}$
x	$c_x = \nu_x \cdot \frac{c_y}{\nu_y} \quad \& \quad P_x = P_y + \frac{(c_y^2)}{\nu_y} - \frac{(c_x^2)}{\nu_x} \quad \& \quad h_x = h_y + \frac{(c_y^2)}{2} - \frac{(c_x^2)}{2}$
d	$\frac{1}{\sqrt{f}} = 2\,log(Re\sqrt{f}) - 0.8 \quad \& \quad c_d = \nu_d \cdot \frac{c_x}{\nu_x} \quad \& \quad h_d = h_x + \frac{(c_x^2)}{2} - \frac{(c_d^2)}{2} \quad \& \quad P_d = \frac{c_x^2}{\nu_x} + P_x - \frac{c_d^2}{\nu_d} - \left[f \cdot \frac{L}{D} \cdot \frac{c_{avg}^2}{2\nu_{avg}}\right]$
C_{new}	$\eta_d = \frac{h_{C_{new,is}} - h_d}{h_{C_{new}} - h_d}$

5-10-3 Appendix C

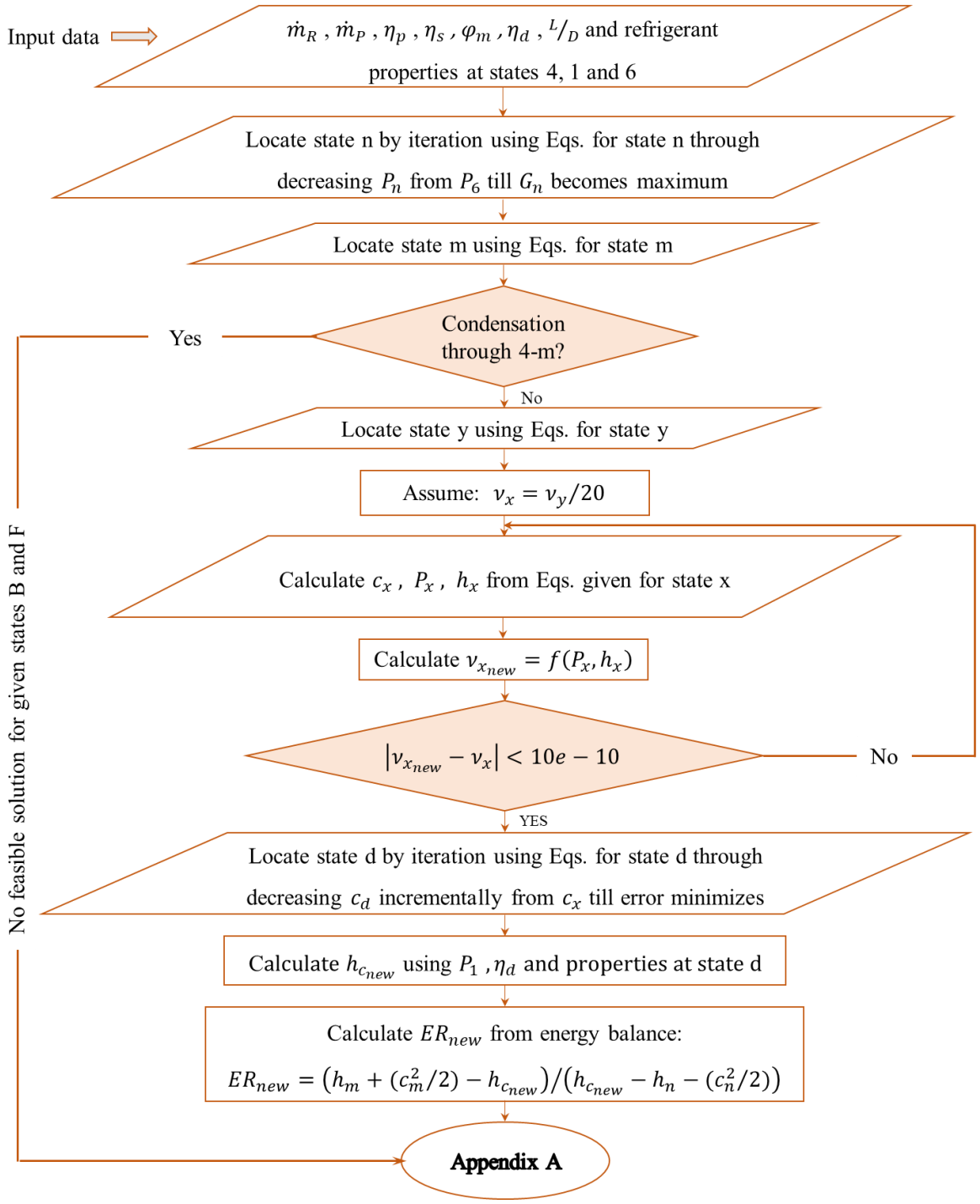

Figure 5-9: ejector's 1-D thermodynamic model

5-11 Nomenclature

A	surface area (m^2)
C	cost rate associated with exergy stream ($/h)
CRF	capital recovery factor
$\dot{E}$	exergy rate (kW)
ER	entrainment ratio
I	component cost, $
N	annual operating hours (hr)
P	pressure (kPa)
$\dot{Q}$	thermal power (kW)
$\dot{S}$	entropy generation rate (kW/K)
T	temperature (°C or K)
$\tilde{T}$	equivalent temperature (K)
UA	thermal conductance (kW/K)
$\dot{W}$	power (kW)
$\dot{Z}$	capital investment cost rate ($/h)
c	velocity (m/s)
c_p	heat capacity at constant pressure (kJ/kg-K)
h	enthalpy (kJ/kg)
i	interest rate (%)
$\dot{m}$	mass flow rate (kg/s)

n	lifetime of system (year)
s	entropy (kJ/kg-K)

Subscripts

C	cooling water
H	high temperature
L	low temperature
$LMTD$	logarithmic mean temperature difference
P	power subcycle
R	refrigeration subcycle
con	condenser
com	compressor
ev	evaporator
exp	expander
txv	thermal expansion valve
gen	generator
f	saturated liquid
g	saturated vapor
is	isentropic
in	inlet
opt	optimal
out	outlet

r	reference state
sh	condenser desuperheating and generator superheating
tot	total

Greek letters

Δ	difference
ν	specific volume (m^3/kg)
η	efficiency
φ	operating and maintenance factor

Chapter 6

EJECTOR DESIGN

This chapter presents the local-scale analysis of the ejector to design the final geometry parameters of the ejector that lead to the optimal operating conditions for the selected working fluid. In the previous chapter, the optimal refrigerant and its operating conditions were determined by using the system-scale optimization and the component-scale design. These conditions cannot be achievable unless the ejector has appropriate geometry characteristics. Since the fluid flow inside an ejector is complex, 1D models cannot accurately predict the ejector geometry parameters. In this case, computational fluid dynamics (CFD) simulation is a useful tool to find the appropriate ejector geometry parameters.

6-1 Ejector geometry parameters

An Ejector is a simple mechanical component, as shown in Figure 5-8, which has drawn the attention of engineers as it has a long lifespan and low maintenance costs. The working process of an ejector is explained in section 5-3. The effectiveness of the ejector depends heavily on its geometry parameters such as converging and diverging angles and the throat diameter of the primary nozzle, nozzle exit position, constant-area duct length and diameter, and diffuser diameter and diverging angle. Yan et al. (Yan, Cai and Li 2012) used a CFD model validated by the experimental results to evaluate the effect of key geometry parameters on the ejector entrainment ratio and found the optimal design parameters. They found that the performance of the ejector is more sensitive to the primary nozzle exit position and the area ratio between the constant-area duct and primary nozzle throat than other geometry parameters. Zhu et al. (Zhu *et al.* 2009) employed the CFD technique to generate 95 different ejector geometries, in order to investigate the influence of primary nozzle exit positions and the mixing (suction) chamber diverging angle on the ejector performance. They stated that the acceleration of the secondary

flow in the suction chamber is proportional to the primary nozzle exit position. Thus, this parameter should be properly selected to have an ejector with a high entrainment ratio. They also showed that a slight change in the mixing chamber diverging angle, especially near its optimum value, can make a significant change in the ejector performance. In another study, Varga et al. (Varga, Oliveira and Diaconu 2009) investigated three geometrical factors, the primary nozzle exit position, the area ratio between the constant-area duct and primary nozzle throat, and constant-area section length by using a CFD model. Their results indicated that although an increase in the area ratio considerably improves the entrainment ratio, this increase results in a decrease in the critical back pressure for the set of operating conditions under investigation. Moreover, their results showed that the constant-area section length does not affect the ejector entrainment ratio.

6-2 CFD Model

In this study, the ejector CFD simulation was performed using the ANSYS Fluent V. 19 commercial software package. This software is based on the finite volume method, in which the computational domain is divided into small volumes. The governing equations are then applied to each subdivision by converting to corresponding algebraic equations that can be solved numerically. The second-order accurate discretization scheme was used in this study for all equations, except for the pressure equation where the PRESTO! (PREssure Staggering Option) scheme that is specially introduced for flow experiencing steep pressure gradients. Moreover, a high-order term relaxation ($f = 0.25$) through the entire computation was applied to guarantee smooth convergence. The set of algebraic equations resulted from the discretization was solved herein using the coupled pressure-based algorithm. This algorithm, first, solves implicitly the pressure-based continuity and the momentum together (ANSYS Inc. 2013). The energy equation is, then, solved in the next step and density is calculated through the gas property model. It must be mentioned that the REFPROP v9.1 database equation was used as the gas property model in this study. Moreover, the ejector flow domain was assumed to be steady state and axi-symmetric.

6-3 Validation

Since there is no experimental test in the literature that was operated with 1butene as its working fluid in the case of the ejector refrigeration system, we applied our proposed CFD model to two different sets of experimental tests with two different working fluids and different ejector geometries. It should be noted that convergence criteria for the CFD model are met when the residual for all equations were under 10^{-5} and mass imbalance is under 1% of the primary mass flow rate. The schematic of the ejector and the main characteristics of both ejectors were illustrated in Figure 6-1 and Table 6-1 respectively.

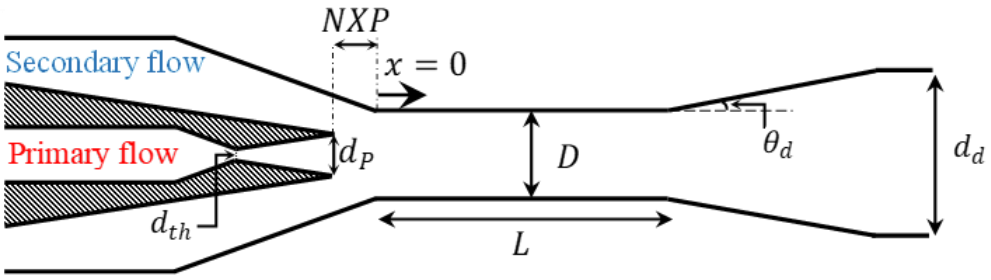

Figure 6-1: Schematic of the ejector geometry

Table 6-1: Main dimensions of the two ejectors used to validate the proposed CFD model, case 1 (Butrymowicz *et al.* 2014) *and case 2* (Croquer 2018)

Geometry parameter	Value	
	Case 1	Case 2
Primary nozzle throat diameter, d_{th}, [mm]	3.50	2.00
Primary nozzle exit diameter, d_P, [mm]	4.69	3.00
Nozzle exit position, NXP, [mm]	-5.00	-5.38
Constant-area section length, L, [mm]	82.00	41.39
Constant-area section diameter, D, [mm]	6.00	4.80
Diffuser diverging angle, θ_d, [deg]	5.00	4.76
Diffuser exit diameter, d_d, [mm]	18.00	20.00
Working fluid	R600a	R134a

The corresponding operating conditions for both cases are summarized in Table 6-2.

Table 6-2: Operating conditions of both cases used to validate the proposed CFD

Operating parameter	Value	
	Case 1	Case 2
Primary flow pressure, [kPa]	940.0	2888.8
Primary flow temperature [°C]	71.5	94.4
Secondary flow pressure, [kPa]	200	414.6
Secondary flow temperature [°C]	13.5	20

Figure 6-2 and Figure 6-3 illustrate the ejector operational curves for case 1 and case 2, respectively. In both figures, three modes, according to the condenser pressure, were identified; namely: double choking (critical mode), single choking (subcritical mode) and back-flow mode (malfunction). During double choking mode, both motive and secondary flows are choked, making the ER remain constant for a fixed set of the primary and secondary flow conditions. Further increase in back pressure above the critical pressure causes the thermodynamic shock wave to move into the mixing chamber and prevents the secondary stream from reaching sonic condition. The secondary flow is no longer choked; thus, the mass flow rate of the secondary flow begins to decrease rapidly. If the condenser pressure is too high, severe backflows may occur and the ejector will lose its function completely (Chunnanond and Aphornratana 2004a). The deviation between the numerical and the experimental entrainment ratio is found to be around 8.91% for case 1 and similarly -8.76% for case 2, in the double-choking modes.

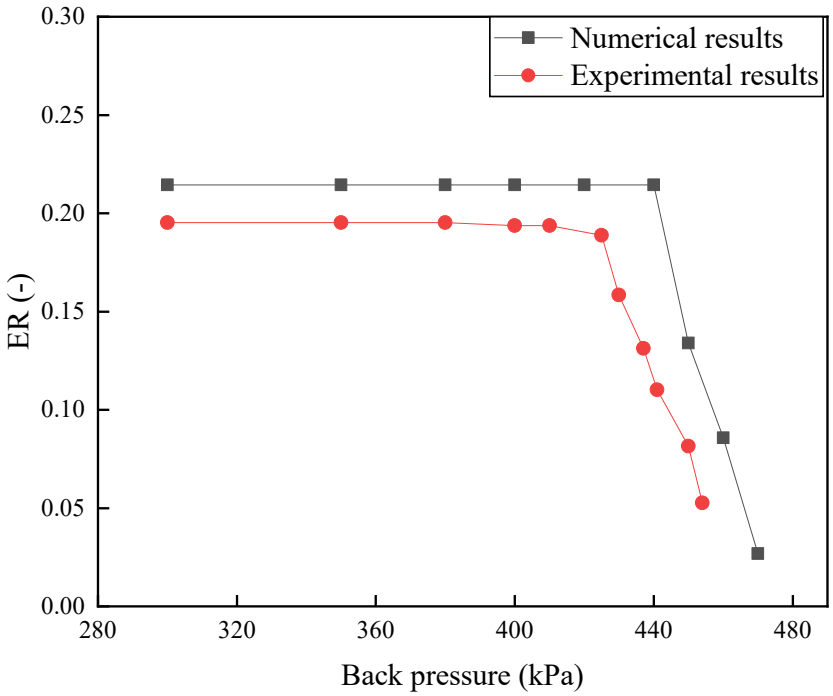

Figure 6-2: Comparison in terms of ejector entrainment ratio between the CFD model and experimental results (Butrymowicz *et al.* 2014) *of case 1*

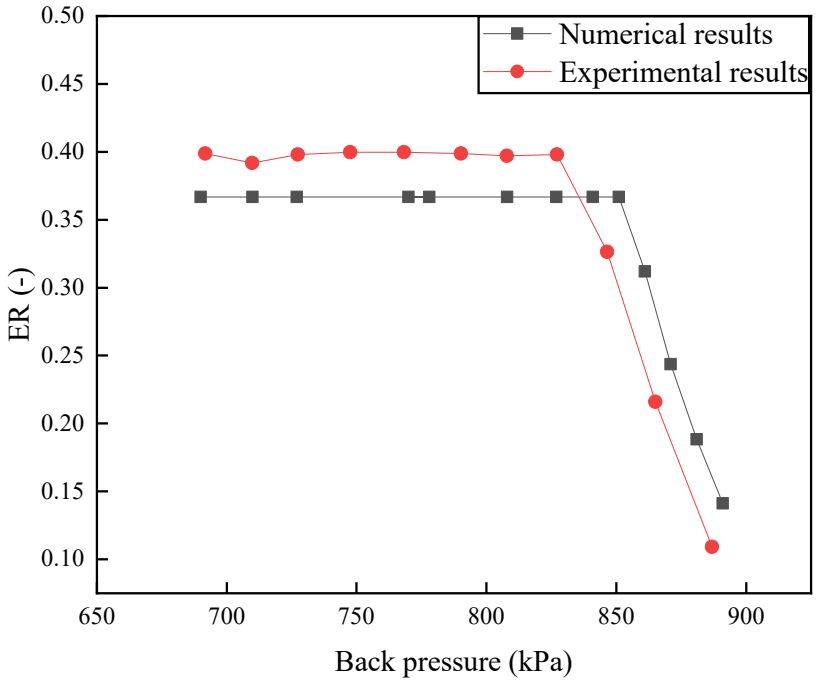

Figure 6-3: Comparison in terms of ejector entrainment ratio between the CFD model and experimental results (Croquer 2018) *of case 2*

6-4 Mesh generation

In this study, the CFD pre-processing tool ICEM was used to mesh the computational domain. As an example, Figure 6-4 shows the mesh generated for the numerical simulations of case 1. The mesh is refined in the vertical direction in order to achieve an acceptable value for the wall coordinate for the application of high-Reynolds approach ($30 < y^+ < 100$) (ANSYS Inc. 2013). A grid convergence study was performed for each case study to ensure overall mesh independent results. In addition to the convergence and stability, the entrainment ratios, pressure and Mach number profiles along the ejector centerline were investigated. The pressure and Mach number profiles comparisons are illustrated in Figure 6-5 and Figure 6-6.

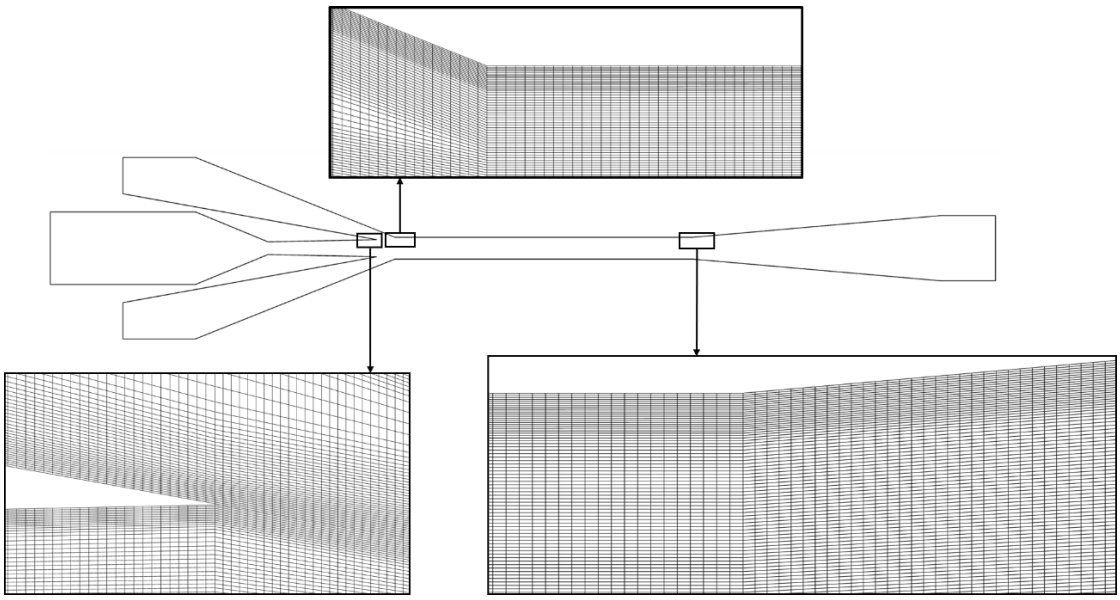

Figure 6-4: Grid structure of the computational domain for numerical simulations

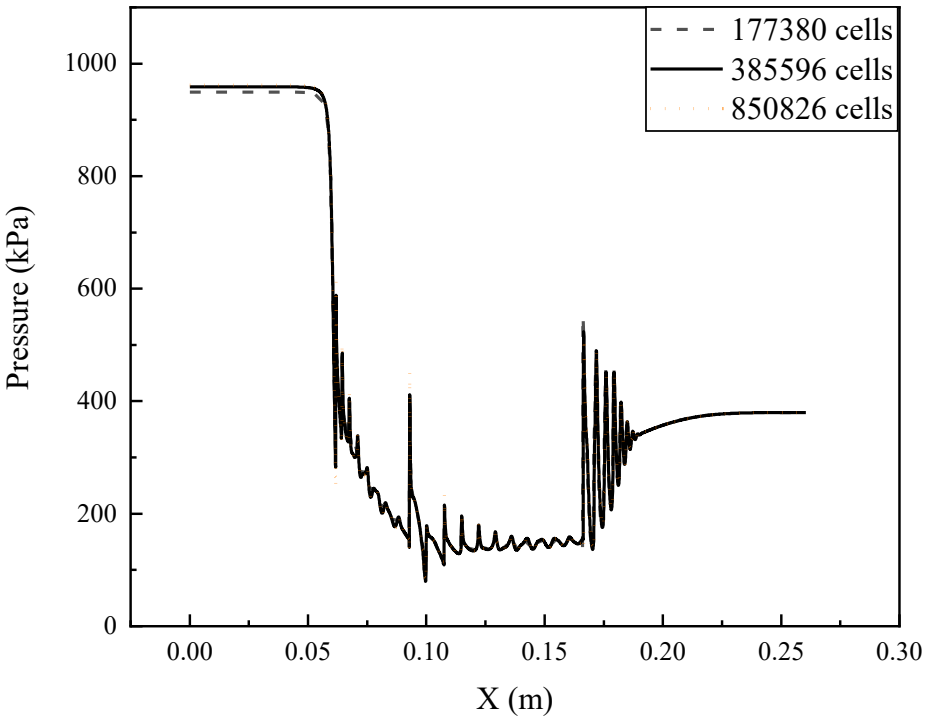

Figure 6-5: Variation of pressure along the ejector centerline with different grid levels for Case 1

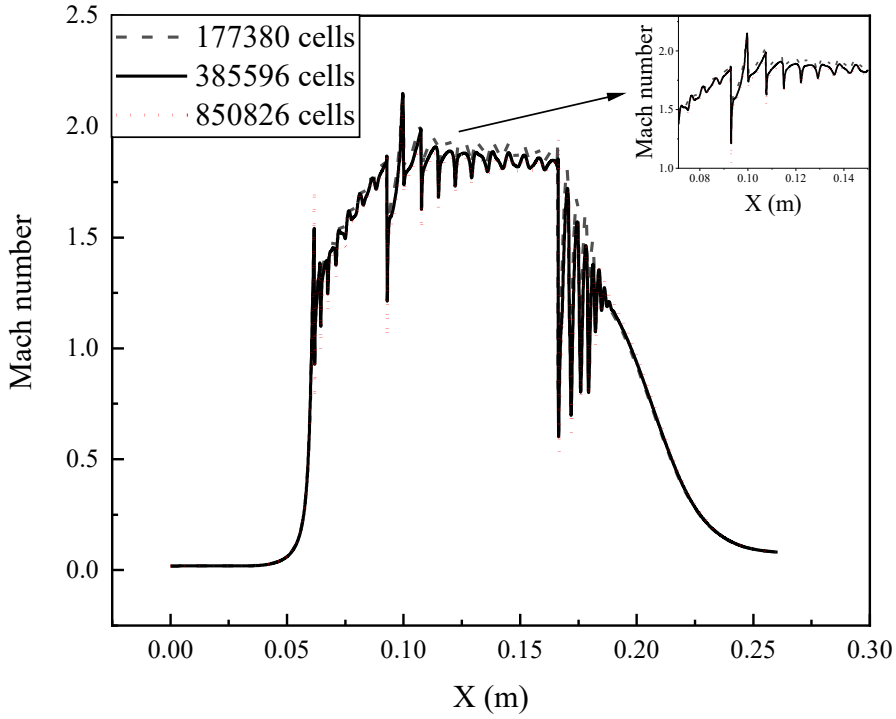

Figure 6-6: Variation of axial Mach number with different grid levels for Case 1

Figure 6-5 and Figure 6-6 show the pressure and Mach number profiles, respectively, for three computational domain comprising 177380, 385559 and 850826 quadrilateral cells that met the entrainment ratio criteria (the deviations of the ERs of the numerical results for computational domains with a lower number of 177380 from those of the corresponding experimental results were not acceptable). Since the geometrical parameters would be changed, the computational domain with 177380 cells which marginally showed good consistencies in the pressure and Mach number profiles compared to the other domains in Figure 6-5 and Figure 6-6, could not be reliable for the proposed study. As a result, the computational domain with 385596 quadrilateral cells was chosen to perform the CDF model.

6-5 Turbulence model

A CFD model requires the selection of a turbulence model. For this study, two well-known turbulence models have been investigated, standard $\kappa - \varepsilon$ and $\kappa - \omega$ SST (Shear Stress Transport) models. Both models belong to the two-equation turbulence category. In two-equation turbulence models, the turbulent length and time scale can be determined by solving two separate transport equations. Turbulence kinetic energy (κ) and its dissipation rate (ε) are two transported variables in the $\kappa - \varepsilon$ model. The standard $\kappa - \varepsilon$ model is known as the workhorse of practical engineering flow calculations in the time since it was introduced (ANSYS Inc. 2013). Its popularity in the industrial applications comes from robustness, economy, and reasonable accuracy for a wide range of turbulent flows. The other turbulence model that was investigated herein is $\kappa - \omega$ SST model. This model is a combination of the standard $\kappa - \omega$ and $\kappa - \varepsilon$ models to benefit from the advantages of both models ($\kappa - \varepsilon$ model shows better performance far from the wall, while $\kappa - \omega$ shows superiority in boundary layer region). It means that near-wall $\kappa - \omega$ model is activated and in the free-stream region and far from the wall $\kappa - \varepsilon$ is activated.

The CFD model for each turbulence model was performed and the results for case study 1, i.e. the computational domain with 385596 cells, have been illustrated in Figure 6-7.

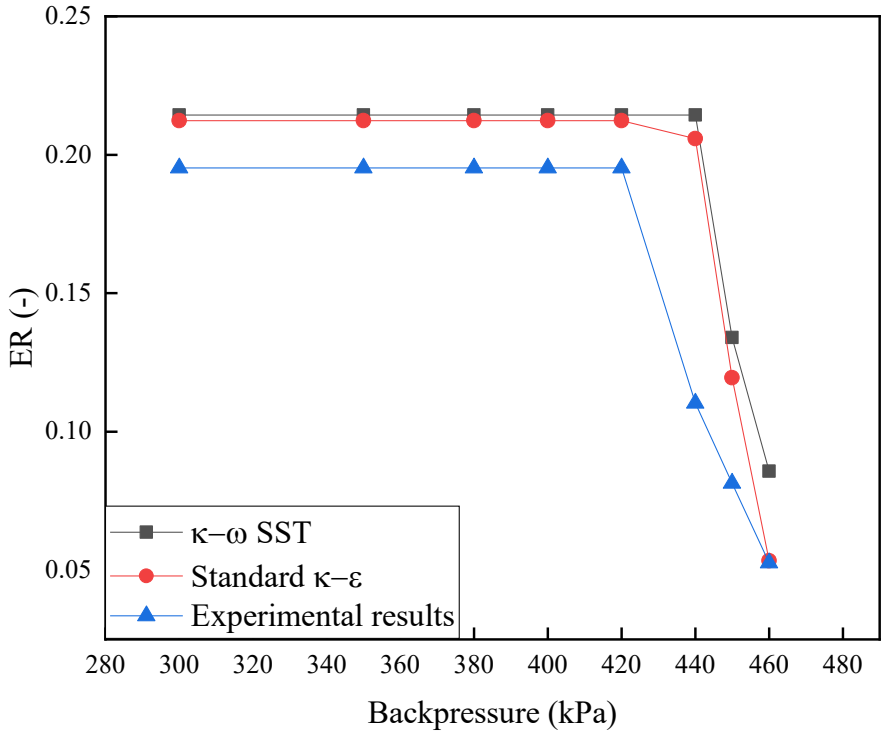

Figure 6-7: Comparison in terms of ejector entrainment ratio between the two turbulence models and experimental results (Butrymowicz *et al.* 2014) *of case 1*

Figure 6-7 shows that the using standard $\kappa - \varepsilon$ turbulence model led to better results in terms of the entrainment ratio and critical back pressure. Thus, this turbulence was used in this study. It should be mentioned that the results are in agreement with the observations of Croquer et al. (Croquer, Poncet and Aidoun 2016).

6-6 Baseline geometry of the ejector

In order to find the geometry design of the ejector which can provide us with the desired ER, the ejector used by Butrymowicz et al. (Butrymowicz *et al.* 2014) will be considered as the baseline. It should be mentioned that the considered ejector respects the length to diameter ratio of the ejector constant-area duct that was proposed as the sole parameter of ejector geometry to perform the 1D thermodynamic model in the previous chapter. Having performed the CFD simulation model on the baseline geometry of the ejector, in which the optimized operating conditions, i.e. Table 6-3, were considered as boundary conditions, the resultant mass flow rates of the primary and secondary flows were obtained, i.e. Table 6-4.

Table 6-3: Desired operating conditions of the ejector based on the optimization approach

Operating parameter	Value
Primary flow pressure, [kPa]	1585.3
Primary flow temperature [°C]	94.4
Secondary flow pressure, [kPa]	216.9
Secondary flow temperature [°C]	15.1
Condenser pressure, [kPa]	460.9
Exit flow temperature, [°C]	59.5

Table 6-4: Mass flow rates calculated by the CFD for the optimized operating conditions and desired mass flow rates

Mass flow rate	Value	
	Baseline ejector	Desired ejector
Primary mass flow rate, [kg/s]	0.0447	0.0415
Secondary mass flow rate, [kg/s]	0.0025	0.016

6-7 Primary mass flow rate

The maximum mass flow rate through a convergent-divergent nozzle depends on the upstream pressure and temperature, as well as the throat area (Rathakrishnan 2019). It means that for a set of inlet conditions of the primary flow, the mass flow rate is the function of the throat area value. According to the literature, a decrease in the primary nozzle throat results in a decrease in the primary mass flow rate (Rathakrishnan 2019). By using the CFD model and examining different values of the throat area, the desired primary mass flow rate can be obtained. Figure 6-8 illustrates the effect of the primary nozzle throat on the primary mass flow rate. According to Figure 6-8, the desired primary mass flow rate was obtained for the throat radius of 1.70 mm. It should be mentioned that the other geometrical parameters remained constant as the baseline ejector geometry.

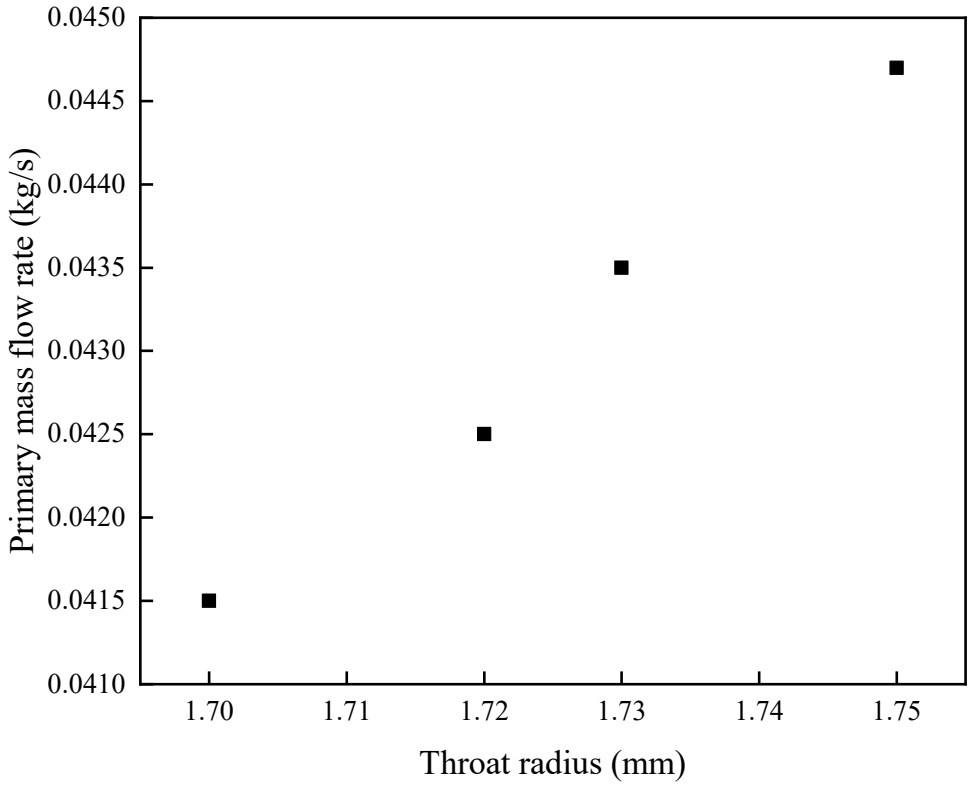

Figure 6-8: Primary mass flow rate vs. nozzle throat radius

Since the flow area in the constant area section is fixed, the decrease of the throat area leads to a higher secondary mass flow rate, Figure 6-9. Thus, the decrease of the throat area has a double effect on the resultant ER by the decrease in the primary mass flow rate and the increase in secondary mass flow rate. It should be noted that the decrease of primary mass flow rate causes the momentum of the mixed flow to drop and consequently the critical back pressure is reduced.

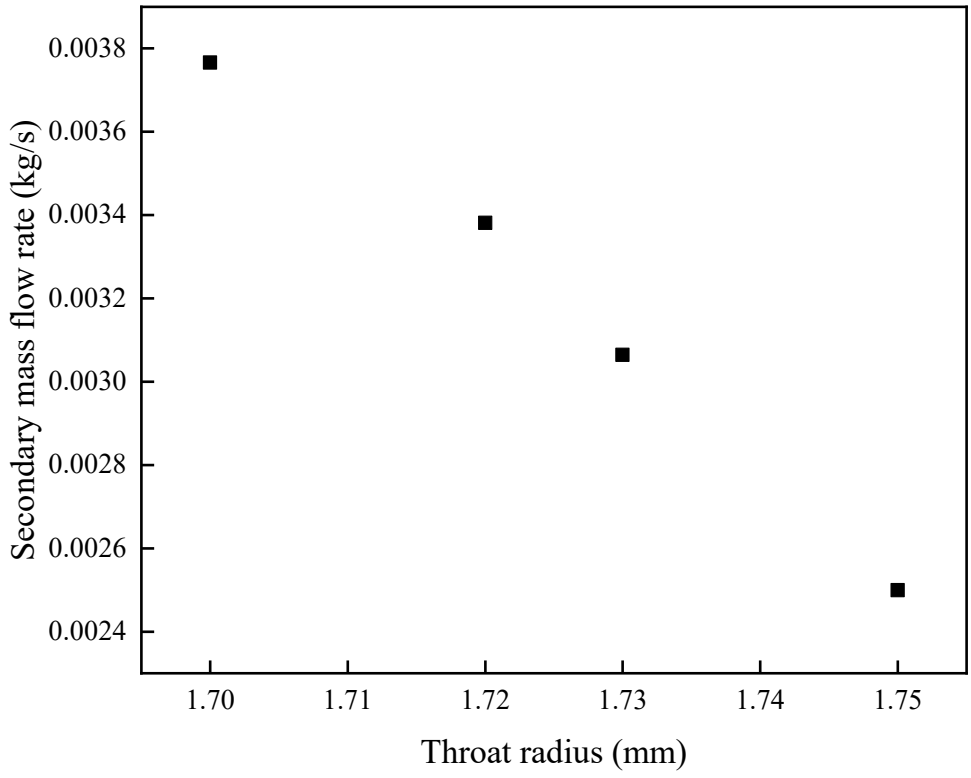

Figure 6-9: Secondary mass flow rate vs. nozzle throat radius

6-8 Secondary mass flow rate

Unlike the primary mass flow rate that depends solely on the primary nozzle throat, secondary (entrained) mass flow rate may be affected by several ejector geometry parameters such as nozzle exit position, constant area length, area ratio, diffuser length, converging angle of the mixing section. Among these geometry parameters of the ejector, nozzle exit position and constant-area section diameter play a more significant role in the ejector performance (Zhu *et al.* 2009; Yan, Cai and Li 2012; Tashtoush, Al-Nimr and Khasawneh 2019). In the following, we will manipulate these parameters to find the appropriate geometry parameters that provide us with the desired secondary mass flow rate.

6-8-1 Nozzle Exit Position, NXP

The ejector can be generally categorized into two main types according to the primary nozzle position (NXP); namely: Constant Area Mixing (CAM) ejector and Constant Pressure Mixing (CPM) ejector. In the constant area mixing type, the primary nozzle outlet is located in the

constant area section as the primary and secondary streams start mixing inside this duct. For the constant pressure mixing type, the primary nozzle outlet is located in the suction chamber and the mixing starts upstream of the constant area section. It was proven that the CPM type is more favorable than CAM type, due to its stable performance at a wider range of back pressures (Chunnanond and Aphornratana 2004b). The influence of the NXP on the ejector performance has been studied by some researchers. It was found that the NXP plays a key role in the ejector performance and its optimum value varies according to the working fluids and corresponding operating conditions (Zhu *et al.* 2009; Yan, Cai and Li 2012). Moreover, retracing the nozzle out of the mixing chamber results in a lower critical back pressure (Chunnanond and Aphornratana 2004a). In order to find out the optimum NXP, seven ejectors were studied by varying the nozzle exit position while other parameters remained constant. Figure 6-10 shows the variation of secondary mass flow rates and resultant ER with different NXPs.

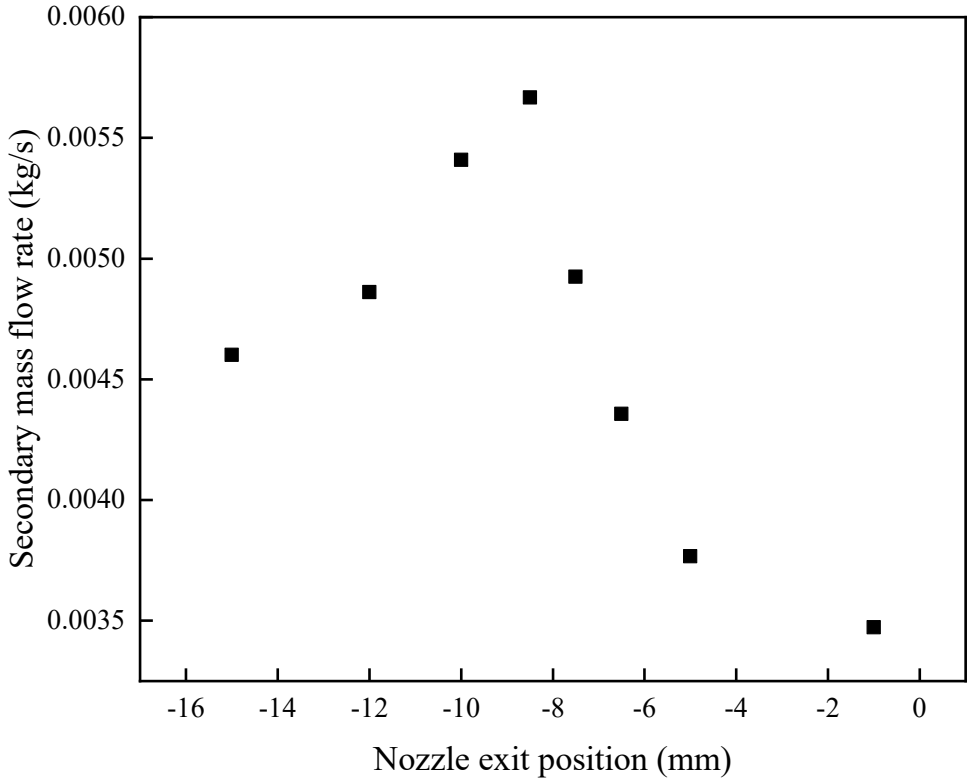

Figure 6-10: Effect of NXP on the secondary mass flow rate

Figure 6-10 reveals that the highest secondary mass flow rate is obtained for NXP=8.5 mm for the proposed set of operating conditions. The figure also shows that the highest secondary mass flow rate equals $0.0057\ (kg/s)$ that is still far from the desired mass flow rate.

It should be mentioned that in all cases, the ejectors operated at critical mode.

6-8-2 Constant-area section diameter:

The entrained mass flow rate of the ejector firstly increases and then decreases with the increase of the diameter of the constant-area section (Yan, Cai and Li 2012; Tashtoush, Al-Nimr and Khasawneh 2019). Elaborately speaking, an increase in the constant-area section diameter results in enhancing the suction of the secondary flow. On the other hand, this increase leads to lower critical back pressure. Thus, the increase of constant-area section diameter can enhance the ER if the ejector operates at the double choking mode.

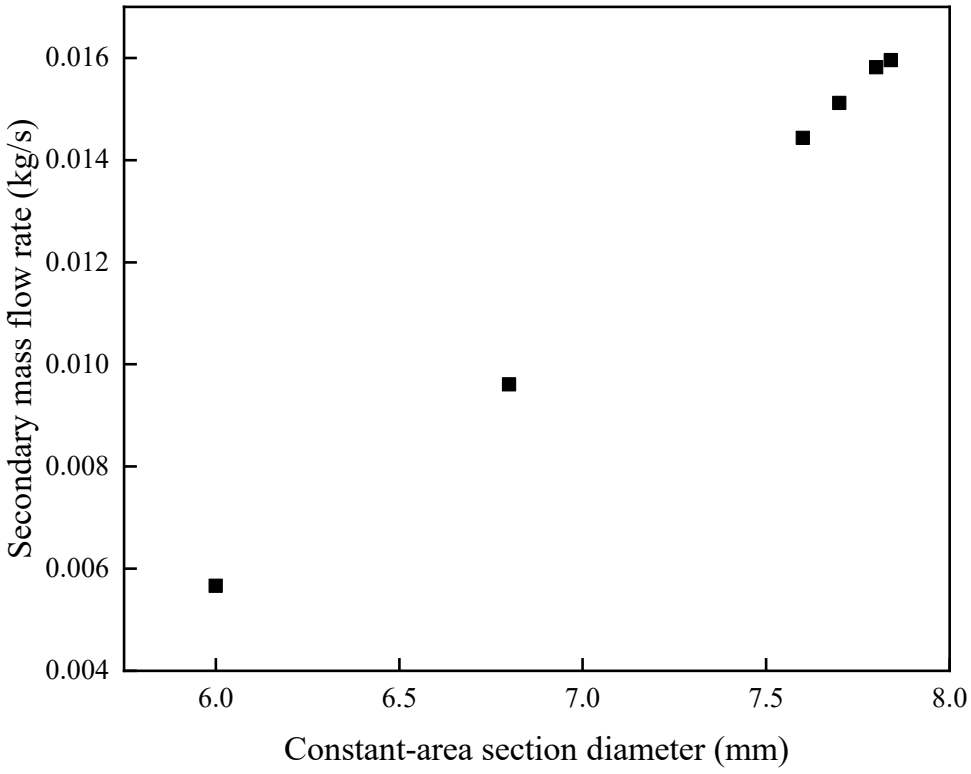

Figure 6-11: Effect of constant-area section diameter on the secondary mass flow rate

Figure 6-11 shows that the secondary mass flow rate increases linearly with the constant area ratio. This remark was already made by previous researchers (Eames *et al.* 1999; Varga, Oliveira and Diaconu 2009; Jia and Wenjian 2012). This figure also reveals that the desired secondary mass flow rate can be obtained for the constant-area section diameter of 7.84 mm. It should be mentioned that since the length to diameter ratio of the ejector constant-area section must be constant (as the sole parameter of ejector geometry for the 1D thermodynamic model); each constant-area section diameter considered in Figure 6-11 has its own constant-area section length. For instance, the desired secondary mass flow rate was obtained for the constant-area section length of 107.2 mm.

6-9 Final geometry parameters

The CFD model results show that the primary nozzle throat diameter, NXP and constant–area section diameter play significant roles in the ejector performance. The final geometry characteristics of the ejector that provide us with the proposed mass flow rates for the optimal operating conditions have been summarized in Table 6-5.

Table 6-5: Final geometry parameters of the desired ejector

Geometry parameter	Value
Primary nozzle throat diameter, d_{th}, [mm]	3.40
Primary nozzle exit diameter, d_P, [mm]	4.69
Nozzle exit position, NXP, [mm]	-8.50
Constant-area section length, L, [mm]	107.20
Constant-area section diameter, D, [mm]	7.84
Diffuser diverging angle, θ_d, [deg]	5.00
Diffuser exit diameter, d_d, [mm]	18.00

Chapter 7

CONCLUSION AND FUTURE VIEW

Conclusion de la thèse

L'objectif principal de cette étude est d'introduire une nouvelle approche systématique pour la conception de systèmes thermodynamiques comprenant la détermination des conditions de fonctionnement et la sélection du fluide de travail le plus approprié, en fonction des conditions de la source externe. Pour atteindre cet objectif, la conception d'un cycle thermodynamique a été divisée en trois étapes séquentielles: optimisation des performances à l'échelle du système, conception à l'échelle des composants et analyse à l'échelle locale. La première étape, à savoir l'optimisation des performances à l'échelle du système, a été introduite pour déterminer l'efficacité maximale possible du système dans des circonstances idéales, sur la base des sources thermiques externes existantes. Dans cette étape, une analyse de génération d'entropie basée sur le concept de température équivalente a été employée pour surmonter les lacunes des méthodes d'optimisation qui existaient dans la littérature. Les résultats de l'optimisation des performances à l'échelle du système étaient indépendants des fluides de travail. Ainsi, ils nous ont fourni la base pour introduire une approche systématique pour la deuxième étape de la conception du cycle. Afin de présélectionner les fluides de travail potentiels, les résultats d'optimisation ainsi que les critères de sécurité et d'environnement ont été utilisés. Ensuite, dans la conception à l'échelle des composants, une procédure de reconstruction a été introduite pour corréler les résultats d'optimisation en termes de températures équivalentes avec les états de fonctionnement réels des fluides de travail présélectionnés. À ce stade, la performance économique de chaque fluide de travail, sur la base des indicateurs économiques, pourrait être évaluée et, par conséquent, le fluide de travail optimal parmi les fluides de travail présélectionnés pourrait être sélectionné. Dans la troisième étape, c'est-à-dire l'analyse à l'échelle locale, les phénomènes au sein des composants sont pris en considération pour concevoir les géométries finales et d'autres caractéristiques des composants du système. L'utilisation de la température équivalente dans le

problème d'optimisation a réduit le nombre de variables d'entrée du problème. En outre, le concept de température équivalente a ouvert la voie à la détermination de la génération d'entropie des composants du système qui a conduit à des résultats optimaux plus précis. De plus, la différence entre la température de saturation et la valeur de température équivalente a posé les bases de la procédure de reconstruction proposée et a entraîné la détermination automatique des degrés de surchauffe et de sous-refroidissement ainsi que le débit massique sans aucune hypothèse préliminaire.

Au chapitre 3, l'approche globale proposée a été appliquée au cycle de réfrigération à compression de vapeur classique. Dans ce cycle, l'analyse de la seconde loi qui a limité l'optimisation des performances à l'échelle du système a été réalisée pour différent rendement isentropiques du compresseur. Ensuite, les résultats d'optimisation et la procédure itérative ont été utilisés pour déterminer les conditions de travail optimales de chaque fluide de travail présélectionné et, à son tour, la sélection du réfrigérant le plus approprié. Dans ce cas, un indicateur économique adimensionnel dans lequel le capital et les coûts d'exploitation ont été pris en compte a été utilisé pour évaluer la performance économique de chaque réfrigérant. Il convient de noter que le facteur économique sans dimension ne faisait pas de distinction entre les valeurs du capital et les coûts d'exploitation.

Au chapitre 4, l'application de l'approche basée sur la température équivalente dans une conception CRO a été présentée. L'approche a été appliquée à deux études de cas différentes qui existaient dans la littérature. Les résultats ont montré que le problème d'optimisation formulé dans la première étape de l'approche proposée a conduit à une solution supérieure par rapport à l'autre approche d'optimisation dans la littérature. De plus, l'approche actuelle nous a donné la capacité d'évaluer davantage de fluides de travail.

Le chapitre 5 peut être vu comme l'extension du modèle équivalent basé sur la température pour les cycles de réfrigération à compression de vapeur et les cycles Rankine organique, afin de concevoir le système de réfrigération à éjecteur. La complexité de l'écoulement de fluide à l'intérieur de l'éjecteur a été simplifiée par l'hypothèse que l'éjecteur était une combinaison d'un détendeur et d'un compresseur hypothétiques. Ensuite, le rendement de l'éjecteur est lié la génération d'entropie du compresseur hypothétique et le processus d'expansion à la génération

d'entropie de l'éjecteur réel. Afin d'évaluer la performance économique des fluides de travail présélectionnés, une analyse économique détaillée, c'est-à-dire une analyse exergoéconomique, a été réalisée pour déterminer le coût de la valeur du produit final du système, c'est-à-dire le coût de la charge de refroidissement pour chaque fluide de travail. L'approche de conception introduite dans cette étude a abouti à de meilleures performances du point de vue des coûts d'investissement et d'exploitation pour tous les fluides de travail étudiés, par rapport à d'autre approches dans la littérature.

Au chapitre 6, un modèle CFD a été utilisé pour déterminer les paramètres de géométrie d'éjecteur appropriés qui devaient atteindre les performances d'éjecteur souhaitées. Le débit massique primaire proposé a été atteint par le changement du diamètre de la gorge de la buse primaire. Les changements de gorge ont non seulement ajusté le débit massique primaire, mais aussi augmenté le débit massique secondaire et, par conséquent, amélioré le rapport d'entraînement de l'éjecteur. Ensuite, afin d'atteindre le débit massique secondaire souhaité, la position de sortie de la buse principale et le diamètre et la longueur de la section à aire constante ont été modifiés jusqu'à ce que le débit massique souhaité soit atteint.

Travail futur et perspective

L’optimisation de la conductance thermique totale des systèmes est un objectif principal dans les problèmes d'optimisation. En effet, une optimisation multi-objectifs incluant la conductance thermique et l'efficacité thermique du système est un sujet essentiel à étudier. Cette étude conduira à la détermination de l'UA optimale par rapport à l'efficacité thermique du système, indépendamment des fluides de travail. En outre, les résultats de ce problème d'optimisation peuvent être considérés comme la limite supérieure des performances du système en fonction des conditions de la source externe.

Il est intéressant de noter que tous les réfrigérants étudiés dans ce projet de recherche s'évaporent et se condensent à des températures constantes. D’autre part, les mélanges non azéotropes ou zéotropes ont des températures d'évaporation et de condensation glissantes ce qui signifie qu’à une pression donnée, la température d'entrée de l'évaporateur dans la région

biphasée sera inférieure à la température de sortie, et la température d'entrée du condenseur (dans la région biphasée) sera supérieure à la température de sortie pour ce type de mélange.

L'application de l'approche basée sur la température équivalente pour les mélanges azéotropes est un volet important à investiguer de même que l'étude de l'application de l'approche présentée pour les fluides supercritiques tels que le dioxyde de carbone.

Thesis conclusions

The main objective of this study was to introduce a novel systematic approach for the design of thermodynamic systems including the determination of operating conditions and the selection of the most appropriate working fluid, according to the conditions of the external source. To achieve this purpose, the design of a thermodynamic cycle was divided into three sequential steps: system-scale performance optimization, component-scale design, and local-scale analysis. The first step, i.e. the system-scale performance optimization, was introduced to determine the maximum possible efficiency of the system under ideal circumstances, based on the existing external thermal sources. In this step, an entropy generation analysis based on the equivalent temperature concept was employed to overcome the shortcomings of the optimization methods existing in the literature. The results of system-scale performance optimization were independent of working fluids. Thus, they provided us with the basis for introducing a systematic approach for the second step of the cycle design. In order to pre-select the potential working fluids, optimization results as well as safety, and environmental criteria have been used. Afterward, in the component-scale design, a reconstruction procedure was introduced to correlate the optimization results which are in terms of equivalent temperatures with the actual operating states of the pre-selected working fluids. In this stage, the economic performance of each working fluids, based on the economic indicators, could be evaluated and, as a result, the optimal working fluid among pre-selected working fluids could be selected. In the third step, i.e. local-scale analysis, the complex flow phenomena within the components were taken into consideration to design the final geometries and other characteristics of the system components. Using the equivalent temperature in the optimization problem reduced the

number of input variables of the problem and consequently decreased the complexity of the problem. Furthermore, the equivalent temperature concept paved the way for the determination of entropy generation of the system components that led to more precise optimum results. Moreover, the difference between the saturation temperature and the equivalent temperature value laid the foundation for the proposed reconstruction procedure and resulted in the automatic determination of superheating and subcooling degrees as well as the mass flow rate without any preliminary assumptions.

In chapter 3, the proposed comprehensive approach was applied to the conventional vapor-compression refrigeration cycle. In this cycle, the second-law analysis that constrained the system-scale performance optimization was conducted for different isentropic efficiencies of the compressor. Then, optimization results and an iterative procedure were used to determine the optimal working conditions of each pre-selected working fluids and, in turn, the selection of the most appropriate refrigerant. In this case, a dimensionless economic indicator in which both capital and operating cost have been taken into account was employed to evaluate the economic performance of each refrigerant. It must be noted that the dimensionless economic factor did not distinguish between the values of capital and operating costs.

In chapter 4, the application of the equivalent-temperature-based approach in an ORC design was presented. The approach was applied to two different case studies existing in the literature. The results showed that the optimization problem formulated in the first step of the proposed approach led to a superior solution compared to the other optimization approach in the literature. The present approach, moreover, gave us the capability to evaluate more working fluids.

Chapter 5 can be seen as the extension of the equivalent temperature-based model for the vapor-compression refrigeration and organic Rankine cycles, in order to design the ejector refrigeration system. The complexity of fluid flow inside the ejector was simplified by the assumption of the ejector as a combination of hypothetical expander and compressor. Then, the ejector efficiency linked the entropy generation of the hypothetical compressor and expansion processes to the entropy generation of the actual ejector. In order to evaluate the economic performance of pre-selected working fluids, a detailed economic analysis, i.e. exergoeconomic

analysis, was conducted to determine the value of the final product cost of the system, i.e., cooling load cost for each working fluid. The design approach introduced in this study resulted in better performances from the capital and operating costs points of view for all working fluids under investigation, compared to another approach in the literature.

In chapter 6, a CFD model was used to determine the appropriate ejector geometry parameters that needed to achieve the desired ejector performance. The proposed primary mass flow rate was achieved by the change of the primary nozzle throat diameter. The throat changes not only adjusted the primary mass flow rate, but also increased the secondary mass flow rate and, as a result, improved the ejector entrainment ratio. Afterward, in order to achieve the desired secondary mass flow rate, the primary nozzle exit position and constant-area section diameter and length were changed until the desired mass flow rate was attained.

Future work and perspective

In the optimization step, the total thermal conductance of systems has been considered as the objective function of the optimization problem. A multi-objective optimization including the thermal conductance and the thermal efficiency of the system can be an interesting subject to study. This study will lead to the determination of optimal UA versus thermal efficiency of the system, independent of working fluids. Furthermore, the results of this optimization problem can be seen as the upper bound of system performance according to the conditions of the external source.

All the refrigerants investigated in this study evaporate and condensate at constant temperatures. Non-azeotropic or zeotropic mixtures have gliding evaporation and condensing temperatures. It means that for a given pressure, the inlet temperature of the evaporator in the two-phase region will be lower than the outlet temperature, and the inlet temperature of the condenser (in the two-phase region) will be higher than the outlet temperature for this kind of mixture. The greatest opportunity for future work can be the application of the equivalent temperature-based approach for azeotropic mixtures. Another subject of future work can be the application of the presented approach for supercritical fluids such as carbon dioxide.

The results of this Ph.D. study have been published in the following international journals and conference:

Journals

- H. Akbari, M. Sorin, B. Marcos, An equivalent temperature based approach for selection of the most appropriate working fluids for refrigeration cycles, Energy Convers. Manag. 174 (2018) 227–238, https://doi.org/10.1016/j.enconman.2018. 08.023**.**
- H. Akbari, M. Sorin, Thermal design and selection of the optimal working fluid for organic Rankine cycles based on the equivalent temperature concept, Appl. Therm. Eng. 168 (2020) 114860. https://doi:10.1016/j.applthermaleng.2019.114860.
- H. Akbari, M. Sorin, Optimal component-scale design of ejector refrigeration systems based on equivalent temperature, Energy Convers. Manag. https://doi.org/10.1016/j.enconman.2020.112627.

Conference

- Akbari H, Sorin M V. Exergetic efficiency of the ejector operating across ambient temperature in a combined power and ejector-refrigeration cycle. 5th International Seminar on ORC Power Systems. Athens, Greece, 2019.

LIST OF REFERENCES

Adefarati T, Bansal RC. Reliability, economic and environmental analysis of a microgrid system in the presence of renewable energy resources. Appl Energy 2019; 236:1089–114.

Aghahosseini S, Dincer I. Comparative performance analysis of low-temperature Organic Rankine Cycle (ORC) using pure and zeotropic working fluids. Appl Therm Eng 2013; 54:35–42.

Ahmadi MH, Ahmadi MA, Mehrpooya M. Thermodynamic and thermo-economic analysis and optimization of performance of irreversible four-temperature-level absorption refrigeration. Energy Convers Manag 2014; 88:1051–9.

Ait-Ali M a. A class of internally irreversible refrigeration cycles. J Phys D Appl Phys 1996;29:593–9.

Ait-Ali MA. Finite-time optimum refrigeration cycles. J Appl Phys 1995; 77:4280–4.

Akbari H, Sorin M. Thermal design and selection of the optimal working fluid for organic Rankine cycles based on the equivalent temperature concept. Appl Therm Eng 2020; 168:114860.

Akbari H, Sorin M, Marcos B. An equivalent temperature-based approach for selection of the most appropriate working fluids for refrigeration cycles. Energy Convers Manag 2018; 174:227–38.

Alefeld G. Efficiency of compressor heat pumps and refrigerators derived from the second law of thermodynamics. Int J Refrig 1987; 10:331–41.

ANSYS Inc. Ansys Fluent Theory Guide., 2013.

ASHRAE Handbook-Fundamentals. IP. American Society of Heating, Refrigerating and Air-Conditioning Engineers, 2017.

Badescu V, Aboaltabooq MHK, Pop H. Avoiding malfunction of ORC-based systems for heat recovery from internal combustion engines under multiple operation conditions. Appl Therm Eng 2019; 150:977–86.

Bejan A. Theory of heat transfer-irreversible power plants. Int J Heat Mass Transf 1988; 31:1211–9.

Bejan A. Theory of heat transfer-irreversible refrigeration plants. Int J Heat Mass Transf 1989; 32:1631–9.

Bejan A. Method of entropy generation minimization, or modeling and optimization based on combined heat transfer and thermodynamics. Rev Générale Therm 1996; 35:637–46.

Bejan A, Tsatsaronis G, Moran M. Thermal Design and Optimization. New York, NY, USA: John Wiley, 1996.

Bejan A, Vargas JVC, Sokolov M. Optimal allocation of a heat-exchanger inventory in heat driven refrigerators. Int J Heat Mass Transf 1995; 38:2997–3004.

Bell IH, Wronski J, Quoilin S. Pure and pseudo-pure fluid thermophysical property evaluation and the open source thermophysical property library coolprop. Ind Eng Chem Res 2014; 53:2498–508.

Bellos E, Tzivanidis C, Tsifis G. Energetic, Exergetic, Economic and Environmental (4E) analysis of a solar assisted refrigeration system for various operating scenarios. Energy Convers Manag 2017; 148:1055–69.

Belman JM, Navarro-Esbrí J, Ginestar D. Steady-state model of a variable speed vapor compression system using R134a as working fluid. Int J Energy Res 2010; 34:933–45.

Besagni G. Ejectors on the cutting edge: The past, the present and the perspective. Energy 2019; 170:998–1003.

Bianchi M, Branchini L, Casari N. Experimental analysis of a micro-ORC driven by piston expander for low-grade heat recovery. Appl Therm Eng 2019; 148:1278–91.

Braimakis K, Karellas S. Energetic optimization of regenerative Organic Rankine Cycle (ORC) configurations. Energy Convers Manag 2018; 159:353–70.

Butrymowicz D, Śmierciew K, Karwacki J. Experimental investigations of low-temperature driven ejection refrigeration cycle operating with isobutane. Int J Refrig 2014; 39:196–209.

Cavazzuti M. Optimization Methods from Theory to Design. Berlin, Heidelberg: Springer Berlin Heidelberg, 2013.

Chen J, Zhu K, Huang Y. Evaluation of the ejector refrigeration system with environmentally friendly working fluids from energy, conventional exergy and advanced exergy perspectives. Energy Convers Manag 2017; 148:1208–24.

Chen L, Sun F, Wu C. Optimal allocation of heat-exchanger area for refrigeration and air-conditioning plants. Appl Energy 2004; 77:339–54.

Chunnanond K, Aphornratana S. An experimental investigation of a steam ejector refrigerator: The analysis of the pressure profile along the ejector. Appl Therm Eng 2004a; 24:311–22.

Chunnanond K, Aphornratana S. Ejectors: Applications in refrigeration technology. Renew Sustain Energy Rev 2004b; 8:129–55.

Croquer S. Combined CFD and thermodynamic analysis of a supersonic ejector with liquid droplets. Ph.D. thesis, Université de Sherbrooke 2018.

Croquer S, Poncet S, Aidoun Z. Turbulence modeling of a single-phase R134a supersonic ejector. Part 1: Numerical benchmark. Int J Refrig 2016; 61:140–52.

Curzon FL, Ahlborn B. Efficiency of a Carnot engine at maximum power output. Am J Phys 1975; 43:22–4.

Dahmani A, Aidoun Z, Galanis N. Optimum design of ejector refrigeration systems with environmentally benign fluids. Int J Therm Sci 2011; 50:1562–72.

Dalkilic AS, Wongwises S. A performance comparison of vapour-compression refrigeration system using various alternative refrigerants. Int Commun Heat Mass Transf 2010; 37:1340–9.

Dimian AC, Bildea CS. Chemical Process Design. Wiley, 2008.

Dincer I. Refrigeration Systems and Applications. THIRD. John Wiley and Sons, Ltd., Publication, 2017.

Eames IW, Wu S, Worall M. An experimental investigation of steam ejectors for applications in jet-pump refrigerators powered by low-grade heat. Proc Inst Mech Eng Part A J Power Energy 1999; 213:351–61.

Eldakamawy MH, Sorin M V, Brouillette M. Energy and exergy investigation of ejector refrigeration systems using retrograde refrigerants. Int J Refrig 2017; 78:176–92.

Energy Information Administration (EIA). International Energy Outlook., 2017.

Farsi A, Mohammadi SMH, Ameri M. Thermo-economic comparison of three configurations of combined supercritical CO_2 refrigeration and multi-effect desalination systems. Appl Therm Eng 2017; 112:855–70.

Grazzini G, Milazzo A, Paganini D. Design of an ejector cycle refrigeration system. Energy Convers Manag 2012; 54:38–46.

Hærvig J, Sørensen K, Condra TJ. Guidelines for optimal selection of working fluid for an organic Rankine cycle in relation to waste heat recovery. Energy 2016; 96:592–602.

Haghparast P, Sorin M V, Nesreddine H. Effects of component polytropic efficiencies on the dimensions of monophasic ejectors. Energy Convers Manag 2018a; 162:251–63.

Haghparast P, Sorin M V., Nesreddine H. The impact of internal ejector working characteristics and geometry on the performance of a refrigeration cycle. Energy 2018b; 162:728–43.

Horlock JH. A brief review of power generation thermodynamics. Advanced Gas Turbine Cycles. Elsevier, 2003, 1–11.

International Energy Outlook, Energy Information Administration (EIA), 2018.

Köhler J, Tischendorf C, Richter C. Experimental and theoretical study of a CO_2 ejector refrigeration cycle. In Vortrag, VDA Winter Meeting. Saalfelden, 2007.

Jia Y, Wenjian C. Area ratio effects to the performance of air-cooled ejector refrigeration cycle with R134a refrigerant. Energy Convers Manag 2012; 53:240–6.

Khan J-R, Zubair SM. Thermodynamic optimization of finite time vapor compression refrigeration systems. Energy Convers Manag 2001; 42:1457–75.

Khan J, Zubair SM. Design and performance evaluation of reciprocating refrigeration systems. Int J Refrig 1999; 22:235–43.

Khennich M, Sorin M, Galanis N. Equivalent temperature-enthalpy diagram for the study of ejector refrigeration systems. Entropy 2014; 16:2669–85.

Lamberts O, Chatelain P, Bartosiewicz Y. Numerical and experimental evidence of the Fabri-choking in a supersonic ejector. Int J Heat Fluid Flow 2018; 69:194–209.

Lawrence N, Elbel S. Analysis of two-phase ejector performance metrics and comparison of R134a and CO2 ejector performance. Sci Technol Built Environ 2015; 21:515–25.

Lazzaretto A, Tsatsaronis G. SPECO: A systematic and general methodology for calculating efficiencies and costs in thermal systems. Energy 2006; 31:1257–89.

Lee TS. Second-Law analysis to improve the energy efficiency of screw liquid chillers. Entropy 2010; 12:375–89.

Li J, Alvi JZ, Pei G. Modelling of organic Rankine cycle efficiency with respect to the equivalent hot side temperature. Energy 2016; 115:668–83.

Linke P, Papadopoulos AI, Seferlis P. Systematic methods for working fluid selection and the design, integration and control of organic Rankine cycles-A review. Energies 2015; 8:4775–801.

Liu W, Meinel D, Gleinser M. Optimal Heat Source Temperature for thermodynamic optimization of sub-critical Organic Rankine Cycles. Energy 2015; 88:897–906.

Lucas C, Koehler J. Experimental investigation of the COP improvement of a refrigeration cycle by use of an ejector. Int J Refrig 2012;35:1595–603.

Luo J, Chen L, Sun F. Optimum Allocation of Heat Exchanger Inventory of Irreversible Air Refrigeration Cycles. Phys Scr 2002;65:410–5.

Luo N, Hong T, Li H. Data analytics and optimization of an ice-based energy storage system for commercial buildings. Appl Energy 2017;204:459–75.

Ma W, Fang S, Su B. Second law-based analysis of vapor-compression refrigeration cycles: Analytical equations for COP and new insights into features of refrigerants. Energy Convers Manag 2017;138:426–34.

Mavrou P, Papadopoulos AI, Seferlis P. Selection of working fluid mixtures for flexible Organic Rankine Cycles under operating variability through a systematic nonlinear sensitivity analysis approach. Appl Therm Eng 2015; 89:1054–67.

Mehrpooya M, Mousavi SA. Advanced exergoeconomic assessment of a solar-driven Kalina cycle. Energy Convers Manag 2018; 178:78–91.

Mills AF. Heat Transfer. Second edi. Boston, MA: Prentice-Hall, 1998.

Mohammadi K, McGowan JG. A thermo-economic analysis of a combined cooling system for air conditioning and low to medium temperature refrigeration. J Clean Prod 2019; 206:580–97.

Molés F, Navarro-Esbrí J, Peris B. Theoretical energy performance evaluation of different single stage vapour compression refrigeration configurations using R1234yf and R1234ze(E) as working fluids. Int J Refrig 2014; 44:141–50.

Muhammad U, Imran M, Lee DH. Design and experimental investigation of a 1 kW organic Rankine cycle system using R245fa as working fluid for low-grade waste heat recovery from steam. Energy Convers Manag 2015; 103:1089–100.

Narimani E, Sorin M, Micheau P, Nesreddine H. Numerical and experimental investigation of the influence of generating pressure on the performance of a one-phase ejector installed within an R245fa refrigeration cycle. Appl Therm Eng 2019; 157:113654.

Neveu P, Azoumah Y. Optimal integration of Rankine cycles in concentrated solar power plant. ECOS 2015 2015.

Nocedal J, Wright JS. Numerical Optimization. Springer New York, 2006.

Nunes TK, Vargas JVC, Ordonez JC. Modeling, simulation and optimization of a vapor compression refrigeration system dynamic and steady state response. Appl Energy 2015; 158:540–55.

Papadopoulos AI, Stijepovic M, Linke P. On the systematic design and selection of optimal working fluids for Organic Rankine Cycles. Appl Therm Eng 2010; 30:760–9.

Qureshi BA. Thermoeconomic considerations in the allocation of heat transfer inventory for irreversible power systems. Appl Therm Eng 2015; 90:305–11.

Rashidi MM, Aghagoli A, Raoofi R. Thermodynamic analysis of the ejector refrigeration cycle using the artificial neural network. Energy 2017; 129:201–15.

Rathakrishnan E. Applied Gas Dynamics., 2019.

Reddick C, Sorin M, Rheault F. Energy savings in CO_2 (carbon dioxide) capture using ejectors for waste heat upgrading. Energy 2014; 65:200–8.

Rostamnejad Takleh H, Zare V. Employing thermoelectric generator and booster compressor for performance improvement of a geothermal driven combined power and ejector-refrigeration cycle. Energy Convers Manag 2019; 186:120–30.

Salah El-Din MM. Performance analysis of heat pumps and refrigerators with variable reservoir temperatures. Energy Convers Manag 2001a; 42:201–16.

Salah El-Din MM. Second law analysis of irreversible heat engines with variable temperature heat reservoirs. Energy Convers Manag 2001b; 42:189–200.

Salhi K, Korichi M, Ramadan KM. Thermodynamic and thermo-economic analysis of compression–absorption cascade refrigeration system using low-GWP HFO refrigerant powered by geothermal energy. Int J Refrig 2018; 94:214–29.

Salimpour MR, Ahmadzadeh A, Al-Sammarraie AT. Comparative investigation on the exergoeconomic analysis of solar-driven ejector refrigeration systems. Int J Refrig 2019; 99:80–93.

Saloux E, Sorin M, Nesreddine H, Teyssedou A. Reconstruction procedure of the thermodynamic cycle of organic Rankine cycles (ORC) and selection of the most appropriate working fluid. Appl Therm Eng 2018; 129:628–35.

Saloux E, Sorin M, Nesreddine H, Teyssedou A. Thermodynamic Modeling and Optimal Operating Conditions of Organic Rankine Cycles (ORC) Independently of the Working Fluid. Int J Green Technol 2019; 5:9–22.

Saloux E, Teyssedou A, Sorin M. Development of an exergy-electrical analogy for visualizing and modeling building integrated energy systems. Energy Convers Manag 2015; 89:907–18.

Samaké O, Galanis N, Sorin M. Thermo-economic analysis of a multiple-effect desalination system with ejector vapour compression. Energy 2018; 144:1037–51.

Sarkar J, Bhattacharyya S. Overall conductance and heat transfer area minimization of refrigerators and heat pumps with finite heat reservoirs. Energy Convers Manag 2007; 48:803–8.

Sayed Ahmed SAE, Ibrahim EZ, Ibrahim MM, Essa, Mohamed A Abdelatief, Mohamed A. El-Sayed, Mohamed N. Heat transfer performance evaluation in circular tubes via internal repeated ribs with entropy and exergy analysis. Appl Therm Eng 2018; 144:1056–70.

Su W, Zhao L, Deng S. Simultaneous working fluids design and cycle optimization for Organic Rankine cycle using group contribution model. Appl Energy 2017; 202:618–27.

Tashtoush BM, Al-Nimr MA, Khasawneh MA. A comprehensive review of ejector design, performance, and applications. Appl Energy 2019; 240:138–72.

Taslimitaleghani S, Sorin M, Poncet S. Energy and exergy efficiencies of different configurations of the ejector-based CO_2 refrigeration systems. Int J Energy Prod Manag 2018; 3:22–33.

Thiel Gregory P, McGovern Ronan K, Zubair Syed M, Lienhard V John H. Thermodynamic equipartition for increased second law efficiency. Appl Energy 2014; 118:292–9.

Varga S, Oliveira AC, Diaconu B. Influence of geometrical factors on steam ejector performance – A numerical assessment. Int J Refrig 2009; 32:1694–701.

Wang Y, Zhao J, Chen G. A new understanding on thermal efficiency of organic Rankine cycle: Cycle separation based on working fluids properties. Energy Convers Manag 2018; 157:169–75.

White MT, Oyewunmi OA, Chatzopoulou MA, Pantaleo A. M, Haslam A. J, Markides C. N. Computer-aided working-fluid design, thermodynamic optimisation and thermoeconomic assessment of ORC systems for waste-heat recovery. Energy 2018; 161:1181–98.

Xu J, Yu C. Critical temperature criterion for selection of working fluids for subcritical pressure Organic Rankine cycles. Energy 2014; 74:719–33.

Xu Weicong, Deng Shuai, Zhao Li, Su Wen, Zhang Ying, Li Shuangjun, Ma Minglu. How to quantitatively describe the role of the pure working fluids in subcritical organic Rankine cycle: A limitation on efficiency. Energy Convers Manag 2018; 172:316–27.

Xu Y, Wang C, Jiang N. A solar-heat-driven ejector-assisted combined compression cooling system for multistory building – Application potential and effects of floor numbers. Energy Convers Manag 2019; 195:86–98.

Xu YC, Chen Q. A theoretical global optimization method for vapor-compression refrigeration systems based on entransy theory. Energy 2013; 60:464–73.

Yan J, Cai W, Li Y. Geometry parameters effect for air-cooled ejector cooling systems with R134a refrigerant. Renew Energy 2012; 46:155–63.

Yang L, Gong M, Guo H. Effects of critical and boiling temperatures on system performance and fluid selection indicator for low temperature organic Rankine cycles. Energy 2016; 109:830–44.

Yari M, Mahmoudi SMS. Thermodynamic analysis and optimization of novel ejector-expansion TRCC (transcritical CO_2) cascade refrigeration cycles (Novel transcritical CO2cycle). Energy 2011; 36:6839–50.

Yi Z, Luo X, Yang Z. Thermo-economic-environmental optimization of a liquid separation condensation-based organic Rankine cycle driven by waste heat. J Clean Prod 2018; 184:198–210.

Çengel Yunus A, Boles, Michael A. Thermodynamics: An Engineering Approach. 6th ed. 8th (ed.). New York, NY, USA: McGraw-Hill Education, 2014.

Zhang C, Liu C, Xu X. Energetic, exergetic, economic and environmental (4E) analysis and multi-factor evaluation method of low GWP fluids in trans-critical organic Rankine cycles. Energy 2018; 168:332–45.

Zhao L, Cai W, Ding X. Model-based optimization for vapor compression refrigeration cycle. Energy 2013; 55:392–402.

Zhou S, Chen L, Sun F. Cooling load density characteristics of an endoreversible variable-temperature heat reservoir air refrigerator. Int J Energy Res 2002; 26:881–92.

Zhu Y, Cai W, Wen C. Numerical investigation of geometry parameters for design of high-performance ejectors. Appl Therm Eng 2009; 29:898–905.